NUREG/CR-4288

Focal Mechanism Analyses for Virginia and Eastern Tennessee Earthquakes (1978-1984)

Prepared by G. A. Bollinger, A. G. Teague, J. W. Munsey/VPISU
A. C. Johnston/MSU

Virginia Polytechnic Institute and State University
and
Memphis State University

Prepared for
U.S. Nuclear Regulatory
Commission

NOTICE

This report was prepared as an account of work sponsored by an agency of the United States Government. Neither the United States Government nor any agency thereof, or any of their employees, makes any warranty, expressed or implied, or assumes any legal liability of responsibility for any third party's use, or the results of such use, of any information, apparatus, product or process disclosed in this report, or represents that its use by such third party would not infringe privately owned rights.

NOTICE

Availability of Reference Materials Cited in NRC Publications

Most documents cited in NRC publications will be available from one of the following sources:

1. The NRC Public Document Room, 1717 H Street, N.W.
   Washington, DC 20555
2. The Superintendent of Documents, U.S. Government Printing Office, Post Office Box 37082, Washington, DC 20013-7982
3. The National Technical Information Service, Springfield, VA 22161

Although the listing that follows represents the majority of documents cited in NRC publications, it is not intended to be exhaustive.

Referenced documents available for inspection and copying for a fee from the NRC Public Document Room include NRC correspondence and internal NRC memoranda; NRC Office of Inspection and Enforcement bulletins, circulars, information notices, inspection and investigation notices; Licensee Event Reports; vendor reports and correspondence; Commission papers; and applicant and licensee documents and correspondence.

The following documents in the NUREG series are available for purchase from the NRC/GPO Sales Program: formal NRC staff and contractor reports, NRC-sponsored conference proceedings, and NRC booklets and brochures. Also available are Regulatory Guides, NRC regulations in the *Code of Federal Regulations*, and *Nuclear Regulatory Commission Issuances*.

Documents available from the National Technical Information Service include NUREG series reports and technical reports prepared by other federal agencies and reports prepared by the Atomic Energy Commission, forerunner agency to the Nuclear Regulatory Commission.

Documents available from public and special technical libraries include all open literature items, such as books, journal and periodical articles, and transactions. *Federal Register* notices, federal and state legislation, and congressional reports can usually be obtained from these libraries.

Documents such as theses, dissertations, foreign reports and translations, and non-NRC conference proceedings are available for purchase from the organization sponsoring the publication cited.

Single copies of NRC draft reports are available free, to the extent of supply, upon written request to the Division of Technical Information and Document Control, U.S. Nuclear Regulatory Commission, Washington, DC 20555.

Copies of industry codes and standards used in a substantive manner in the NRC regulatory process are maintained at the NRC Library, 7920 Norfolk Avenue, Bethesda, Maryland, and are available there for reference use by the public. Codes and standards are usually copyrighted and may be purchased from the originating organization or, if they are American National Standards, from the American National Standards Institute, 1430 Broadway, New York, NY 10018.

NUREG/CR-4288
RA

Focal Mechanism Analyses for Virginia and Eastern Tennessee Earthquakes (1978-1984)

Manuscript Completed: April 1985
Date Published: June 1985

Prepared by
G. A. Bollinger, A. G. Teague, J. W. Munsey, Virginia Polytechnic Institute and State University
A. C. Johnston, Memphis State University

Seismological Observatory
Virginia Polytechnic Institute and State University
Blacksburg, VA 24061

and

Tennessee Earthquake Information Center
Memphis State University
Memphis, TN 38152

Prepared for
Division of Radiation Programs and Earth Sciences
Office of Nuclear Regulatory Research
U.S. Nuclear Regulatory Commission
Washington, D.C. 20555
NRC FINS B6249, B6675
Under Contract Nos. NRC-04-77-134, NRC-04-79-214

TABLE OF CONTENTS

Part One
Focal Mechanism Analyses for Virginia Earthquakes (1978-1984)
by
Jeffrey W. Munsey and G. A. Bollinger

Part Two
Focal Mechanism Analysis for Tennessee Earthquakes (1981-1983)
by
Alan G. Teague, G. A. Bollinger and Arch C. Johnston

TABLE OF CONTENTS

Part One
Focal Mechanism Analyses for Virginia Earthquakes (1978-1984)

Part Two
Focal Mechanism Analysis for Tennessee Earthquakes (1981-1983)

(These appendices may be found in the form of microfiche at the back of this report.)

LIST OF FIGURES

Part One
Focal Mechanism Analyses for Virginia Earthquakes (1978-1984)

Part Two
Focal Mechanism Analysis for Tennessee Earthquakes (1981-1983)

LIST OF TABLES

Part One
Focal Mechanism Analyses for Virginia Earthquakes (1978-1984)

Part Two
Focal Mechanism Analysis for Tennessee Earthquakes (1981-1983)

PART ONE
FOCAL MECHANISM ANALYSES FOR VIRGINIA EARTHQUAKES (1978-1984)

ABSTRACT

Focal mechanisms are presented for 11 earthquakes from the Giles County, Virginia seismic zone and its vicinity and for 12 earthquakes from the Central Virginia seismic zone. These earthquakes ($0 \leq M \leq 4$) were monitored by local networks between January, 1978 and October, 1984. In Giles County, the data base consists of 43 P-wave polarities and 50 SV to P amplitude ratios (SV/P) that yielded six single event focal mechanisms (SEFM's) and five composite event focal mechanisms (CFM's). In Central Virginia 79 P-wave polarities and 51 SV/P ratios are used to determine 11 SEFM's and 4 CFM's. A computer program FOCMEC, which systematically searches the focal sphere for valid mechanism solutions based on pre-defined data error limits, was used to determine the focal mechanism solutions.

The results for the Giles County seismic zone show mainly strike-slip mechanisms on steeply dipping ($73° \pm 16°$) NNE (right lateral motion) and ESE (left lateral motion) trending nodal planes. However, some (4/11) of the solutions show similar movement on nodal planes rotated 45° counterclockwise. The means and standard deviations for the trends and plunges of the P axes are $N46°E \pm 24°$ and $13.5° \pm 20°$, respectively, as computed from the six SEFM's and two CFM's.

Focal mechanisms from Central Virginia exhibit much more scatter in mechanism types and nodal plane orientations than in Giles County. The P axes in Central Virginia are generally northeast trending for shallow earthquakes (>8 km) and northwest trending for deeper ones (<8 km). The focal mechanisms exhibit a mixture of reverse and strike slip faulting on planes that dip $62° \pm 16°$.

In Giles County, where the seismic activity is occurring beneath the Appalachian decollement, faulting and inferred stress orientations are more uniform than in Central Virginia, some 200 km away, where the seismicity is occurring near and above the decollement.

INTRODUCTION

The southeastern United States exhibits a low level of seismic energy release, typical of most intraplate tectonic settings. However, clusters or zones of sporadic seismic activity within the region have been delineated on the basis of the historical record (Bollinger, 1973; Figure 1). Recent seismicity patterns monitored by networks in the southeastern U.S. are very similar to the historical distribution of events (SEUSSN Bulletin 14, 1984, Figure 2). The intensity X, Charleston, South Carolina earthquake of 1886 is the strongest earthquake known to have shaken the region. In addition, approximately a dozen earthquakes of intensity VII or greater have occurred in the southeastern U.S., two of which were located in Virginia (Bollinger, 1973).

The 1875 Goochland County, Virginia (Oaks, 1985) and the 1897 Giles County, Virginia earthquakes (intensities VII and VIII, respectively) are the two largest Virginia earthquakes (Bollinger, 1978). The 1875 earthquake occurred within an area that Bollinger (1973) described as the Central Virginia seismic zone and the 1897 Giles County event took place in the Giles County seismic zone (Bollinger and Wheeler, 1983). These two zones are separated by only 200 km, yet the results reported herein demonstrate that their seismogenic characteristics are quite different.

Emplacement of seismograph networks in the late 1970's, within and around these two zones, has allowed detailed studies of their seismic characteristics. The purpose of this investigation is the determination of focal mechanisms for Virginia earthquakes that occurred during network operation between 1978 and 1984. The data base consists of P-wave polarities and SV to P amplitude ratios (SV/P); the FORTRAN program, FOCMEC (Snoke and others, 1984) is used to analyze the data. The two study areas, Giles County, Virginia and Central Virginia, are first discussed separately and then subsequently compared and contrasted.

DATA COLLECTION

Installation of what is now a 20 station network of vertical, short-period seismographs began in the latter part of 1977 (Figure 3). The seven station Giles County sub-network in southwestern Virginia and the nine station Central Virginia sub-network were positioned to monitor seismic activity in those two areas of the state possessing a record of historical earthquakes.

The Bath County sub-network in the northwestern part of the state occupies what has been a virtually aseismic area (Bollinger and Gilbert, 1974). However, construction of a large pumped-storage reservoir project there has required that a seismic monitoring program be conducted to determine the background, pre-reservoir filling seismicity characteristics. The seismicity of the Bath County area was described by Todd (1982).

In Giles County, the data base consists of 43 P-wave polarities and 50 SV/P amplitude ratios from 11 earthquakes. Those earthquakes had duration magnitudes of 2.2 or less and their focal depths ranged from 7 to 20 km. In Central Virginia, 79 polarities and 51 SV/P

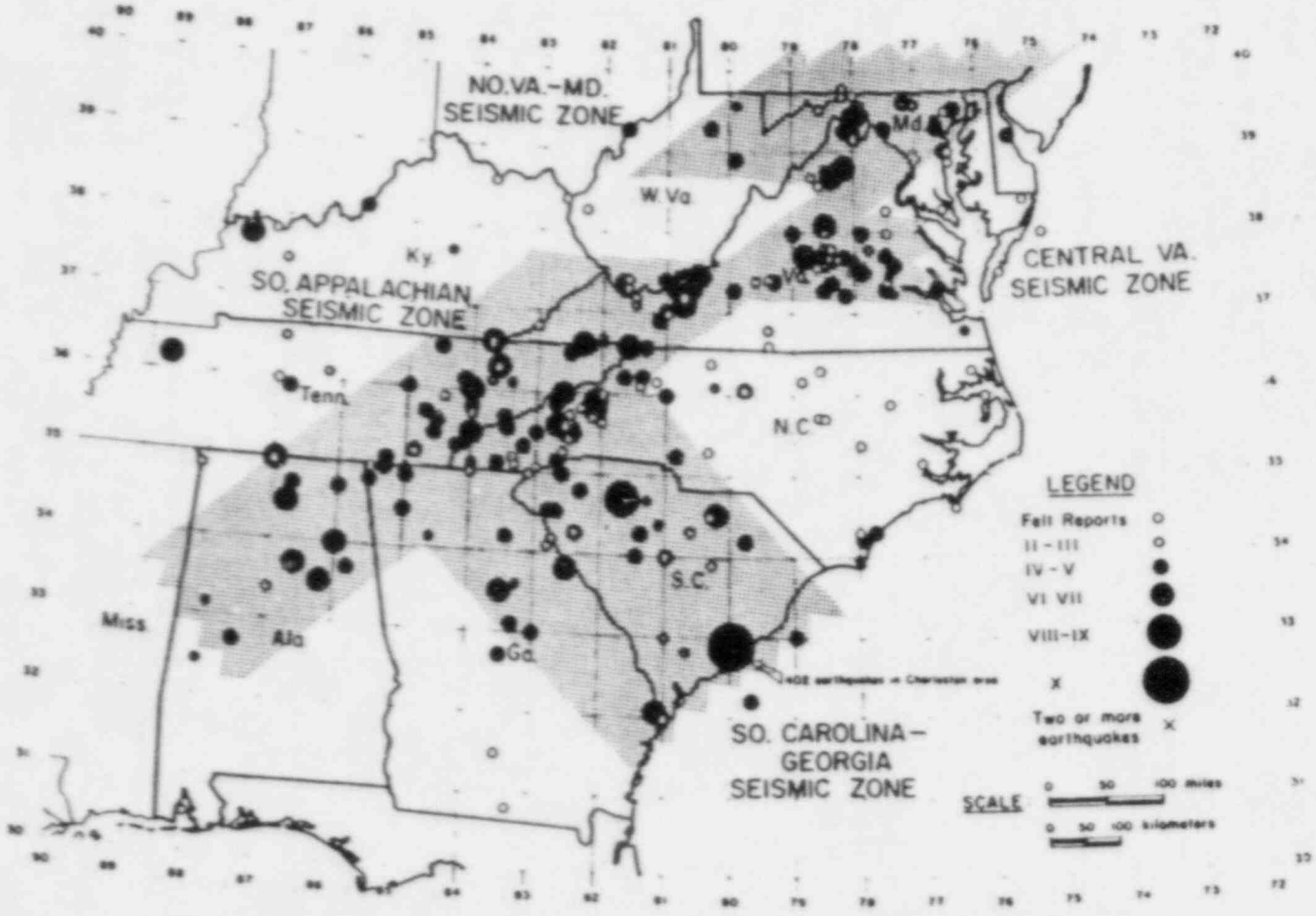

Figure 1: Historical earthquake locations based on isoseismals in the southeastern U.S. prior to 1972 are shown by circles scaled to magnitude. Seismic zones defined by Bollinger (1973) are also identified (after Bollinger, 1973).

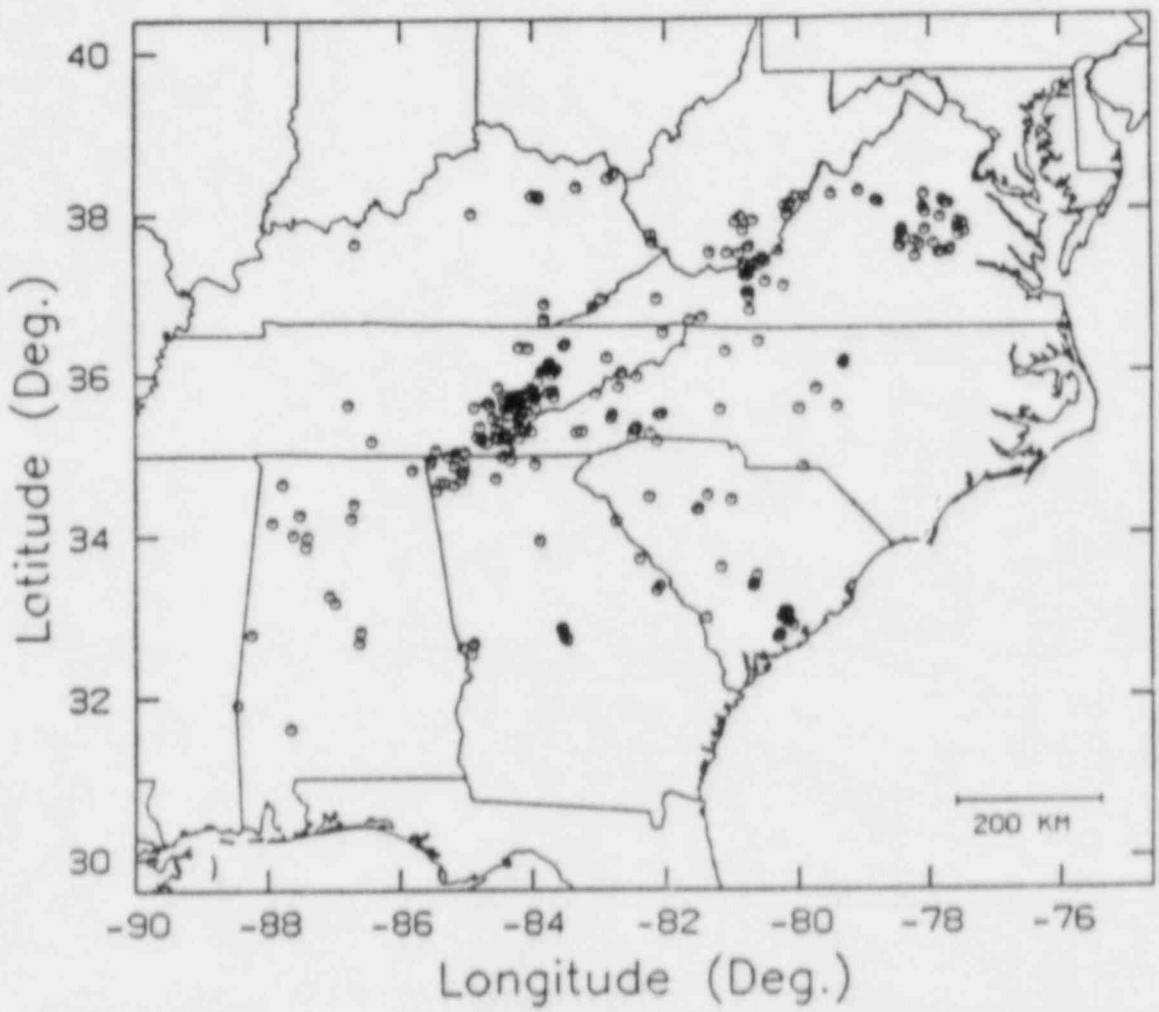

Figure 2: Open circles depict network monitored seismicity in the southeastern U.S. from January 1977 - June 1984 (after SEUSSN Contributors, 1984). Note the similarity in seismicity distribution to that of Figure 1.

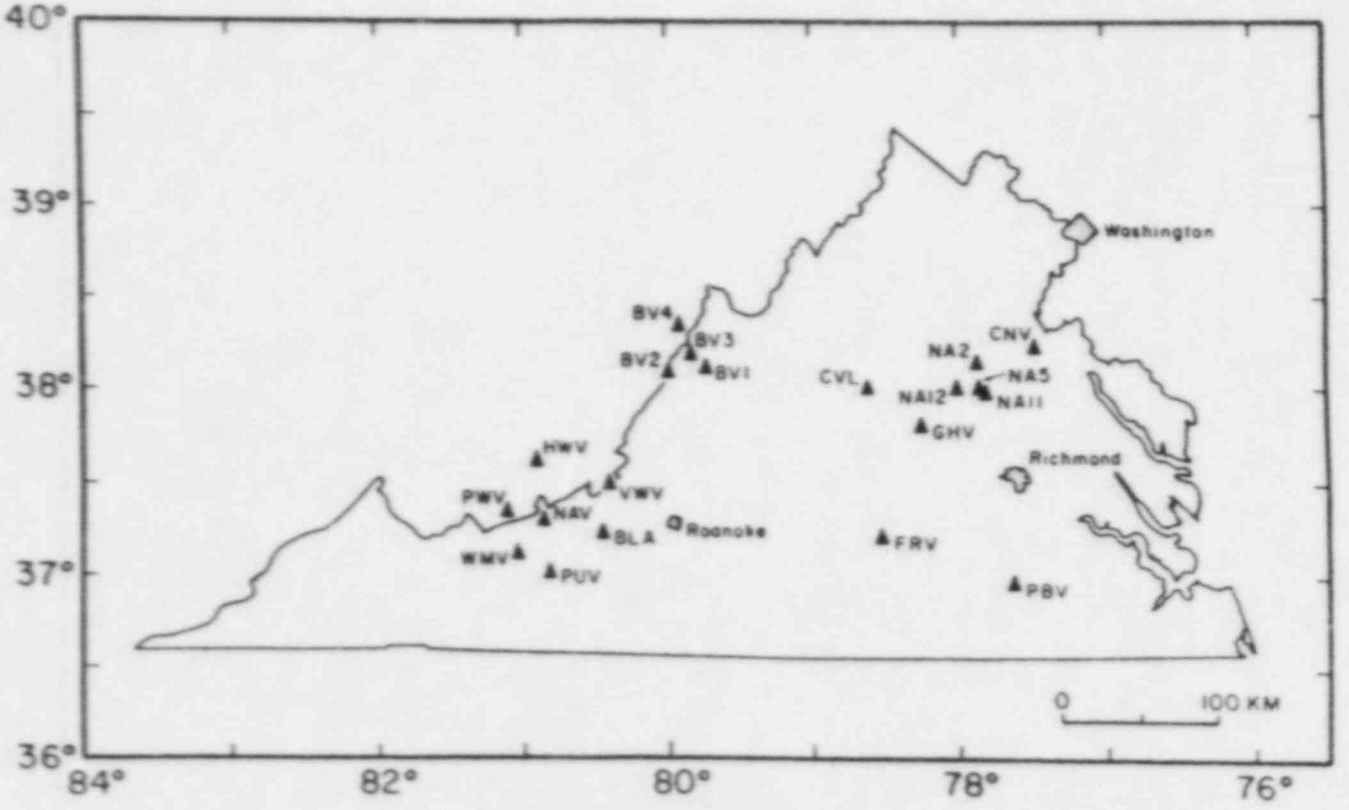

Figure 3: Seismic stations from the three sub-networks in Virginia are indicated by solid triangles. The Giles County network occupies southwestern Virginia and northwestern Virginia is the site of the Bath County network. The remaining stations at North Anna and in Central Virginia constitute the Central Virginia seismic network.

ratios from 12 earthquakes were used in the analysis. The Central Virginia events ranged in magnitude from 0.3 to 4.0 and had depths from 3 to 15 km. Pre-network events were also considered for focal mechanism analysis but because of one or both of the following shortcomings they are not considered herein: (1) a poorly constrained hypocenter, usually in depth; (2) lack of good quality polarity and, more often, amplitude ratio data.

Only impulsive P-wave polarities and the ratio of the vertical components of the maximum SV to P amplitudes (SV/P) within the first 1½ cycles of each phase are employed to determine focal mechanisms. Quality control for the input data included the reading of all polarity and amplitude ratio data by two or more independent observers, usually on more than one type of recording medium. The fidelity of P-wave polarities for the study earthquakes was assured by comparing the polarities of teleseismic P waves at the WWSSN station BLA with those at each network station for impulsive P-waves from teleseismic shocks that occurred both before and during the study period. SV/P amplitude ratios were measured only for stations with epicentral distances of 100 km or less for two reasons. First, restricting the distance range minimizes the effect that potential differences in P and S wave anelastic attenuation would have on the amplitude ratio. Secondly, the distance restriction eliminates the possibility of interference from Pg-Pn or Sg-Sn crossover amplitudes. Quality control measures relating directly to event location accuracy are discussed in the following section.

DATA PROCESSING

Velocity Models and Earthquake Location Procedures

The earthquake location program HYPOELLIPSE (Lahr, 1980) was used to locate all events. The use of locale-specific crustal velocity models significantly upgraded the precision and reliability of hypocenter estimates (Table 1). Such local velocity models had previously been developed for Giles County and Central Virginia (Moore, 1979 and Chapman, 1979). Also, joint relocation studies of Virginia earthquakes (Viret and others, 1984) have shown that the individual hypocenter estimates obtained by HYPOELLIPSE for Central and Southwestern Virginia earthquakes are reliable and have no significant biases resulting from the different network configurations employed in their locations.

Revisions of earlier locations (SEUSSN Bulletin 12A, 1983) were conducted because accurate ray take-off angles and azimuths are essential to achieve reliable focal mechanisms (see Appendix A). These revised locations incorporated the two layered, locale-specific velocity models. After relocation, only those earthquakes with vertical and horizontal errors (90% confidence level) of 5 km or less were retained for analysis. Location revision efforts included rereading of some arrival times, employing consistent arrival time residual and distance weighting schemes, and, in some cases, the incorporation of new arrival time data. Finally, the coordinates of two Central Virginia stations were found to be slightly in error, and the correct coordinates were included in the relocation runs.

Table 1

Velocity Models

MODEL	P WAVE VELOCITY (KM/SEC)	DEPTH (KM)	THICKNESS (KM)	GRADIENT (KM/SEC/KM)	VP/VS
GC01	5.63	0.0	5.7	Constant	1.64
	6.05	5.7	9.0	Constant	1.72
	6.53	14.7	36.0	Constant	1.70
	8.18	50.7		Constant	1.71
GCGR	5.63	0.0	50.7	0.035	1.70 or 1.72
	7.40	50.7			1.70 or 1.72
	8.18	50.7		Constant	1.70 or 1.72
CVNA	6.09	0.0	15.0	Constant	1.73
	6.50	15.0	21.0	Constant	1.72
	8.18	36.0		Constant	1.73
CVGR	6.09	0.0	36.0	0.016	1.73
	6.67	36.0			1.73
	8.18	36.0		Constant	1.73

The use of layered velocity models in focal mechanism determinations results in only direct arrival take-off angles and one possible (critical refraction) take-off angle for each layer boundary below the earthquake hypocenter. This artifact of layered models will result in a plot of rings of focal mechanism data when stations are distant enough from the source to record critical refractions as first arrivals. To alleviate this problem, postulated gradient velocity models were applied to the data in both study areas. However, our selection of focal mechanism solutions are derived from the layered velocity model results and all subsequent interpretations will be based upon these layered model findings.

In Giles County, the postulated gradient velocity model is characterized by a surface P wave velocity of 5.63 km/sec, a gradient of 0.035 km/sec/km to a depth of 50.7 km, and a sub-MOHO P-wave velocity of 8.18 km/sec (Table 1). The S wave velocity model was identical except that it was divided by the Vp/Vs ratios of 1.70 or 1.72 depending on the layer in which the seismic event was located using the discrete layer model. The gradient velocity model in Giles County was used to relocate the seismic events and it was chosen to minimize differences in the event locations produced by it and the layered model. Thus, while the hypocenters found by both Giles County layered and gradient velocity models are similar, and differences in take-off angles are primarily a function of the nature of the models and not of small differences in focal depth.

The gradient velocity model in Central Virginia was chosen in a manner somewhat different from the one for Giles County. In Central Virginia, the gradient model hypocenters were fixed to remain the same as the layered model ones. The gradient that produced the lowest total arrival time RMS error for the five events analyzed was chosen as the Central Virginia gradient model. The model selected had a surface P wave velocity of 6.05 km/sec with a 0.016 km/sec/km gradient to the MOHO at 36 km depth. The sub-MOHO P wave velocity is 8.18 km/sec. The Central Virginia gradient velocity model employs a 1.73 Vp/Vs ratio for all locations.

It must be emphasized that these gradient velocity models were subjectively and NOT rigorously developed. They were employed to illustrate the possible variation in focal mechanisms that is obtained from ONE possible gradient velocity model in comparison to a layered one.

The Giles County locations are generally more reliable than the Central Virginia ones. This is the result of the tighter and more evenly distributed Giles County network stations than are present in Central Virginia. Also, the distance between the earthquake and closest recording seismograph station is generally smaller in Giles County than in Central Virginia.

Focal Mechanism Data Reduction

The P-wave polarity is a discrete-valued parameter. It is either a compression or a dilatation. However, the observed SV/P amplitude ratios produce a continuum of values between zero and infinity. Body wave amplitudes potentially require application of three types of corrections to recover their value at the source: (1) Boundary

transmission effects (free surface and internal), (2) Geometrical spreading and (3) Anelastic attenuation. The differences in body wave amplitudes between the source and station depend on the radiation pattern, the velocity structure and the density and anelastic attenuation (Q) values of the medium.

Free surface effect corrections were applied to all SV/P data. SV/P amplitude ratios with emergence angles of 30° to 37° were deleted because the free surface effects change very rapidly in that range. Transmission coefficients are virtually the same for P and S across a velocity boundary for any angle of incidence, except when the density and/or Poisson's (Vp/Vs) ratio are significantly different across the boundary. The difference in the Vp/Vs ratio for the Giles County layered velocity model causes transmission differences of more than 10% between P and S rays that are incident upon the bottom of the top layer at angles of less than 20°. Thus, for that velocity model, transmission corrections were applied to the SV/P ratios.

Geometrical spreading affects P and S waves differently only when the Vp/Vs ratio changes along a raypath. Otherwise, the geometrical attenuation is exactly the same for both waves. Additionally, when variable Vp/Vs ratios are assumed, amplitude ratios from raypaths with take-off angles within approximately $\pm 2°$ of horizontal were not utilized because the differences in raypath length for P and S waves become too sensitive to the take-off angle in that range.

As mentioned earlier, anelastic attenuation is ASSUMED to create negligible differences between P and S amplitudes at epicentral distances of 100 km or less. No effort was made to correct the SV/P amplitude ratios for this effect and the validity of this assumption was not tested.

Several other assumptions about the data processing and analysis should be noted explicitly: (1) the velocity model employed for event locations is an adequate approximation of the actual velocity structure, and the take-off angles and azimuths as well as surface emergence angles, derived from the velocity model are correct, (2) when velocity models with variable Vp/Vs ratios are used, the amplitude ratio corrections used different P and S take-off angles at the source for a given epicentral distance are correct. However, theoretical amplitude ratios at the source are calculated with the same take-off angle for P and S. This inconsistency is assumed to be negligible when comparing the corrected observed amplitude ratio and the theoretical value because differences in P and S wave take-off angles were almost always less than two degrees. (3) Finally, the wave frequency at which both P and S amplitudes were read is assumed to be virtually the same. In practice, the P wave frequency (approximately 5 Hz) is usually slightly higher than the S wave frequency. Without this assumption, however, the frequency response of seismographs would have to be considered to obtain the correct relative amplitude.

FOCAL MECHANISM ANALYSIS

Stauder (1962) gave an excellent review of the historical development of double-couple focal mechanism theory. More recently, Herrmann (1975) presented a straightforward discussion of the use of

P-wave polarity and S-wave polarization angles to determine focal mechanisms. Kisslinger (1980; and others, 1981; and others, 1982) developed the theory and use of SV/P amplitude ratios to obtain a focal mechanism solution by non-linear least squares iterations.

Focal Mechanism Analysis by FOCMEC

The computer program, FOCMEC, (Snoke and others, 1985) was used in this study to determine focal mechanism solutions. This program is a refinement and extension of the algorithm written by Tzeng and Long (1982). FOCMEC incorporates P-wave polarities and/or SV/P amplitude ratios and differs from Kisslinger's approach in that it uses the SV/P data to constrain possible solutions, not to converge to a single one. FOCMEC systematically searches the focal sphere to find mechanism solutions consistent with pre-specified numbers of polarity and/or amplitude ratio errors. Acceptable ratios are those which fall within a pre-defined error allowance range. FOCMEC can search over any desired interval or increment of the focal sphere, but in this study a 5° search grid is used which generates more than 25,000 possible solutions. The set of solutions that satisfies the data within the pre-defined error allowances is called the family of solutions.

Some experience factors gained from this study's application of FOCMEC should be mentioned. In general, polarity data were judged to be more reliable than amplitude ratios. Too, any raypath errors present in polarity data must also be present for amplitude ratios. Mislocating station data on the focal sphere will thereby affect both types of data. Moreover, such mislocation is potentially more serious for amplitude ratios than polarities because of the raypath-dependent corrections to which ratios are subject. Finally, picking the S-wave onset time is in general less certain than the P-wave arrival time. This implies that the S wave amplitude, and hence the SV/P amplitude ratio, probably tends to be suspect more often than the P-wave polarity.

The above considerations pertain to any data set. However, composite focal mechanism (CFM) solutions are observed to generally have a higher percentage of agreement with polarity than amplitude ratio data. That tendency is not as strong for single event solutions. This may be due in part to the subjective compositing scheme that usually groups events on the basis of spatial association, similarity of stress axes, and/or similarity of polarity distributions, but generally not on the basis of amplitude ratio patterns. Nonetheless, some of the poorer SV/P agreement observed for composite solutions is likely related to the continuous, as opposed to discrete, nature of the amplitude ratio distributions.

Large disparities between the percentage of polarity and amplitude ratio errors indicates that some aspect of the resulting focal mechanism solution set is suspect. For example, when no polarity errors are found but 9 out of 10 ratios must be declared in error to obtain solutions, then the polarity data which may have errors present, is probably over-restricting the set of solutions. In cases such as this, allowing one polarity error will usually increase greatly the percentage of amplitude ratio data found to be in agreement. Except in rare cases when all the polarity and SV/P data

are acceptable, two or more sets of error specifications should be applied in an attempt to assess the data quality and mechanism solution stability.

The primary criteria for selection of a single preferred mechanism from a family of possible mechanisms is the root mean square (RMS) error for those ratios that fit the solutions, in combination with the RMS error for all ratios. The RMS error is defined as the square root of the squared differences between the theoretical and observed $\log_{10}$ SV/P amplitude ratios. Usually, greater emphasis is placed on choosing the lowest RMS error for the acceptable ratios than for all ratios because one or two ratios could be grossly in error and thereby make the overall RMS error misleading. However, when half or fewer of the ratios are acceptable, then the total ratio RMS error has been given more weight. In all cases, both types of RMS error are considered in choosing the preferred solution. The number of ratio errors for each solution within a family of solutions and the agreement in type of any one solution with all others from that family were judged to be secondary considerations in the choice of a preferred mechanism.

The data and solutions for each focal mechanism family are presented in the following on equal area, lower focal hemisphere projections. Except where noted specifically to the contrary, the figure format will be as follows: (1) nodal planes from the family of solutions on the left, (2) polarity and amplitude ratio data with the preferred solution in the center, and (3) the family of P (maximum compressive stress), T (minimum compressive stress) and B (null) axes corresponding to the nodal planes in (1) on the right. The convention for slip angles in Tables 4 and 8 is 0° = left-lateral, 90° = reverse, 180° or -180° = right-lateral, and -90° = normal slip.

THE GILES COUNTY, VIRGINIA SEISMIC ZONE

Geology and Seismicity

Most of Giles County lies within the Valley and Ridge physiographic province. The extreme northwest part of the County extends into the Cumberland plateau. Sedimentary rocks ranging in age from Early Cambrian (Rome Formation) to Mississippian (Pennington Group) crop out at the surface (Geologic Map of Virginia, 1963). Igneous and metamorphic rocks underlie the sedimentary cover at depths from about 3 to 7 km with the contact being deeper to the southeast (Bollinger and Wheeler, 1982). The strike of the sedimentary units is generally N60°-65°E. With the exception of that small portion of the county in the Cumberland Plateau, where flat-lying unfaulted rocks are the rule, these Paleozoic rocks have been folded and thrust-faulted northwestward to form several long, sub-parallel, linear ridges. The New River flows through the center of the County and cuts directly across these long, east-northeasterly trending ridges.

Bollinger and Wheeler (1983) have described the characteristics of the Giles County seismic zone. A summary of their results, modified somewhat by additional data and reevaluations of the complete data base follows. Seismicity in Giles County is concentrated at depths of 7 to 20 km (Figure 4). This places the seismic activity in the basement and below the overthrust sedimentary rocks. Epicenters

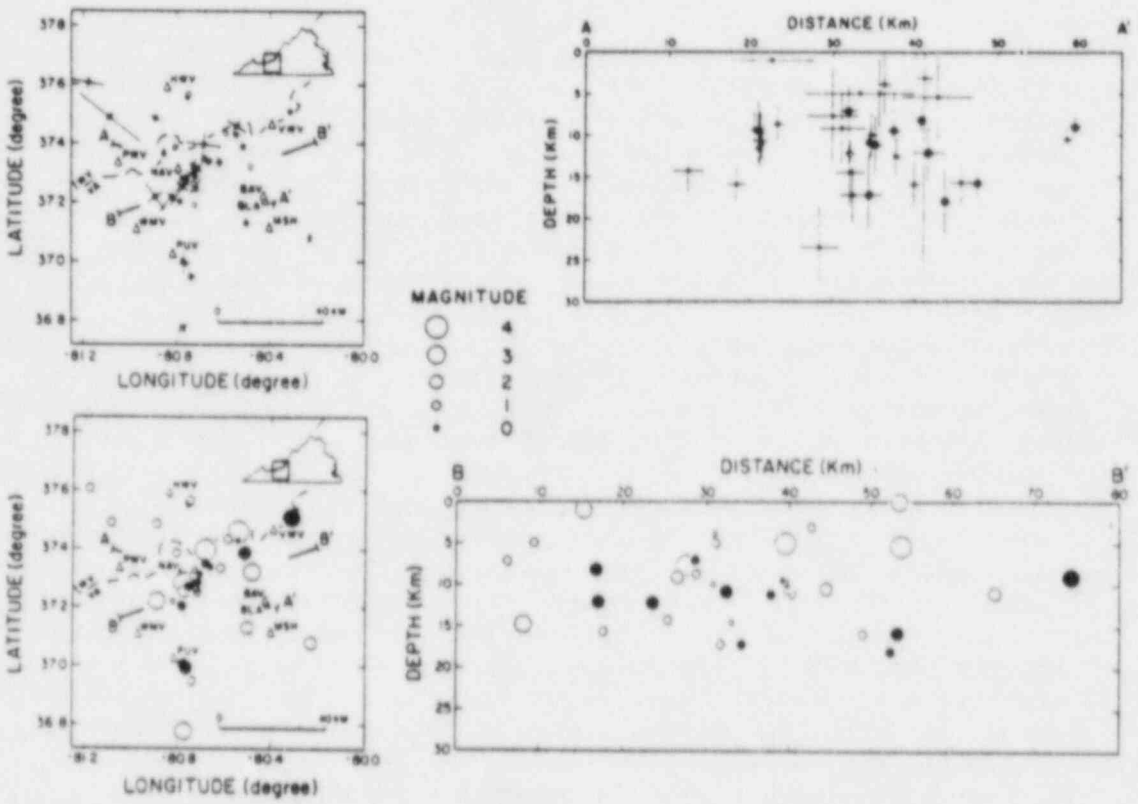

Figure 4: Upper left (4a): Network located and pre-network Dewey and Gordon relocated events in Giles County and vicinity are shown with horizontal error axes. Dark circles are study events and stations are represented by open triangles. Upper right (4b): The events in cross section A-A' of Figure 4a are shown with their vertical and horizontal error axes. The larger circles are study events. This cross-section is oriented perpendicular to a strike of N20°E which is the trend of one of the nodal planes for CFM A in Figure 6. Lower left (4c): Same map as Figure 4a except that events are scaled to magnitude. Again, darkened circles are study events. Lower right (4d): The events in cross section B-B' from Figure 4c are shown. This cross section is included because it is perpendicular to a trend of N25°W which is the trend of one of the nodal planes for CFM C in Figure 8.

from the main zone as defined by Bollinger and Wheeler, form an alignment striking N45°E. In section, these events form a near vertical plane. An important subset of earthquakes in the main zone consists of events from the southwestern and central portions of the zone. This sub-portion of the zone strikes N30°E and its significance will be discussed later in the context of composite focal mechanisms.

Since 1959, nine felt events have been recorded in the Giles County area. Dewey and Gordon (1982) relocated several of these earthquakes and they are included with the network located seismicity in Figure 4. Unfortunately, the local network was not yet in operation for any of these events. Thirty-five seismic events have, however, been detected by network monitoring in the last seven years with the largest event having a duration magnitude of 2.2.

Previous Focal Mechanism Studies

Herrmann (1979) computed a focal mechanism for the 1969 Elgood, West Virginia earthquake based primarily on surface wave data. That event occurred about 15 km northwest of the Giles County seismic zone. His mechanism indicated primarily strike-slip motion on near-vertical northeast and northwest trending nodal planes with left-lateral motion on the northeast striking plane. Conversely, Wheeler and Bollinger (1982) had projected right-lateral reverse motion on a near vertical, northeast trending plane on the basis of a few impulsive P-wave first motions and in-situ stress estimates from core data. The mechanism proposed by those two workers is consistent with the east-northeast maximum compressive stress typical of the midcontinent stress regime of Zoback and Zoback (1980).

Focal mechanisms results from the Bath County, Virginia area northeast of Giles County exhibited both strike-slip and reverse motions (Todd, 1982). However, the orientation of the maximum compressive stress (P) axes from that Central Appalachian setting was unlike that proposed for the Southern Appalachian Giles County. Generally, focal mechanism results from Bath County showed P axes with west to northwest trending, moderately plunging orientations.

Teague (1984) obtained focal mechanisms for earthquakes from eastern Tennessee using the same analysis method as in this study. Teague's study area is roughly along strike with and some 325 km southwest of the Giles County seismic zone, and his focal mechanisms showed mainly strike slip motion on north-south (right lateral) and east-west (left lateral) trending nodal planes. The mean P axis trend for Teague's composite focal mechanisms was N54°E with a plunge of 12°.

Focal Mechanism Results and Interpretations

A total of six single event focal mechanisms (SEFM's) and five composite event focal mechanisms (CFM's) solutions were obtained from earthquakes occurring along and in the near vicinity of the Giles County seismic zone. In addition to the primary family of focal mechanism solutions found using the layered Giles County velocity model (Figure 5; Table 2), focal mechanisms for some of the data sets include alternative solution families for the layered model and/or

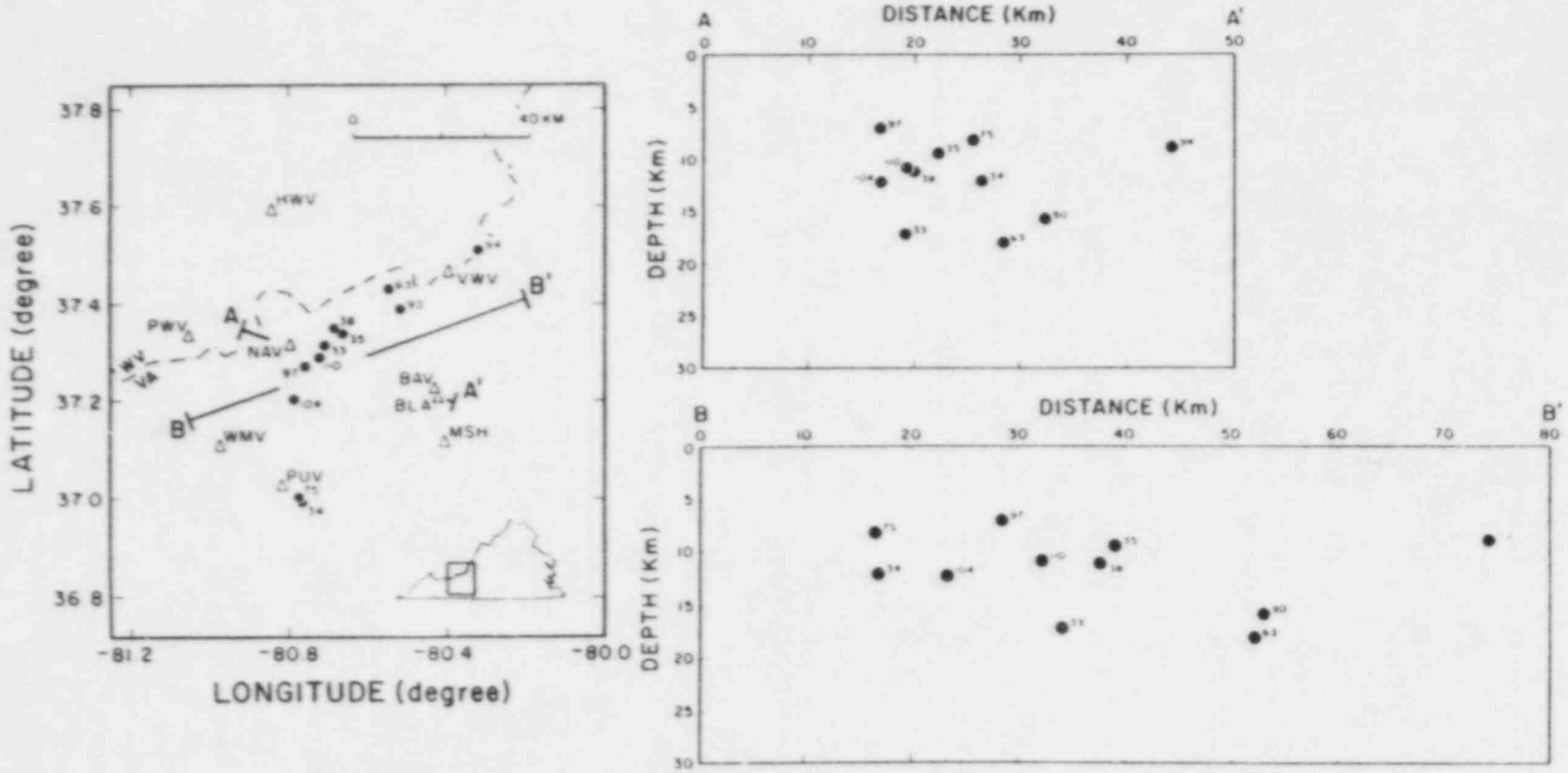

Figure 5: Left (5a): The darkened circles represent the locations of all Giles County study events and are numbered for reference. The cross section orientations and station symbols are the same as in Figure 4. Upper right (5b): Cross section A-A' of Figure 5a. Lower left (5c): Cross section B-B' of Figure 5a.

Table 2

Giles County Hypocenters*

EVT	DATE (M/D/Y)	TIME (UCT)	LAT (DEG N)	LONG (DEG W)	DEPTH (KM)	MAG	GAP (DEG)	DMIN (KM)	RMS (SEC)	ERH (KM)	ERZ (KM)
33	5/10/78	04:19	37.3112	80.7072	17.2	0.3	160	8	0.18	4.2	4.5
34	5/25/78	08:30	36.9903	80.7677	12.1	1.5	259	6	0.28	4.3	3.2
35	6/01/78	01:33	37.3360	80.6593	9.5	-0.2	153	12	0.16	1.6	4.6
38	8/30/78	02:19	37.3472	80.6812	11.2	0.5	151	11	0.18	1.7	3.5
63	12/02/80	07:47	37.4275	80.5427	18.0	0.4	113	25	0.16	1.2	3.8
75	12/04/81	02:35	36.9980	80.7743	8.2	2.0	136	5	0.2	1.3	1.6
90	1/25/83	20:38	37.3863	80.5137	15.8	1.8	81	14	0.24	0.8	1.5
94	5/26/83	01:04	37.5060	80.3152	9.0	2.2	103	8	0.24	0.8	1.4
97	7/10/83	14:05	37.2690	80.7558	7.1	1.0	89	6	0.26	1.1	2.9
104	12/9/83	00:11	37.2015	80.7857	12.2	1.1	98	13	0.22	0.7	1.1
110	7/02/84	19:51	37.2858	80.7180	10.8	1.4	89	8	0.19	1.0	2.0

*GC01 velocity model
EVT - event number
MAG - duration magnitude
GAP - greatest azimuthal separation of stations relative to epicenter
DMIN - distance of closest station from epicenter
ERH,ER2 - horizontal and vertical error estimates, respectively, at the 94% confidence level

solutions found by using a gradient velocity model. Alternative solution families for the layered velocity model are also shown when the choice of a preferred family of solutions is not clear, or when the secondary solution family more closely resembles solutions from other nearby events than does the primary family. Gradient velocity model mechanisms were obtained as an aid in the assessment of the stability of the layered model results. Appendices C and D present the complete set of focal mechanism results for both velocity models.

The character and distribution of the focal mechanism data indicates that four sub-groupings to form CFM's are appropriate (Table 3) for the Giles County events. Data from events 33, 35, 38, 97, 104 and 110 combined to form CFM A. Earthquakes 97, 104 and 110 also yielded SEFM. CFM group A occupies the southwestern and central portions of Bollinger and Wheeler's (1983) original seismic zone. Results for this CFM are shown in Figure 6. A group B CFM is derived from earthquakes 63 and 90. These two events lie at the northeastern end of the Giles County zone. Both events gave SEFM's and Figure 7 portrays the results for CFM B. To the south of and apart from the main zone, seismic events 34 and 75 were composited as Group C to give the results shown in Figure 8. Event 94 occurred 25 km northeast of the zone, and because it is spatially isolated and exhibits a somewhat different type of mechanism from the other events, it will not be discussed in detail. The preferred solutions for all of the SEFM and CFM are shown in Figures 9 and 10, respectively (also see Table 4).

The results from CFM's A and B attest to the complexity of faulting within the zone. The trend of the nodal planes and the spatial relationship of events in the northeastern and southwestern parts of the zone for these two sets of solutions make it unlikely that the seismicity results from a single, 40 km long northeasterly trending fault. Two hypotheses may be postulated from consideration of these differing mechanisms. First, seismicity on the southwestern and central parts of the zone is occurring on one or several very closely spaced, north-northeasterly striking, near vertical faults. The trend of epicenters in the southwestern and central portion of the zone is approximately N28°E which differs by only 8° from the N20°E nodal plane trend obtained from the CFM of these events. Motion on these faults is primarily right-lateral strike slip with a small reverse component. The activity at the northeastern end of the zone can be interpreted to result from a north-northwesterly trending, vertical fault with motion divided evenly between right-lateral and reverse slips. The spatial pattern of seismicity in the northeastern end of the zone, especially the alignment of epicenters, would support but not require this interpretation (Figure 5).

A second explanation for seismic source mechanisms within the zone would propose that the southwestern and northeastern ends of the zone lie on distinct, but sub-parallel faults. CFM D, which includes all eight events on the zone (Figure 11), satisfies all input data well, especially the polarities. Motion on faults in the northeastern end of the zone would be very similar to motion on faults in the southwestern portion of the zone.

The focal mechanisms will allow for either hypothesis. Analysis of future additional events, especially those with larger magnitudes, will be required to better define the nature of faulting within the zone.

Table 3

Giles County Composites

COMPOSITE	EVENTS	AVE DEPTH (KM)	MAX MAG
A	33,35,38,97,104,110	11.3	1.4
B	63,90	16.9	1.8
C	34,75	10.2	2.0
D	33,35,38,97,104,110, 63,90	12.7	1.8
E	33,35,38,97,104,110, 63,90,34,75,94	11.9	2.2

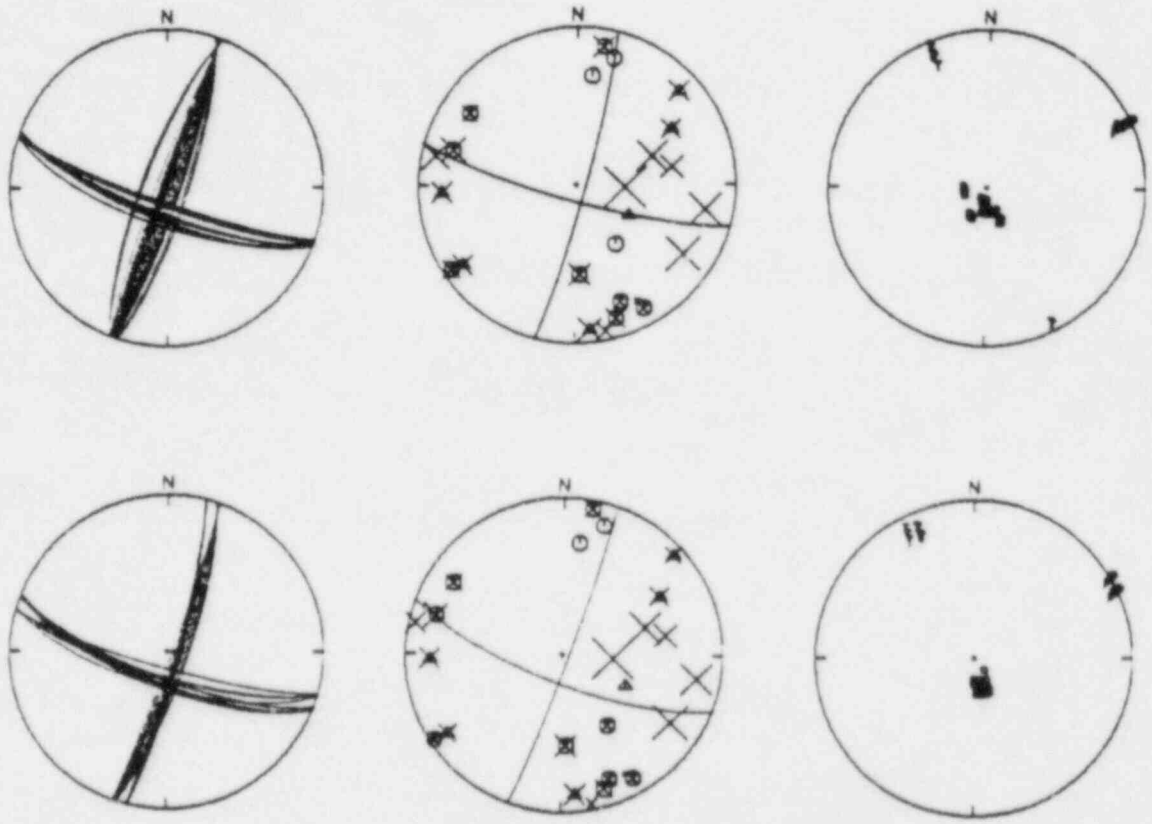

Figure 6: Top row, from left to right: (1) The family of nodal plane solutions, (2) the preferred nodal planes with polarity and SV/P amplitude data, and (3) the family of maximum (P) and minimum (T) compressive stress axes and the null (B) axes are shown on equal area, lower hemisphere projections. These solutions for CFM A were obtained using the Giles County layered velocity model. Second row: The solutions are presented in same order as above. These solutions are obtained by using the Giles County gradient velocity model as applied to CFM A. For the middle diagrams in both rows, circles represent compressions, triangles are dilatations and the size of the X's are proportional to the log of the SV/P corrected amplitude ratios.

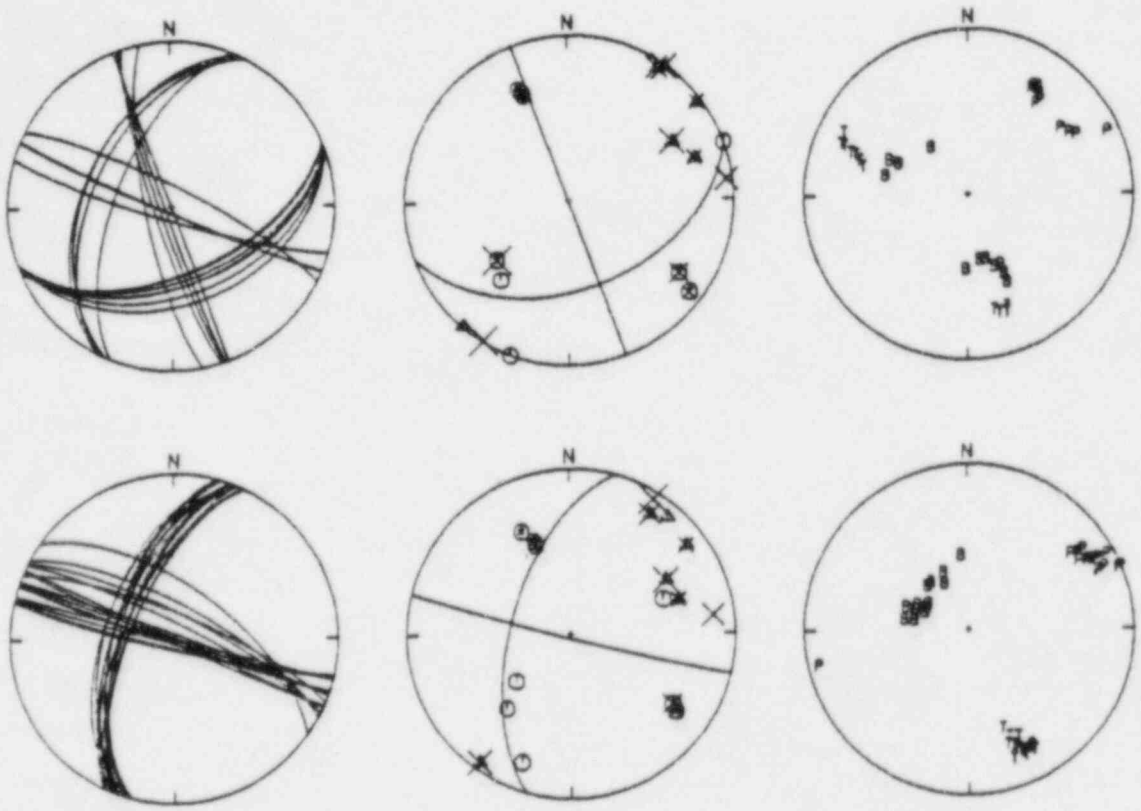

Figure 7: CFM B is analyzed using the Giles County layered (top row) and gradient velocity models (bottom row). Symbols and intra-row order are the same as in Figure 6.

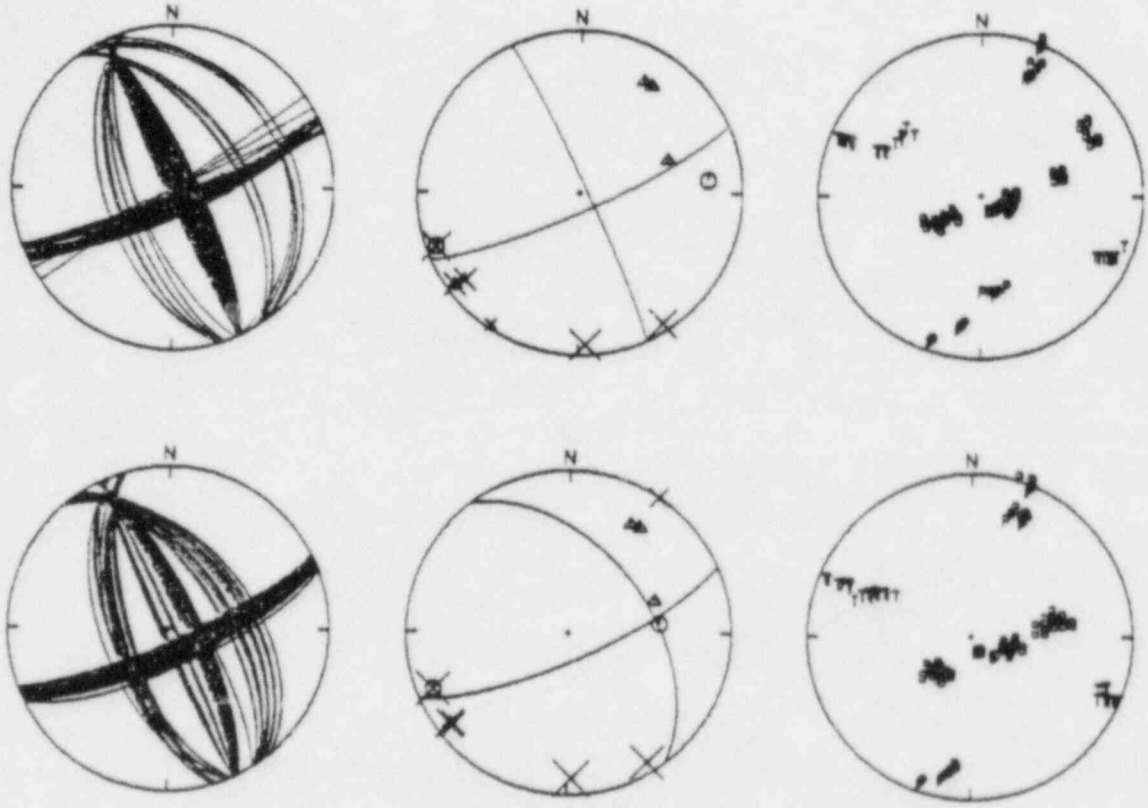

Figure 8: CFM C is analyzed by the Giles County layered (top row) and gradient velocity models (bottom row). Symbols and intra-row order are the same as in Figure 6.

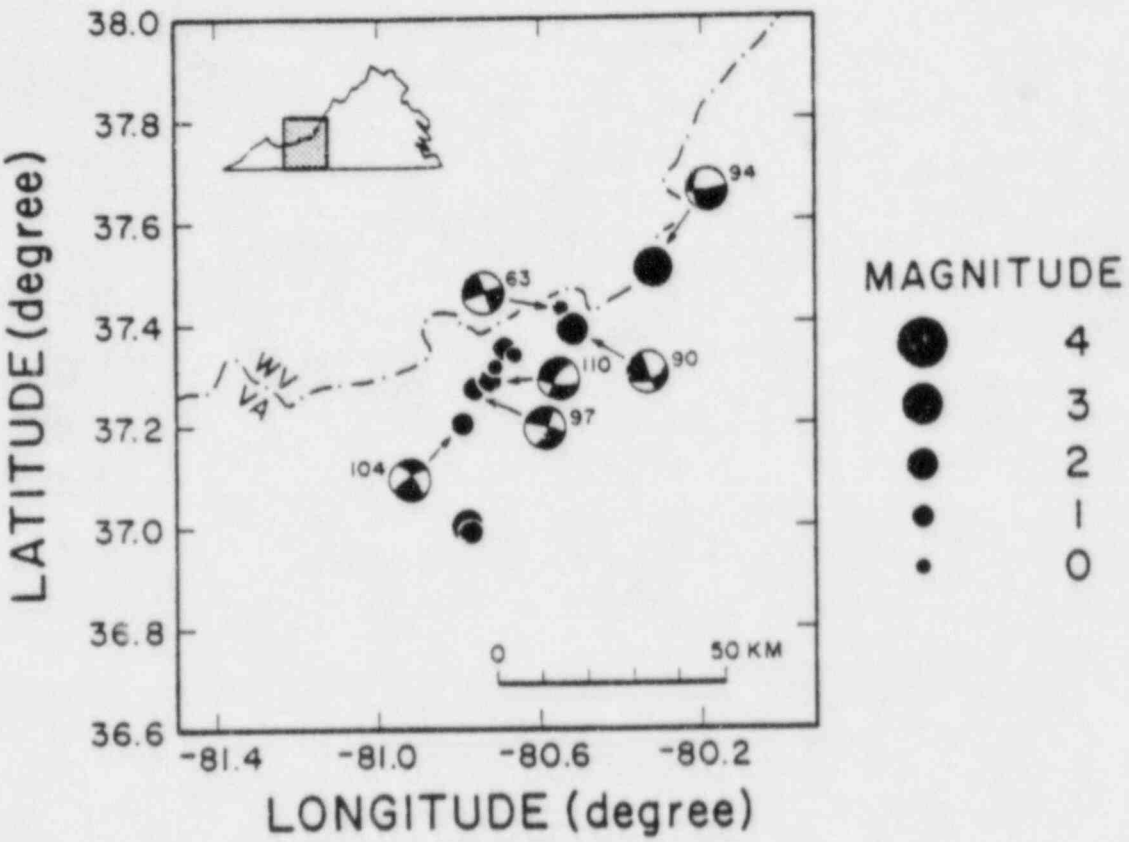

Figure 9: The six SEFM preferred nodal planes for Giles County obtained by the layered velocity model are presented. The shaded areas are compressional quadrants and the white areas are dilatational quadrants.

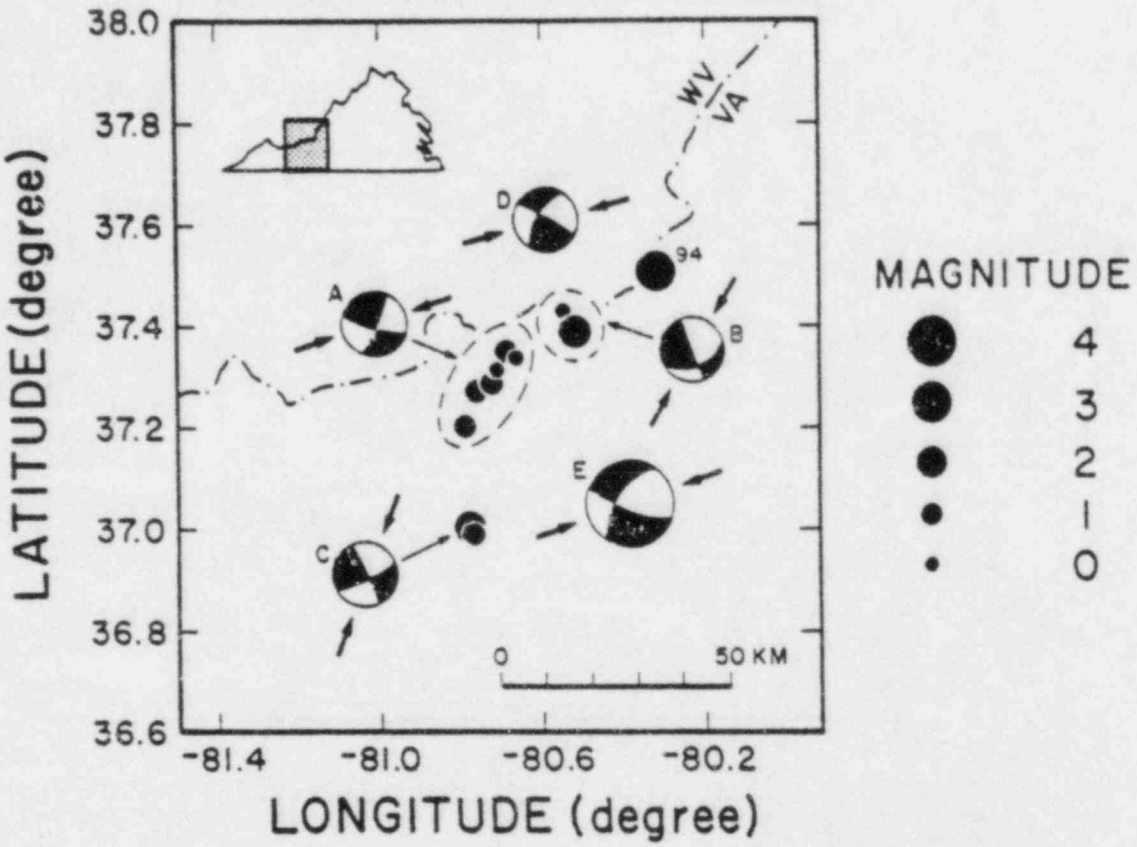

Figure 10: The preferred nodal planes from the five Giles County CFM using the layered velocity model are shown. Quadrant shading is the same as in Figure 9. The HEAVY arrows correspond to the trend of the P axes for each CFM. See Table 3 for the earthquakes that are included in each CFM.

Table 4

Giles County Preferred Solutions

EVT	STRIKE	DIP	SLIP	P(TREND,PLUNGE)	T(TREND,PLUNGE)	B(TREND,PLUNGE)
63	N20°W	85°E	-178°	S25°W,5°	N65°W,2°	N45°E,85°
	S70°W	88°N	-5°			
90	N20°W	90°E	145°	N31°E,24°	N71°W,24°	S20°E,55°
	N70°E	55°S	0°			
94	S	30°W	-171°	N21°E,42°	S33°E,34°	S80°W,30°
	N82°E	86°S	-60°			
97	N20°E	82°E	-174°	S65°W,10°	N25°W,1°	N70°E,80°
	N70°W	84°N	-8°			
104	S26°W	64°NW	164°	N73°E,7°	S13°E,29°	N30°W,60°
	N57°W	76°NE	27°			
110	S27°W	66°NW	-147°	N67°E,40°	N26°W,3°	S60°W,50°
	S78°E	60°S	-28°			
A	N20°E	86°E	165°	N66°E,7°	N26°W,13°	S5°W,75°
	S69°E	75°S	4°			
B	N20°W	90°E	135°	N35°E,30°	N75°W,30°	S20°E,45°
	N70°E	45°S	0°			
C	N25°W	86°NE	171°	N20°E,3°	N70°W,9°	S50°E,80°
	N65°E	81°SE	4°			
D	S29°W	60°NW	177°	N71°E,19°	S11°E,23°	N55°W,60°
	N59°W	88°NE	30°			
E	S30°W	60°NW	-161°	N67°E,34°	S17°E,9°	S85°W,55°
	S70°E	73°S	-31°			

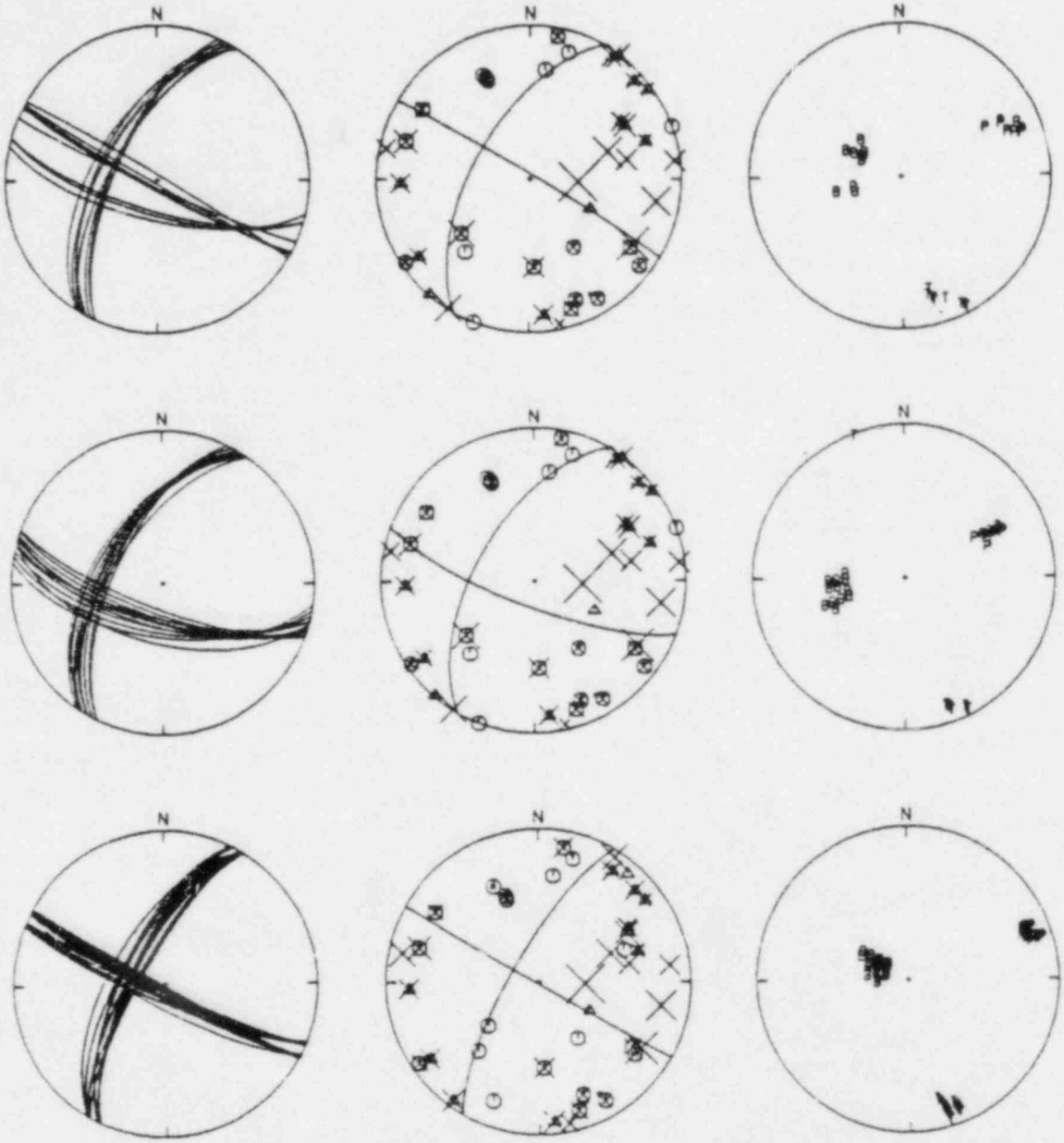

Figure 11: Upper row: Preferred solution set for CFM D using the layered velocity model is shown. Middle row: The alternative solution set for CFM using the layered velocity model is shown. Bottom row: The solutions set for CFM D using the gradient velocity model is shown. All symbols and intra-row order are the same as in Figure 6.

Interestingly, CFM C, which consists of two events about 35 km south of the zone, produced a preferred solution whose fault geometry strongly resembles that of the preferred solution for CFM B. Thus, seismicity at the ends of the zone may be occurring on nearly identical fault planes with the trend of fault planes in the center of the zone differing from those at the ends by 40°-45° (N20°E versus N25°W).

For the Giles County analysis, the percentage of acceptable amplitude ratios was usually higher for the gradient velocity model solutions than the layered velocity model (Table 5 and Appendix C). This is probably a consequence of the inclusion of amplitude ratio corrections, namely, geometrical spreading and transmission coefficient corrections, in the layered velocity model data. The Giles County layered velocity model includes variable Vp/Vs ratios that differ enough between layers to imply significant geometrical spreading and transmission coefficient corrections. The gradient model assumes a constant Vp/Vs ratio, hence, these two corrections are not necessary. In this case, a literal application of ratio corrections implied by the layered velocity model seems to be inappropriate.

One of the most interesting results of this study was the consistency in the orientation of the stress and null axes throughout the entire Giles County area (Figure 12). The preferred P axis from CFM E (all events, Figure 13) has a trend of N66°E and plunge of 33°. The T axis trend was S17°E with a plunge of 9°. The mean and standard deviation for the trend and plunge of the preferred P axes from SEFM's 63, 90, 94, 97, 104 and 110 and CFM's A and C are N46°E$\pm$24° and 13.5°$\pm$20°, respectively. Corresponding values for the trend and plunge of the T axis are S41°E$\pm$24° and 1°$\pm$20°. Note that the mean P and T axes agree within one standard deviation of the values for the preferred P and T axes of CFM E. Both of these measurements are in good agreement with the previously inferred principal stress directions for the region by Wheeler and Bollinger (1981). They proposed a maximum horizontal compressive stress trend of N65°E. Our results herein also support the continuation of the Midcontinent stress province of Zoback and Zoback (1980) into the basement rocks beneath Giles County.

Bollinger and Wheeler (1982) have proposed that seismicity in Giles County is occurring on reactivated normal faults that were formed originally during Iaeptan time as the proto-Atlantic began to open. These faults would lie within the basement beneath the Valley and Ridge, but at an angle to the lineated surface structural trend. The focal mechanisms shown here support that hypothesis. However, faults at cross-trends to the strike of the rifted margin are also an obvious possibility. In light of these focal mechanism results, the reactivation of Iaeptan rift-associated faults below Giles County as a plausible explanation for present day seismicity in this area is supported.

Table 5

Error Allowances for Giles County Events

EVT	MODEL	POL	POL ERR	RAT	RAT ERR	ERR ALL	QUAD	SOL
63	GCO1	3	0	3	0	0.25	3	20
90	GCO1	12	1	10	6	0.25	4	32
94	GCO1	5	0	9	1	0.25	2	40
97	GCO1	4	1	6	2	0.15	4	27
104	GCO1	5	1	5	1	0.15	4	38
110	GCO1	5	0	4	1	0.25	4	48
A	GCO1	17	2	22	13	0.25	4	19
	GCGR	17	3	21	10	0.25	4	14
B	GCO1	15	1	13	8	0.25	4	11
	GCGR	15	1	12	6	0.25	4	17
C	GCO1	6	0	6	2	0.25	4	44
	GCGR	6	0	6	2	0.25	4	40
D	GCO1	32	4	35	26	0.25	4	14
	GCO1(2)	32	3	35	28	0.25	4	12
	GCO1R	32	4	33	23	0.25	4	27
E	GCO1	43	6	50	38	0.25	4	10
	GCGR	43	6	47	37	0.25	4	15

POL - number of polarities
POL ERR - number of specified polarity errors
RAT - number of SV/P ratios
RAT ERR - number of SV/P ratio errors
ERR ALL - $\log_{10}$ SV/P ratio error allowance
QUAD - number of focal sphere quadrants that contain data for the preferred solution
SOL - number of acceptable solutions found by FOCMEC
GCO1 - Giles County layered velocity model primary family of solutions
GCO1(2)-Giles County layered velocity model secondary family of solutions
GCGR - Giles County gradient velocity model family of solutions

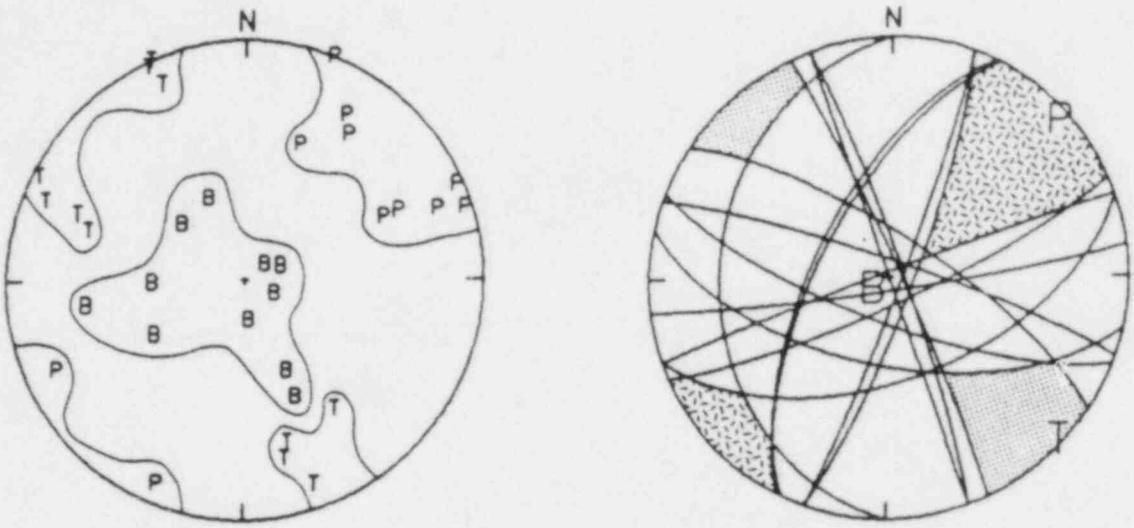

Figure 12: The focal hemisphere on the left shows and outlines the set of eight preferred P, T and B axes from the Giles County focal mechanisms (see text). The other focal sphere shows the nodal planes corresponding to these eight sets of axes and shows the positions of the mean P, T and B axes from that set. The nodal planes are used to restrict the area in which the P (dilatational quadrants) and T (compressional quadrants) axes may lie. These restricted areas (two differnt stipple patterns) are drawn under the assumption that the maximum compressive stress must lie within the dilatational quadrant (McKenzie, 1969) and that all of the earthquakes were reacting to the same regional stress field.

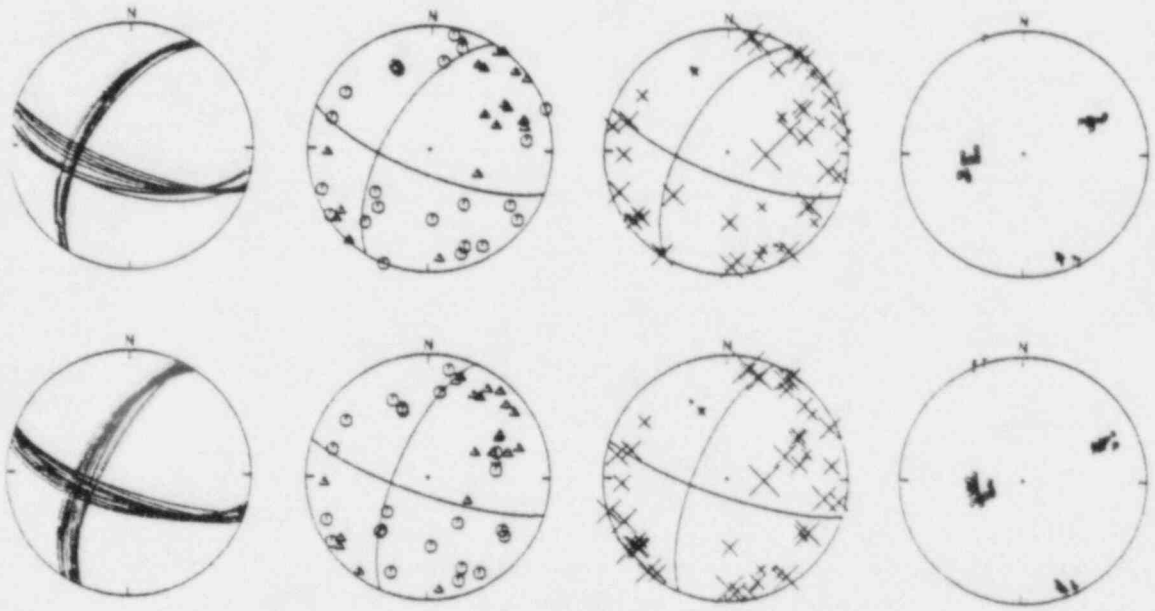

Figure 13: Top row: The solution set for CFM E using the layered velocity model is shown. The middle two figures in each row have the preferred solution superimposed on the polarity and SV/P data, separately, for clarity. Bottom row: The solution set for CFM E using the gradient velocity model is shown. The symbols are the same as in Figure 6.

THE CENTRAL VIRGINIA SEISMIC ZONE

Geology and Seismicity

The Central Virginia seismic zone extends some 150 km from the Fall Line on the east to the western edge of the Piedmont near Lynchburg (Figure 14). From north to south, the zone is about 120 km wide. Geologic units ranging from Grenville to Cretaceous age are present at the surface (Geologic Map of Virginia, 1963). However, the majority of the area is covered by rocks at least as old as Cambrian. The dominant lithologies are metamorphics, meta-volcanics and granitic intrusives. Sedimentary rocks are present in the Triassic basins and Coastal Plain sediments abut the eastern edge of the zone. In addition to the Triassic basins, Triassic-Jurassic age dikes are scattered over the area and strike generally north to northwest. Collisional tectonics during the Paleozoic resulted in extensive, northwest-directed overthrusting in the area. The Triassic basins and Mesozoic dikes are indicative of later extensional tectonics related to continental rifting (Glover and others, 1985).

Low ridges and hills characterize the western part of the area and the topography becomes less pronounced eastward. The James River bisects the seismic zone in an east-west direction.

Seismicity within the zone is diffuse. No obvious lineations are apparent although there are some indications of clustered activity (Figure 14). Most of the events are located no deeper than 10 km and all of the well-located events have depths of 15 km or less (Figure 15; Table 6). There is some tendency for earthquake sequences to occur in Central Virginia (Bollinger and Sibol, 1985). Recently, for example, in February, 1981 three earthquakes, all of magnitude about 3, occurred near Scottsville, Virginia within eight minutes (Sibol and Bollinger, 1981). Focal mechanisms for these and other events are presented below.

Previous Focal Mechanism and Crustal Stress Studies

Originally, Zoback and Zoback (1980) suggested that the entire United States Atlantic Coastal Plain and much of the Piedmont is undergoing northwest directed, maximum compressive stress. Several other authors (Yang and Aggarwal, 1981; Wentworth and Mergner-Keefer, 1981; Aggarwal and Sykes, 1978), some of whose work Zoback and Zoback (1980) cited, have proposed reverse faulting on north and northeast planes to be the dominant mode of faulting in the Piedmont and Atlantic Coastal Plain provinces of Eastern North America. This mode and orientation of faulting would imply a horizontal, east to southeast trending, maximum compressive stress. However, a study by Pulli and Toksoz (1981) showed focal mechanisms for the entire northeast U.S. with east to northeast trending P axes. In addition, recent hydrofracturing tests and reevaluations of some earlier focal mechanism results from the northeast U.S. (M.L. Zoback, personal communication, 1984) indicate that the whole northeastern United States may indeed be subject to northeast trending, horizontal maximum compressive stress. Thus, the stress field of the northeastern U.S. may be quite similar to Zoback and Zoback's (1980) midcontinent stress

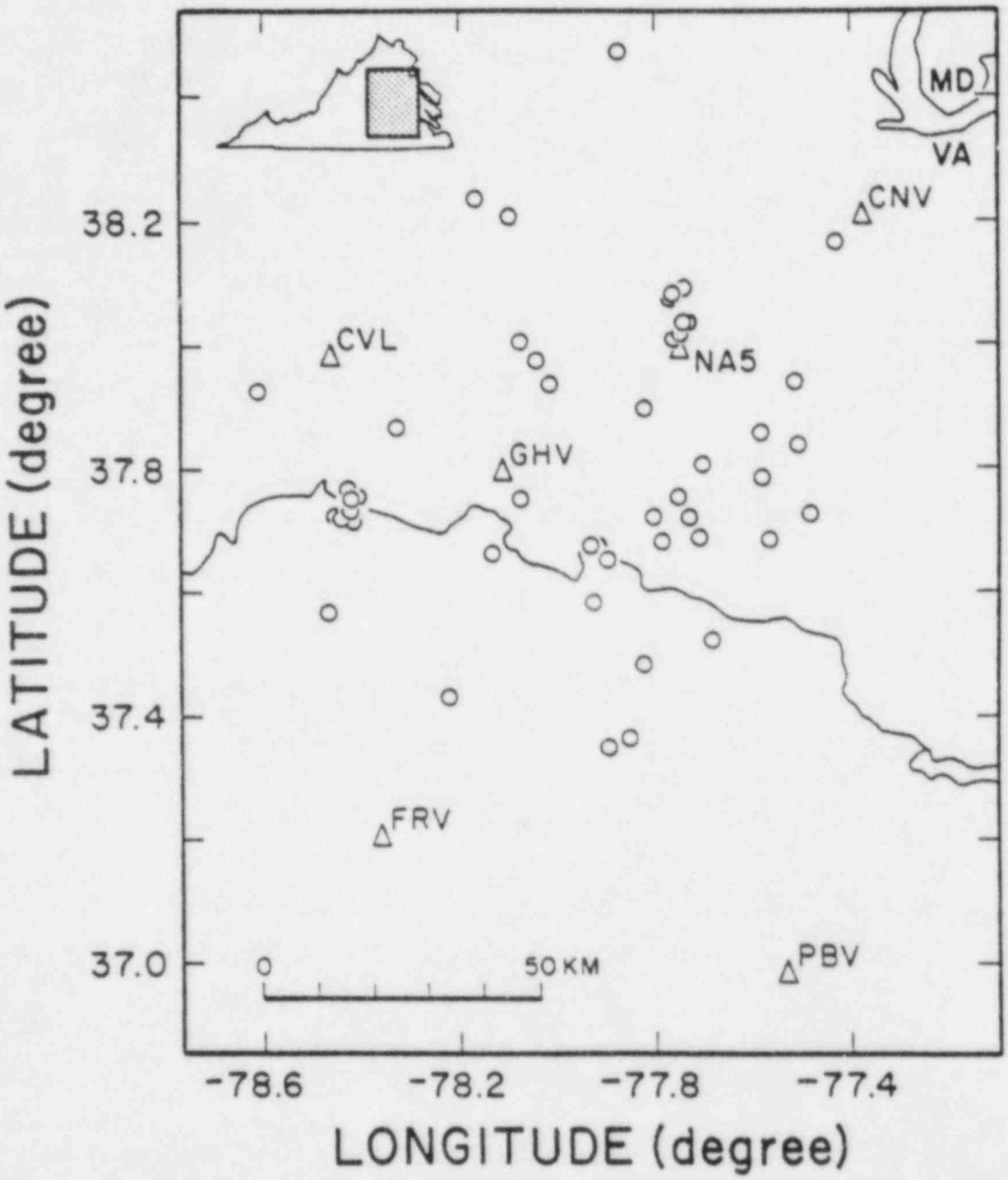

Figure 14: Central Virginia epicenters (open circles) are shown that were located by network monitoring or relocated by Dewey and Gordon (1982). These earthquakes, all of which are not study events, have horizontal errors of 10 km or less and vertical errors of 30 km or less. Station symbols are as in Figure 4.

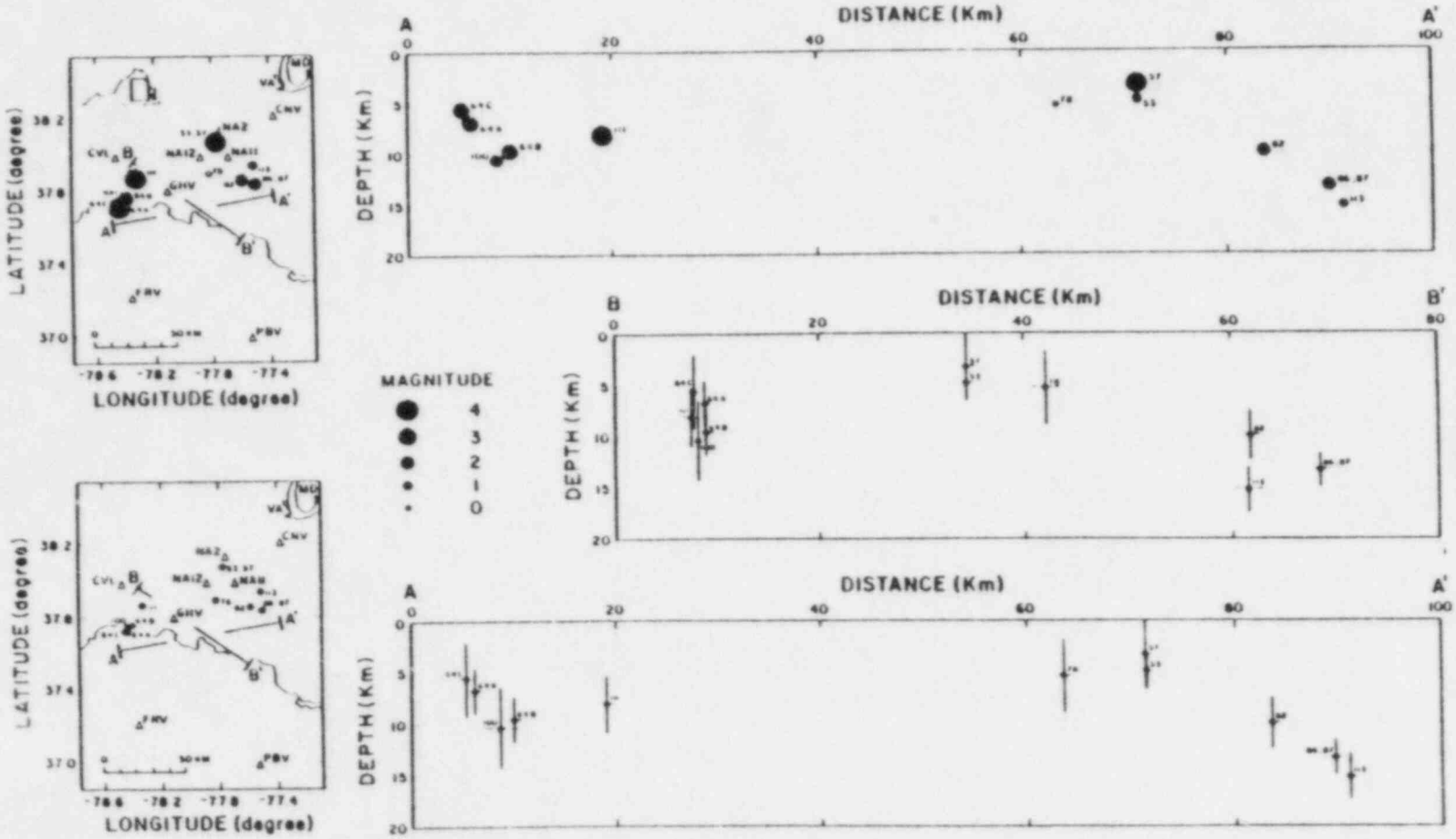

Figure 15: Upper left (15a): The locations of the Central Virginia study events are shown by dark circles scaled to magnitude. Triangles denote seismic stations. Upper right (15b): Events from cross sections A-A' of Figure 15a are shown. Cross section A-A' strikes perpendicular to a N10°W trend. Many of the Central Virginia nodal planes have a NNW trend. Lower left (15c): This figure is the same as 15a except that the event locations are not scaled to magnitude. Middle right (15d): Events in cross section B-B' from Figure 15c are shown with their vertical and horizontal error axes. Lower right (15e): The horizontal and vertical error axes of events from cross section A-A' of Figure 15c are shown.

Table 6

Central Virginia Hypocenters**

EVT	DATE (M/D/Y)	TIME (UCT)	LAT (DEG N)	LONG (DEG W)	DEPTH (KM)	MAG	GAP (KM)	DMIN (KM)	RMS (SEC)	ERH (KM)	ERZ (KM)
53	8/4/80	10:13	38.0718	77.7673	4.9	0.9	115	6.4	0.17	0.8	1.8
57	9/26/80	01:31	38.071	77.7678	3.3	1.0	102	6.5	0.16	1.0	3.4
64A	2/11/81	13:44	37.7168	78.4388	6.8	3.4*	123	29.4	0.16	1.1	2.3
64B	2/11/81	13:50	37.7543	78.4033	9.6	3.2*	156	25.7	0.20	2.4	2.3
64C	2/11/81	13:51	37.7208	78.4492	5.6	2.9*	129	28.9	0.14	0.9	3.7
78	1/18/82	06:11	37.8932	77.8193	5.4	0.3	183	11.3	0.11	1.6	3.7
82	5/6/82	07:18	37.8553	77.5792	10.0	2.1	153	17.2	0.19	1.0	2.5
86	6/25/82	23:03	37.835	77.5033	13.4	1.9	166	23.1	0.14	1.1	1.8
87	9/20/82	12.15	37.8352	77.5032	13.4	1.6	166	23.1	0.16	1.0	1.4
100	8/10/83	12.29	37.7505	78.4177	10.4	1.9	157	25.9	0.19	2.7	4.0
111	8/17/84	18:05	37.8662	78.3242	8.1	4.0	103	17.5	0.22	1.7	2.9
113	10/17/84	08:57	37.9372	77.5100	15.3	1.1	201	16.2	0.17	2.7	2.3

** - CVNA velocity model
EVT - event number
MAG - duration magnitude except * is m_b(LG)
GAP - greatest azimuthal separation of stations relative to epicenter
DMIN - distance of closest station from epicenter
ERH,ERZ - horizontal and vertical error estimates, respectively, at 94% confidence level

regime, but the detailed stress orientations within the Piedmont and Coastal Plain provinces of the southeastern U.S., of which Central Virginia is a part, are still unclear.

Dames and Moore (1976) obtained focal mechanisms from the vicinity of the North Anna Nuclear Power Plant in Mineral, Virginia, near the northern boundary of the Central Virginia seismic zone. These mechanisms did in fact show reverse faulting on north to northeast trending planes. However, due to those earthquakes' very shallow depths and locations near the North Anna reservoir, they may be a reservoir-induced "skin effect."

Two possible CFM's for events 64A and 64B near Scottsville, Virginia, some 60 km to the southwest of the North Anna site, were obtained using 29 P-wave polarities (Sibol and Bollinger, 1981). One of their CFM's shows mainly reverse faulting on north and northwest trending planes and is very similar to the focal mechanism developed for those events in this study through the use of both polarity and SV/P ratio data.

Focal Mechanism Results and Interpretations

At first glance the results from Central Virginia are both puzzling and surprising (Figure 16; Table 8). The diffuse character of seismicity in the zone itself is mimiced in the scatter present in the focal mechanisms. Preferred mechanisms for the eleven SEFM and four CFM event range in type from almost pure dip slip to pure strike-slip. Additionally, the principal stress axes have different orientations throughout the zone (Figure 17). For example, the trend of the P axes (heavy arrows in Figure 16) depict both NE and NW directed maximum compressive stress for the four CFM's. The mechanism data and families of solutions for these four CFM's, F,G,H,I (Table 7), are shown in Figures 18-21. Spatial proximity of hypocenters and input data compatibility were the primary compositing criteria for the Central Virginia events. Spatial lineations of epicenters appear to be much less meaningful for compositing purposes in Central Virginia than they are in Giles County and were, therefore, not used.

Yet another complication is that two earthquakes (86 and 87, Figure 16) with identical hypocenters and separated in time by only three months may have markedly different focal mechanisms. The difference in focal mechanisms for these two events could be real or it may be exaggerated by rather poor data coverage on the focal sphere.

Finally, none of these focal mechanisms have nodal planes with northeast strikes and subhorizontal dips which Glover and others (1985) have proposed on the basis of reflection seismic data as probable faults for the current Central Virginia seismicity. Possible explanations are offered below for these puzzles.

Some important relationships between nodal planes, stress axes and focal depth are shown in the four graphs in Figure 22. Figure 22a suggests that there is no relationship between event magnitude and P axis trend. To illustrate this lack of any relationship between stress axes orientation and magnitude consider, CFM F (events 64A, B and C) and SEFM 111. Event 64A had a m_b(Lg) of 3.4 and event 111's magnitude was 4.0. However, as Figures 18 and 23 show, the mechanisms

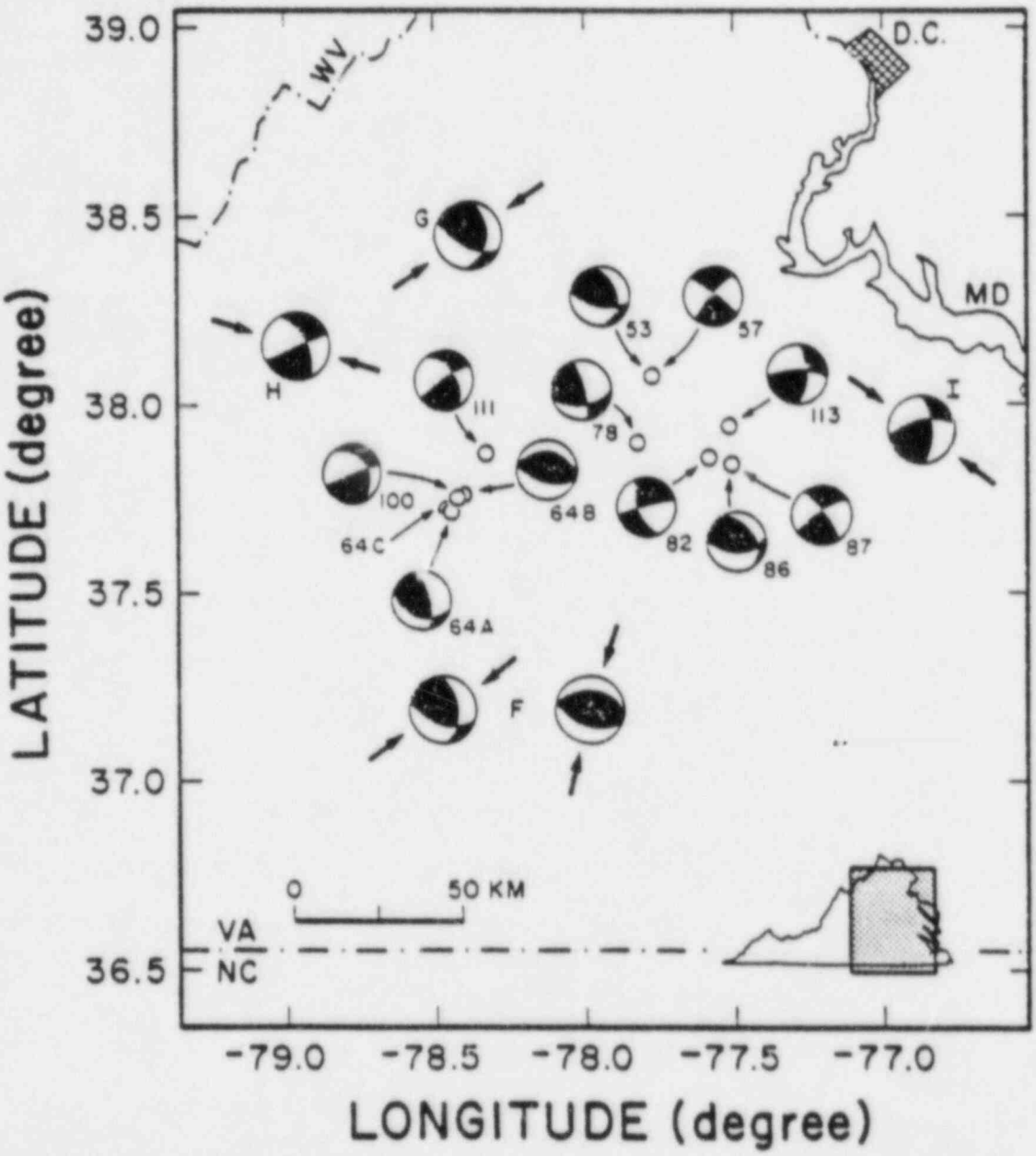

Figure 16: The preferred nodal planes for all central Virginia SEFM and CFM solutions are shown. Smaller mechanisms are SEFM events and CFM have HEAVY arrows showing their P axis trend. Shaded areas are compressional, and white areas are dilatational quadrants. Open circles are event locations. Note that two preferred solutions are shown for CFM F.

Table 7

Central Virginia Composites

COMPOSITE	EVENTS	AVE DEPTH (KM)	MAX MAG
F	64A,64B,64C	7.3	3.4*
G	53,78	5.2	0.9
H	100,111	9.3	4.0
I	82,87,113	12.9	2.1

* - indicates m_b(LG) instead of duration magnitude

Table 8

Central Virginia Preferred Solutions

EVT	DIP	STRIKE	SLIP	P(TREND,PLUNG)	T(TREND,PLUNGE)	B(TREND,PLUNGE)
53	41°W	N19°W	139°	S34°W,13°	N32°W,57°	S60°E,30°
	64°S	S76°E	56°			
57	82°NW	S40°W	174°	N85°E,1°	S5°E,10°	N10°W,80°
	84°NE	N50°W	8°			
64A	67°E	N14°W	117°	N56°E,18°	N66°W,58°	S25°E,25°
	35°SW	S67°E	42°			
64B	35°N	N82°W	81°	S14°W,10°	N41°E,79°	N75°W,5°
	55°S	S72°E	96°			
78	79°E	N14°W	136°	N43°E,21°	N64°W,38°	S25°E,45°
	47°S	N86°E	15°			
82	61°W	S22°E	-8°	S61°E,26°	N22°E,14°	S85°W,60°
	83°N	S72°W	-151°			
86	42°NE	N44°W	129°	S19°W,9°	N52°W,63°	S75°E,25°
	59°S	N89°E	60°			
87	79°NE	N33°W	17°	S81°E,3°	S11°W,20°	N0°,70°
	74°SE	S53°W	168°			
100	45°NE	N27°W	-5°	N60°W,33°	S11°W,27°	N70°E,45°
	86°SE	N66°E	-135°			
111	59°NE	N25°W	16°	N72°W,11°	S11°W,33°	N35°E,55°
	76°NW	S56°W	148°			
113	63°E	N3°E	14°	N42°W,10°	S42°W,28°	N65°E,60°
	78°N	S87°W	152°			
F(1)	35°N	N82°W	81°	S14°W,10°	N41°E,79°	N75°W,5°
	55°S	S72°E	96°			
F(2)	58°E	N9°W	132°	N52°E,4°	N44°W,55°	S35°E,35°
	51°S	S69°E	43°			
G	48°E	N1°W	141°	S56°W,8°	N23°W,54°	S40°E,35°
	52°S	S72°E	49°			
H	65°NE	N24°W	2°	N67°W,16°	S17°W,19°	N60°E,65°
	88°N	S85°W	155°			
I	66°E	N4°W	26°	N55°W,0°	S35°W,35°	N35°E,55°
	66°N	S74°W	154°			

Table 9

Error Allowances for Central Virginia

EVT	MODEL	POL	POL ERR	RAT	RAT ERR	ERR ALL	QUAD	SOL
53	CVNA	5	1	7	2	0.2	3	19
57	CVNA	5	0	2	0	0.14	4	89
64A	CVNA	9	0	3	0	0.25	2	17
64B	CVNA	7	1	5	2	0.25	2	23
78	CVNA	3	0	4	0	0.17	3	27
82	CVNA	5	0	6	1	0.25	2	76
86	CVNA	7	0	6	2	0.25	3	13
87	CVNA	4	0	8	2	0.25	3	14
100	CVNA	3	0	3	1	0.17	2	45
111	CVNA	24	2	0	-	-	4	7
	CVGR	24	2	0	-	-	4	7
113	CVNA	6	0	5	1	0.20	4	34
F	CVNA	17	1	10	5	0.25	2	7
	CVGR	17	1	10	5	0.25	3	10
G	CVNA	8	1	11	4	0.25	4	6
	CVGR	8	1	11	4	0.25	4	3
H	CVNA	27	4	3	1	0.25	4	30
	CVNA(2)	27	3	3	2	0.25	3	6
	CVGR	27	4	3	1	0.25	4	5
I	CVNA	15	1	19	9	0.25	4	36
	CVGR	15	1	19	9	0.25	4	28

POL - number of polarities
POL ERR - number of specified polarity errors
RAT - number of SV/P ratios
RAT ERR - number of SV/P ratio errors
ERR ALL - $\log_{10}$ SV/P ratio error allowance
QUAD - number of focal sphere quadrants that contain data for the preferred solution
SOL - number of acceptable solutions found by FOCMEC
CVNA - Central Virginia layered velocity model primary family of solutions
CVNA(2) - Central Virginia layered velocity model secondary family of solutions
CVGR - Central Virginia gradient velocity model family of solutions

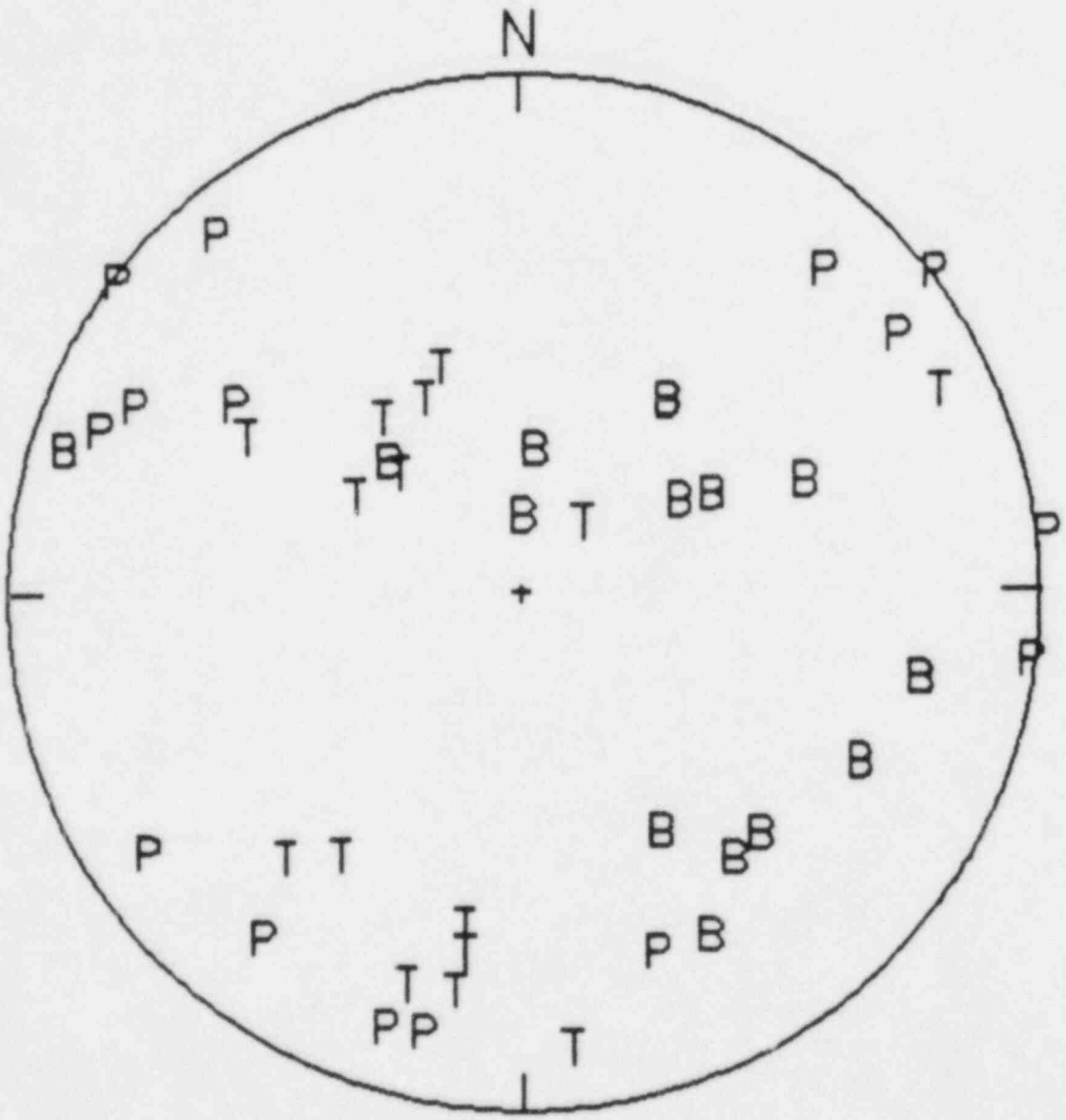

Figure 17: The preferred P, T and B axes for all Central Virginia SEFM and CFM solutions are shown. Note the scatter in the axes' locations.

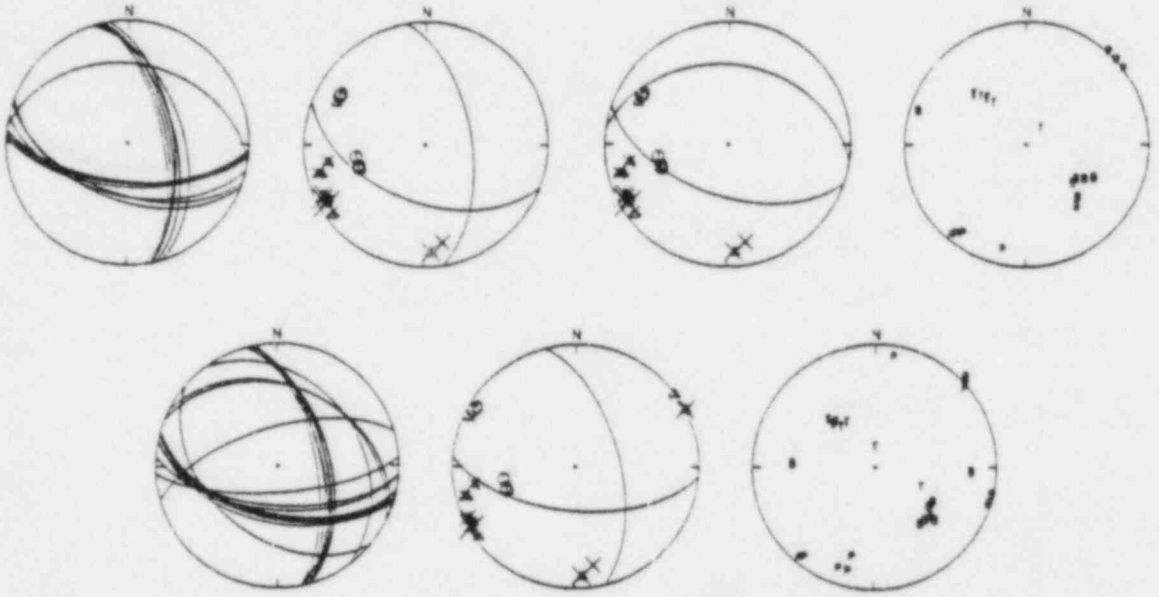

Figure 18: Upper row: The solution set for CFM F using the Central Virginia layered velocity model is shown. Note that two preferred solutions are shown. Bottom row: The solution set for CFM F using the Central Virginia gradient velocity model is shown. The symbols and order are the same as in Figure 6.

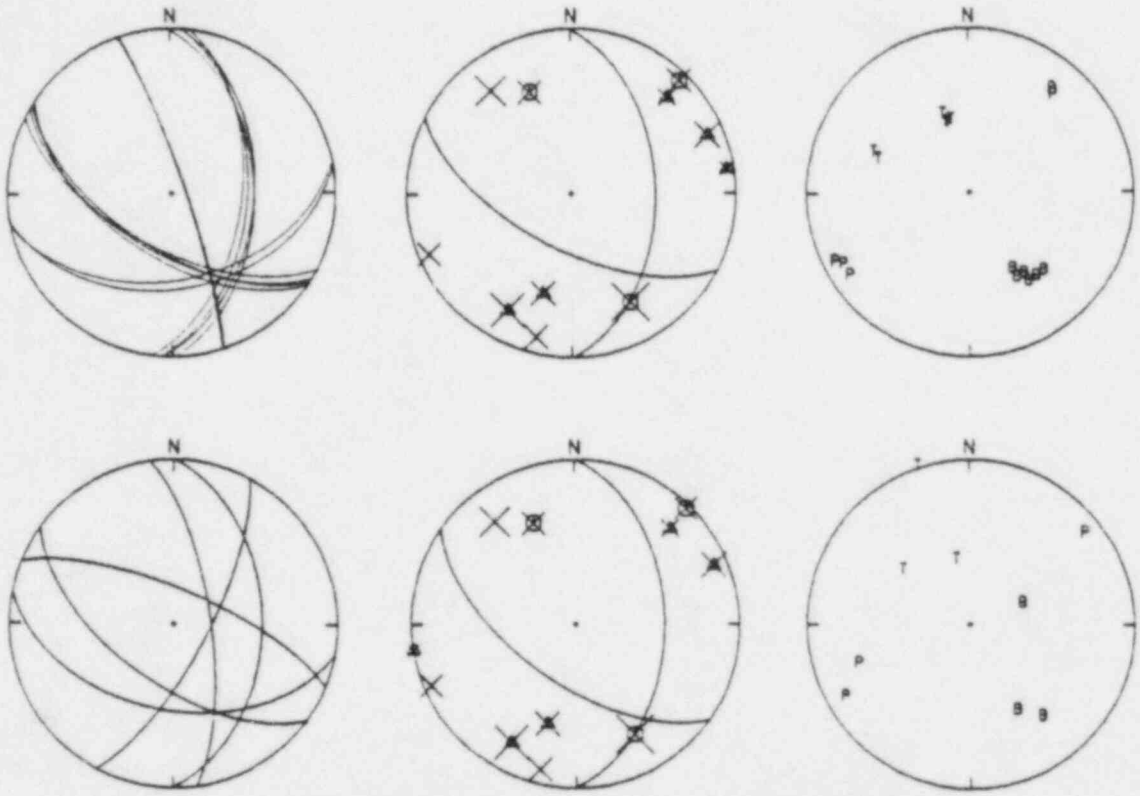

Figure 19: Upper row: The solution set for CFM G using the Central Virginia layered velocity model is shown. Bottom row: The solution set for CFM G using the gradient velocity is shown. The symbols and order are the same as in Figure 6.

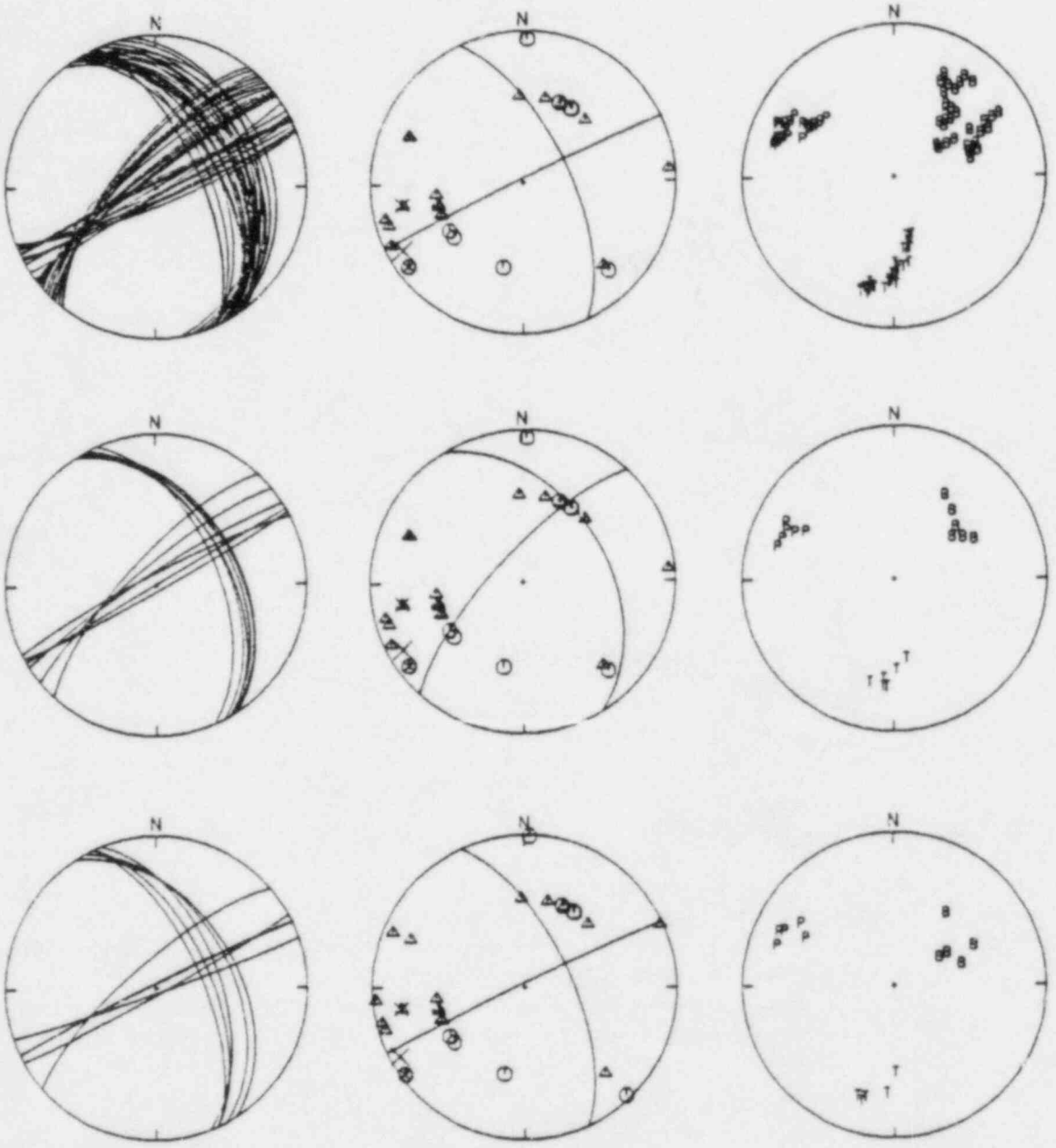

Figure 20: Upper row: The solution set for CFM H using the Central Virginia layered velocity model is shown. Middle row: An alternative solution set for CFM H is shown as obtained by the Central Virginia layered velocity model. Bottom row: The solution set for CFM H using the Central Virginia gradient velocity model is shown. The symbols and order are the same as in Figure 6.

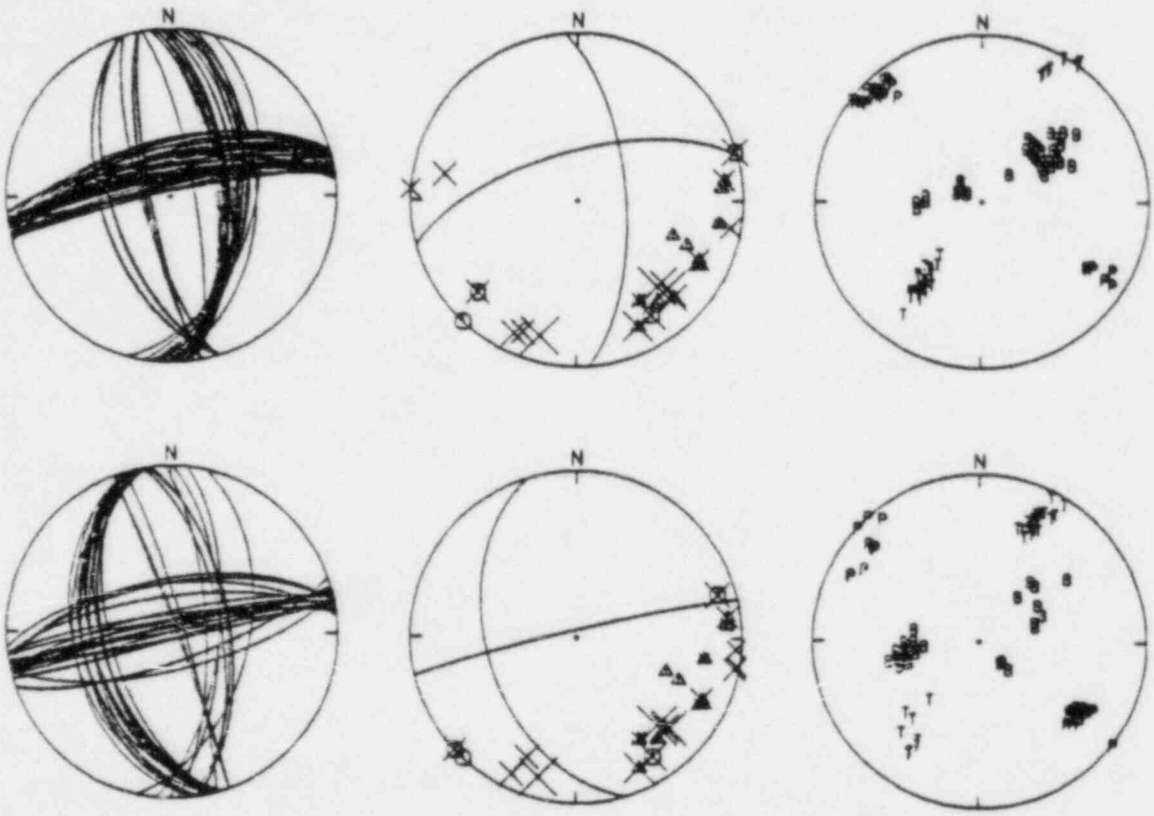

Figure 21: Upper row: The solution set for CFM I using the Central Virginia layered velocity model is shown. Bottom row: The solution set for CFM I using the Central Virginia gradient velocity model is shown. The symbols and order are the same as in Figure 6.

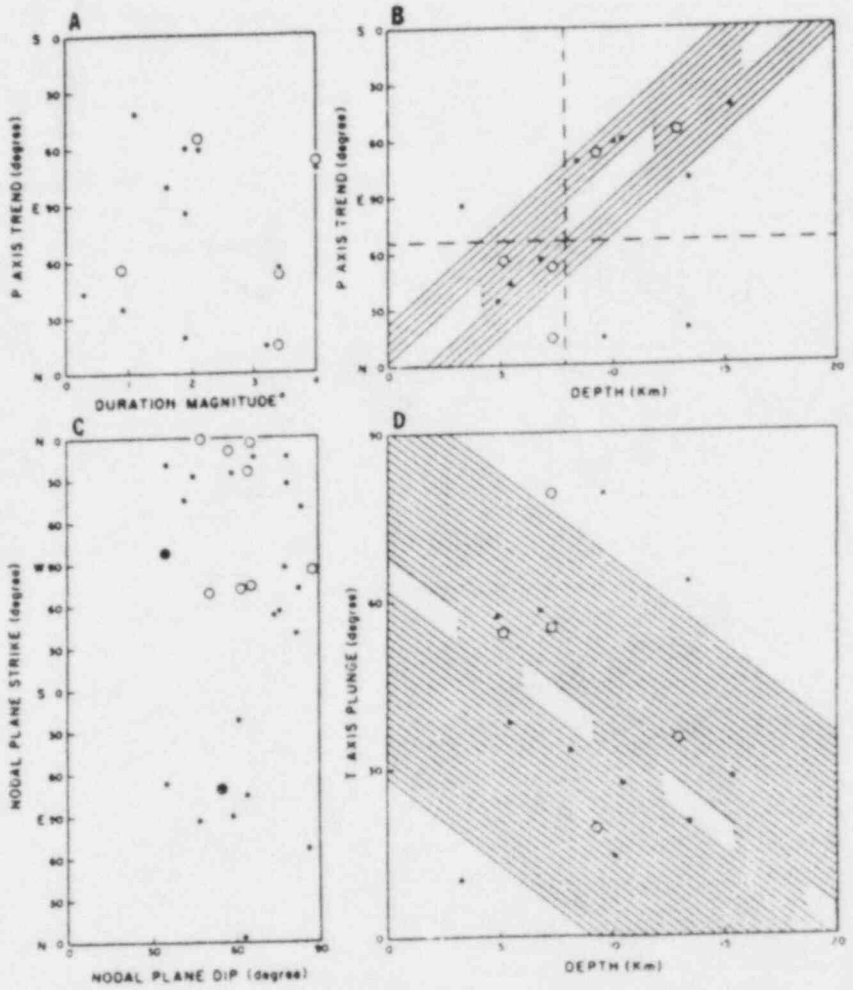

Figure 22: Upper left (22a): The graph plots duration magnitude (m_b(LG) for 64A and 64B) versus the preferred P axes trends for single SEFM (solid dots) and CFM (open circles) solutions. Upper right (22b): The graph plots focal depth versus the preferred P axes' trends from Figure 22a. The banded area is ±35° of a fit by eye line. The 70° band corresponds to the area within which σ_1 should lie relative to the focal mechanism P axis. Lower left (22c): The orientations of all 16 pairs of preferred nodal planes in Central Virginia are shown. Note the absence of nodal planes with dips less than 30° and the sparsity (two) of planes with northeast strikes. Lower right (22d): This plot shows focal depth versus preferred T axes' plunges for all Central Virginia SEFM and CFM. The 70° band should include σ_3. The decreasing T axis plunge with depth implies a change in slip from reverse to strike slip with depth in the presence of a horizontal P axis.

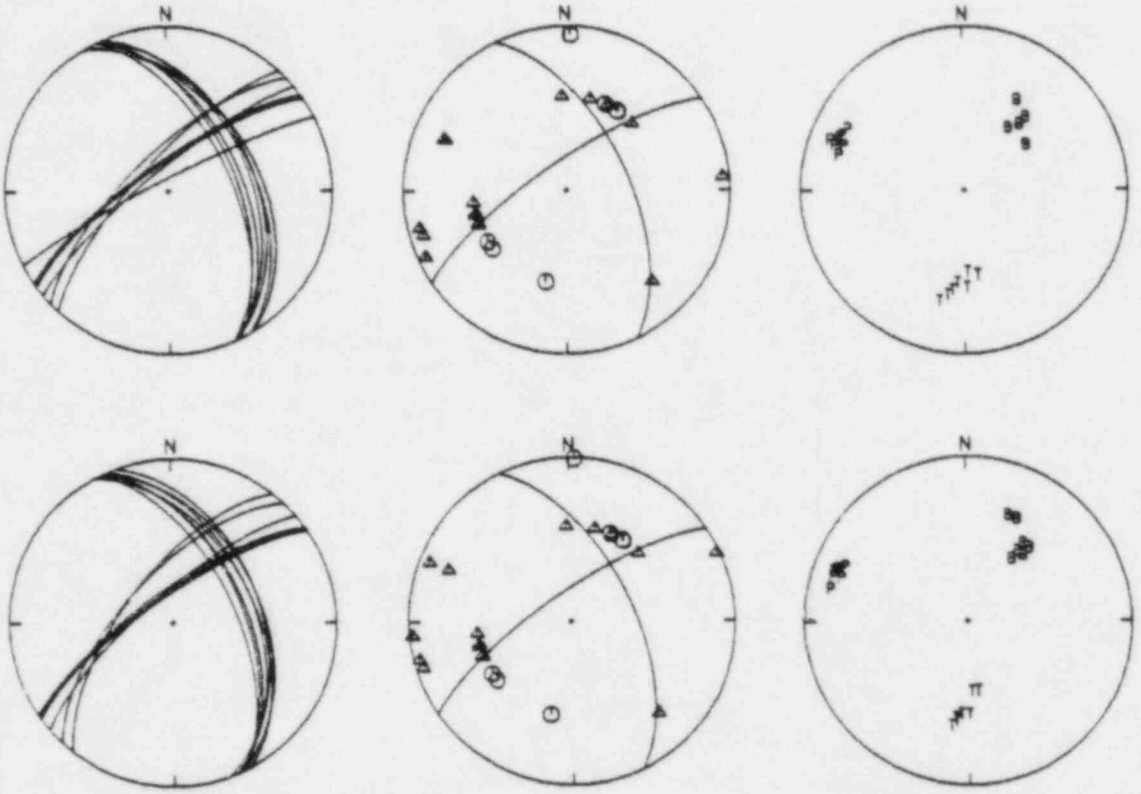

Figure 23: Upper row: The SEFM 111 obtained by the Central Virginia layered velocity model is shown. No ratio data was available for this event, but 22 of 24 polarities were satisfied by this solution. Bottom row: The SEFM 111 obtained by the Central Virginia gradient velocity model is shown. The symbols and order are the same as in Figure 6.

for CFM F and SEFM 111 are different: CFM F exhibits mainly reverse faulting on west or north striking nodal planes while SEFM 111 shows predominantly strike-slip motion on northwest and southwest striking nodal planes.

Figure 22b can be interpreted as showing a linear relationship between P axis trend and depth. A 70° band is included around a line fit by eye. McKenzie (1969) has shown that theoretically the in-situ maximum compressive stress (sigma-one) could lie anywhere within the focal mechanism's dilatational quadrant. The 70° band is included because Rayleigh and others (1972) showed that, for the Rangely, Colorado, study area, on pre-existing faults the orientation of sigma-one generally differed from the focal mechanism's P axis by no more than $\pm 35°$.

Another possible interpretation of Figure 22b would be that a change in P axis trend from northeasterly to southeasterly results as earthquakes occur above and below 8 km. Of the 7 solutions whose depths or average depths are less than 8 km, only one has a P axis trend outside of N14°-60°E. The change, if real, could mean that the decollement is acting to decouple the stress fields. That is, different stress fields may be operative above and below about 9 or 10 km because the decollement serves as a mechanical discontinuity.

Glover and others (1985) suggested that the basal detachment and ramp faults identified by reflection seismic and geological studies in Central Virginia are acting as seismogenic structures for the contemporary seismicity there. Those faults strike northeast and dip at 45° or less. While it is true that most or all of the seismicity is occurring in the allochthonous, thrust faulted block, the focal mechanisms presented here do not agree with the Glover and others proposed seismogenic structures. Additionally, only two of 32 total nodal planes have strikes between due north and N70°E and neither of these planes dip at less than 45°. Therefore, reactivation of northeast trending, shallow to moderately dipping fault planes in the Central Virginia Piedmont is strongly discouraged by these focal mechanisms. Seismogenic structures other than the northeasterly trending ramp faults and the subhorizontal basal detachment postulated by Glover and others (1985) appear to be present in Central Virginia.

A final observation about faulting in Central Virginia is the general trend of predominantly dip slip giving way to mainly strike-slip motion as the events become deeper. The P axis for virtually all of the solutions is horizontal to sub-horizontal. Consequently, the plunge of the T axis will determine whether the mechanism is more reverse slip (steeply plunging T axis) or more strike slip (shallowly plunging T axis). Figure 22d plots the T axis plunge against depth and shows a general tendency for the plunge of the T axis to become more horizontal with depth. Again, a 70° band is included to account for possible variations in the in situ minimum compressive stress (sigma-three) from the double couple T axis. A shift of the T axis such as this could be accomplished by interchanging the orientations of the intermediate and least compressive stresses in response to increasing lithostatic pressure. Such shifts have been reported in the literature. For example, Talwani (1982) finds reverse faulting for shallow events and strike-slip for deeper events in the Charleston, S.C. area, which is consistent with the results of this study.

Because Glover and others (1985) proposal for seismogenic structures in Central Virginia is in conflict with the Central Virginia focal mechanism results, an alternative hypothesis is now suggested that may explain at least some of the seismicity there. Fox (1970) noted the association of Triassic dikes with seismicity in the Piedmont of the Eastern U.S. More recently, McKeown (1978) has suggested that much of Eastern U.S. seismicity is related to mafic intrusives. Additionally, Campbell (1978) concluded that serpentized mafic intrusives may act to concentrate stresses more than 200% above their average regional values.

These preferred focal mechanisms from Central Virginia are generally consistent with an association of Mesozoic dikes and seismicity because 10 of the 32 possible nodal planes strike between N50°W and N5°E and have dips within 35° of vertical. The mapped dikes (Geologic Map of Virginia, 1963) in Central Virginia trend northwest and north and supposedly dip vertically to near vertically. In addition to dikes mapped in the field, many other mafic dikes are indicated throughout the Virginia Piedmont by aeromagnetic anomalies (Aeromagnetic Map of Virginia, 1977). This correlation is suggestive, but not conclusive, evidence for the dikes or associated fracturing acting as seismogenic structures. The widespread distribution of these dikes could also explain the diffuse character of the Central Virginia seismic zone.

The Virginia Mesozoic dikes are observed to extend across the Blue Ridge into the Valley and Ridge west of Charlottesville, Virginia. Dennison and Johnson (1971) noted that this westward excursion of Mesozoic or younger dikes is one of only three places where they cross the Blue Ridge Anticlinorium and penetrate the western Appalachians. The existence of the Central Virginia seismic zone is itself enigmatic. Perhaps the westward excursion of these dikes northwest of and roughly parallel to the trend of the zone is related in some manner to the reason for the existence of the seismicity there.

SUMMARY AND CONCLUSIONS

New focal mechanism analytical techniques have been applied to data sets from the Giles County and Central Virginia seismic zones. In Giles County, the seismicity lies within the autochthonous basement rocks and below the decollement. In Central Virginia, only some 200 km to the east, earthquakes are occurring near the basal detachment or above it in the allochthonous block. The methods of focal mechanism evaluation were the same exactly in both areas but the results are markedly dissimilar in these two geologically different locales.

In Giles County, a consistent stress regime is present throughout the area. The P axis trend as determined from eight different sets of solutions has a mean and standard deviation of N46°E$\pm$24° and the plunge is 14°$\pm$20°. The mean and standard deviation for the T axis trend and plunge are S41°E$\pm$24° and 1°$\pm$20°, respectively. The Giles County seismic zone as defined by Bollinger and Wheeler (1983) is corroborated by these focal mechanism results. However, portions of the zone are probably more complex than originally defined.

One of the two nodal planes and the trend of epicenters for shocks from the southwestern and central portions of the zone indicate a north-northeast striking fault. Motion on this near vertical plane is almost pure right-lateral strike-slip. Faulting at the northeast end of the zone may be occurring on a vertical plane that strikes N20°W. This geometry would be consistent with that found for a two event CFM from south of the zone. Alternatively, faulting at the northeast end of the zone may occur on faults sub-parallel to the fault(s) in the southwestern part of the zone. Faulting throughout the zone and for nearby events is primarily strike-slip with some reverse motion.

Despite the spatial proximity of the two seismic zones in Virginia the focal mechanism results are quite different. The uniformity of stress axes found in Giles County does not hold for the seismicity in Central Virginia. In Central Virginia, the trend of the generally sub-horizontal P axis appears to rotate from northeast to southeast as the events become deeper. An obvious alternative interpretation is that there is an offset in the P axis trend from northeast for events occurring above 8 km to southeast for those below this level. The scarcity of data from larger earthquakes ($M \geq 4$) may mean that neither of these generalizations is valid, and even if one of them is, the answer will require additional focal mechanisms.

There is a tendency for strike-slip to dominate over dip slip as a mode of faulting for the deeper events in Central Virginia. This result is consistent with the increase in lithostatic pressure with depth which can interchange the roles of the three principal stresses.

A more complete and detailed geologic interpretation of seismicity in Central Virginia is an objective for our future research. The lack of northeast striking, gently dipping nodal planes implies that structures identified from reflection seismic and geological studies in Central Virginia (Glover and others, 1985) are probably not directly responsible for the recent seismicity. The widespread distribution of Mesozoic dikes, their near vertical orientations and their spatial correlation with focal mechanism nodal planes suggest that these features may be associated with present day seismicity in Central Virginia.

Several important experience factors have been gained in focal mechanism analysis through the use of a powerful new analytical tool, FOCMEC. Insights related to the use of both P-wave polarity and SV/P amplitude ratio data are:

(1) The inclusion of amplitude ratio data has allowed the definition of well-constrained focal mechanism solutions where P-wave polarities alone would not,

(2) At least two combinations of P-wave polarity and amplitude ratio error allowances should be applied to all data sets which do not satisfy all the input polarity and SV/P data. A sound general approach is to find a family of solutions with the least number of polarity errors possible, then increase the number of polarity errors by one and reevaluate the results to see if other combinations of polarity-amplitude ratio errors are appropriate,

(3) When either the specified number of polarity or amplitude ratio errors is overly restrictive to obtain solutions, the other type of data will often indicate this by also being in poor agreement with that family of solutions
(4) In general, composite solutions match a much greater percentage of polarity data than the ratio data.

ACKNOWLEDGMENTS

Dr. J. Arthur Snoke generously gave of his time in answering questions and he wrote the analysis program (FOCMEC) used herein. Dr. Edwin S. Robinson made suggestions on the manuscript. This work benefited from discussions with Alan Teague, and he also verified the data base. Paul Dysart and Martin Chapman critically reviewed the manuscript. Discussions with Matt Sibol contributed to our understanding of the Virginia earthquake data base. Lisa Gotow drafted many of the illustrations and Sharon Chiang offered comments on the presentation of these illustrations.

This research was supported in part by the Office of Nuclear Regulatory Research under contract NRC-04-77-134.

REFERENCES

Aggarwal, Y. P., and L. R. Sykes (1978). Earthquakes, faults, and nuclear power plants in southern New York and northern New Jersey, Science 200, 425-429.

Bollinger, G. A. (1973). Seismicity of the Southeastern United States, Bull. Seism. Soc. Am. 63, 1785-1808.

Bollinger, G. A., and M. C. Gilbert (1974). A reconnaissance microearthquake survey of the Hot Springs, Virginia area, Bull. Seism. Soc. Am. 64, 1715-1720.

Bollinger, G. A. (1978). Seismic hazard in Virginia, Virginia Minerals 24, 29-35.

Bollinger, G. A., and Russell L. Wheeler (1982). The Giles County, Virginia, seismogenic zone - Seismological results and geological interpretations, U.S. Geol. Survey Open - File Report 82-585, 136 p.

Bollinger, G. A., and Russell L. Wheeler (1983). The Giles County, Virginia, seismic zone, Science, 219, 1063-1065.

Bollinger, G. A., M. S. Sibol, and E. C. Mathena, eds. (1984). Seismicity of the southeastern United States, January 1, 1984 - June 30, 1984, SEUSSN Bulletin 14, 53 p.

Bollinger, G. A., and M. S. Sibol (1985). Seismicity, seismic reflection studies, gravity and geology in the central Virginia seismic zone: Part I. Seismicity, Geol. Soc. Am. Bull. 96, 49-57.

Calver, J. L., C. R. B. Hobbs, Jr., R. C. Milici, C. T. Spiker, and J. M. Wilson (1963). Geologic map of Virginia, Va. Div. Min. Res.

Campbell, David L. (1978). Investigation of the stress - concentration mechanism for intraplate earthquakes, Geophys. Res. Lett. 5, 477-479.

Chapman, M. C. (1979). Seismic velocity structure of central Virginia, Virginia Polytechnic Institute and State University, M.S. Thesis, 146 p.

Dames and Moore (1976). Summary Report of the in-progress seismic monitoring program at the North Anna site, prepared for Virginia Electric and Power Company, 117 p.

Dennison, J. M., and R. W. Johnson, Jr. (1971). Tertiary intrusions and associated phenomena near the thirty-eight parallel fracture zone in Virginia and West Virginia, Bull. Geol. Soc. Am. 82, 501-508.

Dewey, James W., and David W. Gordon (1985). Seismicity of the eastern United States and adjacent Canada, 1925-1976, U.S. Geol. Survey Prof. Paper, 106 p.

Fox, F. L. (1970). Seismic Geology of the Eastern United States, Bull. Assoc. Eng. Geol. 7, 21-44.

Glover, Lynn, III, J. K. Costain, C. Coruh, N. H. Evans, G. A. Bollinger, S. S. Farrar, and M. S. Sibol (1985). Seismicity, seismic reflection studies, gravity and geology of the Central Virginia seismic zone: Part IV, Tectonic history and current seismicity, Geol. Soc. Am. Bull. 96, in press for January, 1985.

Herrmann, R. B. (1975). A student's guide to the uses of P and S wave data for focal mechanism determination, Eqke. Notes 46, 29-39.

Herrmann, R. B. (1979). Surface wave focal mechanisms for eastern North American earthquakes with tectonic implications, J. Geophys. Res. 84, 3543-3552.

Kisslinger, Carl (1980). Evaluation of S to P amplitude ratios for determining focal mechanisms from regional network observations, Bull. Seism. Soc. Am. 70, 999-1014.

Kisslinger, C., J. R. Bowman, and K. Koch (1981). Procedures for computing focal mechanisms from local $(SV/P)_z$ data, Bull. Seism. Soc. Am., 71, 1719-1730.

Kisslinger, C., J. Roger Bowman, and Karl Koch (1982). Determination of focal mechanism from SV/P amplitude ratios at small distances, Phys. Earth Planet. Int. 30, 172-176.

Lahr, J. C. (1980). HYPOELLIPSE/MULTICS: A computer program for determining local earthquakes hypocentral parameters magnitude and first motion pattern, U.S. Geological Survey Open-File report 80-59, revised April 1980, for version II, 59 p.

McKenzie, D. P. (1969). The relationship between fault plane solutions for earthquakes and the directions of the principal stresses, Bull. Seism. Soc. Am. 59, 591-601.

McKeown, F. A. (1978). Hypothesis: Many earthquakes in the central and southeastern United States are causally related to mafic intrusive bodies, J. Res. U.S. Geol. Survey 6, 41-50.

Moore, T. P. (1979). Crustal velocity structure in southwestern Virginia, Virginia Polytechnic Institute and State University, M.S. Thesis, 75 p.

Oaks, S. D., and G. A. Bollinger (1985). The epicenter of the December 22, 1875 Central Virginia earthquake: New findings from documentary sources, Eqke. Notes 55, 11.

Pulli, Jay J., and M. Nafi Toksoz (1981). Fault plane solutions for northeastern United States earthquakes, Bull. Seism. Soc. Am. 71, 1875-1882.

Raleigh, C. B., J. H. Healy, and J. D. Bredehoeft (1972). Faulting and crustal stress of Rangely, Colorado, in Flow and Fracture of Rocks, Geophys. Monogr. Ser. 16, edited by H. C. Heard and others, 275-284.

Sibol, M. S., and G. A. Bollinger (1981). A note on recent seismic activity in the Scottsville, Virginia, area, Eqke. Notes 52, no. 4, 11-22.

Sibol, M. S., and G. A. Bollinger, eds. (1983). Hypocenter listing from southeastern U.S. seismic network Bulletins 1-12, July, 1977 to July 1983, SEUSSN Bulletin 12 A, 44 p.

Snoke, J. A., J. W. Munsey, A. G. Teague, and G. A. Bollinger (1985). A program for focal mechanism determination by combined use of polarity and SV-P amplitude ratio data, Eqke. Notes 55, 15.

Stauder, W. (1962). The focal mechanisms of earthquakes, Adv. Geophys. 9, 1-76.

Talwani, Pradeep (1982). An internally consistent pattern of seismicity near Charleston, South Carolina, Geology 10, 654-658.

Todd, E. D. (1982). Seismicity of the Bath County, Virginia Locale, Virginia Polytechnic Institute and State University, M.S. Thesis, 100 p.

Tzeng, W. S., and L. T. Long (1982). Investigation of SV- to P-wave amplitude ratio for determining focal mechanism, Eqke. Notes 53, no. 3, 39-40.

Viret, Marc, G. A. Bollinger, J. A. Snoke, and J. W. Dewey (1984). Joint hypocener relocation studies with sparse data sets--A case history: Virginia earthquakes, Bull. Seism. Soc. Am., 74, 2297-2321.

Wentworth, C. M., and M. Mergner-Keefer (1981). Reverse faulting along the eastern seaboard and the potential for large earthquake, in Beavers, J. E. (Ed.), Earthquakes and Earthquake Engineering: The Eastern United States, Vol. 1, Ann Arbor Science Publications, Michigan, 109-128.

Wheeler, R. L., and G. A. Bollinger (1982). Stress orientations on the Giles County, Virginia, seismogenic zone, Eqke. Notes 53, no. 3, 32-33.

Yang, J. P., and Y. P. Aggarwal (1981). Seismotectonics of northeastern United States and adjacent Canada, J. Geophys. Res. 86, 4981-4998.

Zietz, I., James L. Calver, S. S. Johnson, and J. R. Kirby (1977). Aeromagnetic map of Virginia, Virginia Div. Min. Res.

Zoback, M. L., and M. Zoback (1980). State of stress in the conterminous United States, J. Geophys. Res. 85, 6113-6156.

APPENDIX A.

APPENDIX B.

APPENDIX C.

APPENDIX D.

These appendices may be found in the form of microfiche in the jacket at the back of this report.

PART TWO

FOCAL MECHANISM ANALYSES FOR EASTERN TENNESSEE EARTHQUAKES (1981-1983)

ABSTRACT

To investigate the neotectonic processes in the Southern Appalachians, eleven single event focal mechanisms (SEFM) and seven composite focal mechanisms (CFM) were determined from 37 events that occurred in eastern Tennessee between September 1981 and July 1983. Both P-wave polarities and (SV/P)z amplitude ratios are input to a computer program that systematically searches the focal sphere for solutions acceptable within pre-set error limits. Hypocenter locations, azimuth and departure angles are taken from locations obtained by the Tennessee Earthquake Information Center (TEIC) with a four layer velocity model (GCO1). A second velocity model (STEP2), developed to improve focal depth estimates and to provide continuously varying (rather than discrete) departure angles, is used to relocate the seismic events for which SEFM and CFM solutions are obtained. The two different velocity models each produced focal mechanisms with similar nodal plane and P-axis orientations, indicating stable and reliable mechanism solutions; the differences between average strike, dip, and rake angles of the two data sets range from 2° to 11°.

Both SEFM and CFM solutions exhibit predominantly strike-slip motion along nearly vertical north-south (right-lateral) or east-west (left-lateral) oriented nodal planes. Standard deviations for average strike, dip, and rake angles are generally less than 20°. P-axis trends average about N50°E, with a nearly horizontal average plunge, and both trend and plunge estimates have standard deviations of 25° or less. Thus, the earthquakes in the study area all appear to result from a maximum compressive stress trending between N40°E and N70°E and plunging between 10° and -30°.

INTRODUCTION

The record of historic seismicity for the southeastern United States depicts a diffuse regional distribution of low to moderate earthquake activity constrained roughly to zones trending both parallel and transverse to the regional Appalachian structure (Bollinger, 1973). Some clustering of events exists within these zones, most notably in the vicinity of Giles County, Virginia, and near Charleston, South Carolina, locus of the largest shock to occur in the region (MMI = X) in 1886. Recent seismic network monitoring has revealed seismicity patterns similar to those expressed in the historic record. However, for the eastern Tennessee region, the current level of seismicity is somewhat higher than that for the surrounding locales. That is, for the last three years, over one-third of all earthquakes recorded, and about one-third of all felt events in the Southern Appalachian region have occurred in eastern Tennessee (Sibol and others, 1984). Unlike the Giles County Seismic Zone (Bollinger and Wheeler, 1982; Bollinger and Wheeler, 1983) some 300 km to the northeast, hypocenters in eastern Tennessee exhibit no obvious lineation(s).

The purpose of this study is to obtain earthquake focal mechanism solutions for earthquakes in the eastern Tennessee region. Input data are P-wave polarities and (SV/P)z amplitude ratios as recorded by short-period vertical (SPZ) seismometers. Thirty-seven events that occurred between September 1981 and July 1983 in the region extending from 35.5° to 36.5° north latitude and from 83° to 85° west longitude are considered (Figure 24). HYPO71 horizontal and vertical error estimates for the foci of these earthquakes are less than 2 km. Duration magnitudes range from 0.8 to 3.5, and focal depths range from 3 to 23 km, averaging 13 km (Sibol and Bollinger, 1984; Nava and Everett, 1984).

The computer program, FOCMEC (Snoke and others, 1984), is used to determine families of permissible focal mechanism solutions that are consistent, within pre-defined error allowances, with the P-wave polarities and the (SV/P)z amplitude ratios. FOCMEC is a refinement and extension of the FOCALSR program written by Tzeng and Long (1982), and features a more efficient and systematic searching algorithm along with a more complete and detailed output listing.

Twenty-eight of the original 37 events are used to determine 11 single event focal mechanisms (SEFM) and 7 composite focal mechanisms (CFM) using locations determined by a layered velocity model. The effects of various velocity model parameters on hypocentral locations, and ultimately on the resulting focal mechanism solutions, are evaluated. A gradient velocity model, approximated by 12-layers with variable Vp/Vs ratios, is also used to relocate earthquakes from which focal mechanisms are obtained. The resulting focal mechanism solutions are then compared to those solutions determined by using the original locations found by the Tennessee Earthquake Information Center (TEIC) employing the layered velocity model. The multiple mechanism solutions obtained collectively place strong constraints on the possible orientations of the regional in-situ stresses.

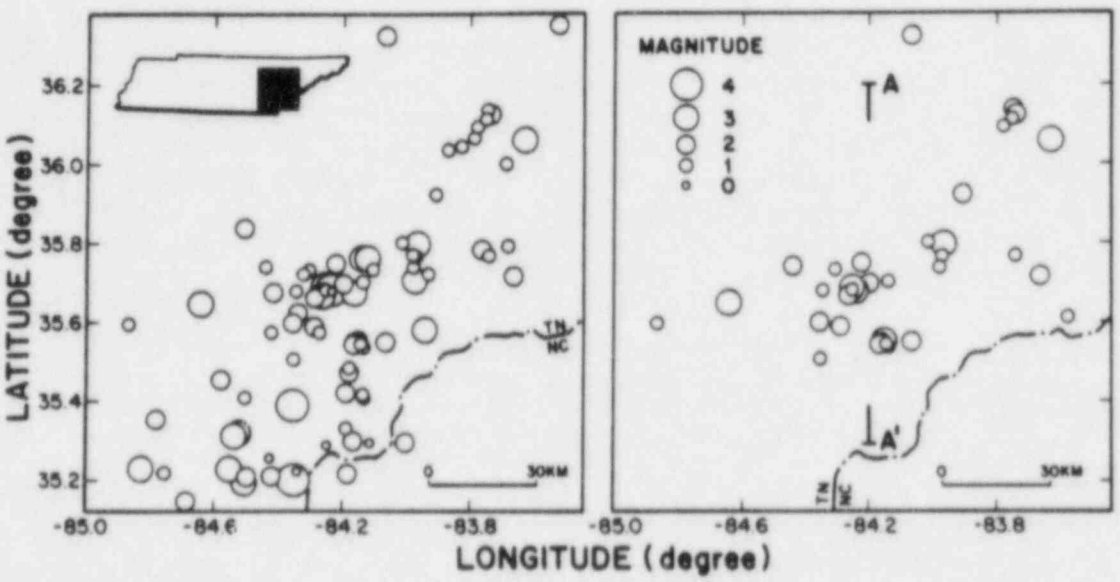

Figure 24: Eastern Tennessee Seismicity. Left: Total seismicity in eastern Tennessee region between 1981 and 1983. Study area shown by inset (shaded) map. Right: Earthquakes used to obtain focal mechanisms in this study. Location of A-A' profile as shown in Figure 27. All epicenters (open circles) scaled according to duration magnitudes.

Regional Geology

The geology of eastern Tennessee can be generalized into three major geologic divisions: the western portion of the Blue Ridge province, the Valley and Ridge province, and the eastern portion of the Cumberland Plateau province (Figure 25). The western portion of the Blue Ridge is characterized by an approximately 5 to 6 km thick allochthonous sheet of highly metamorphosed Proterozoic and lower Paleozoic volcanic, sedimentary, and plutonic rocks with metamorphic grade increasing eastward. Large thrust blocks have been transported tens to hundreds of kilometers westward along low-angle thrust faults. The associated thrust faults coalesce into a single sole fault above relatively unmetamorphosed lower Paleozoic sediments (Cook and others, 1979), which are underlain by crystalline basement. The Blue Ridge thrust fault separates the Blue Ridge province to the east from the Valley and Ridge province on the west.

The Valley and Ridge province consists of an approximately 5 km thick sequence of unmetamorphosed and linearly folded sedimentary rocks. West to east imbricated thrust faults coalesce into a decollement above crystalline basement rocks (Harris, 1976). Fold and fault axes trend N45°E through most of eastern Tennessee. The intensity of folding and faulting decreases westward toward the Cumberland Plateau. That geologic division is composed of some 4 km of relatively flat-lying Paleozoic platform sedimentary rocks that overlie Grenville basement, and marks the western extent of Appalachian style deformation.

Seismicity

The historic seismicity of the Southern Appalachian region can be characterized as a diffuse zone of moderate activity that extends from central Alabama to southern West Virginia, with epicenters concentrated in the Valley and Ridge province of Tennessee, the Blue Ridge province of North Carolina, and the Giles County region in the Valley and Ridge province of Virginia (Bollinger, 1973; Bollinger and Wheeler, 1983). The largest earthquake known to have occurred in the region is the MMI VIII, mb 5.8 Giles County earthquake of 1897 (Bollinger and Wheeler, 1982). An intensity VII earthquake that occurred in 1913 near Knoxville is the largest known earthquake in the eastern Tennessee area of this study (Bollinger,1973; Coffman and others, 1982). Dewey and Gordon (1984) report the relocation of three earthquakes with magnitudes greater than 4 that occurred in eastern Tennessee since 1925.

Until late-1981, most eastern Tennessee earthquakes were located either by widely spaced regional seismograph stations and/or by isoseismal maps and thus have potentially large locational errors (see Dewey and Gordon, 1984). Studies by Bollinger and others (1976) and Guinn (1980) of the 1973 eastern Tennessee earthquake sequence, initiated by a 4.6 mainshock, made use of temporary, portable seismograph networks. They were, however, unable to obtain definitive focal mechanism solutions. That is, the P-wave first motion data could not distinguish between primarily strike-slip motion along northeast or northwest trending nodal planes, and dip-slip motion

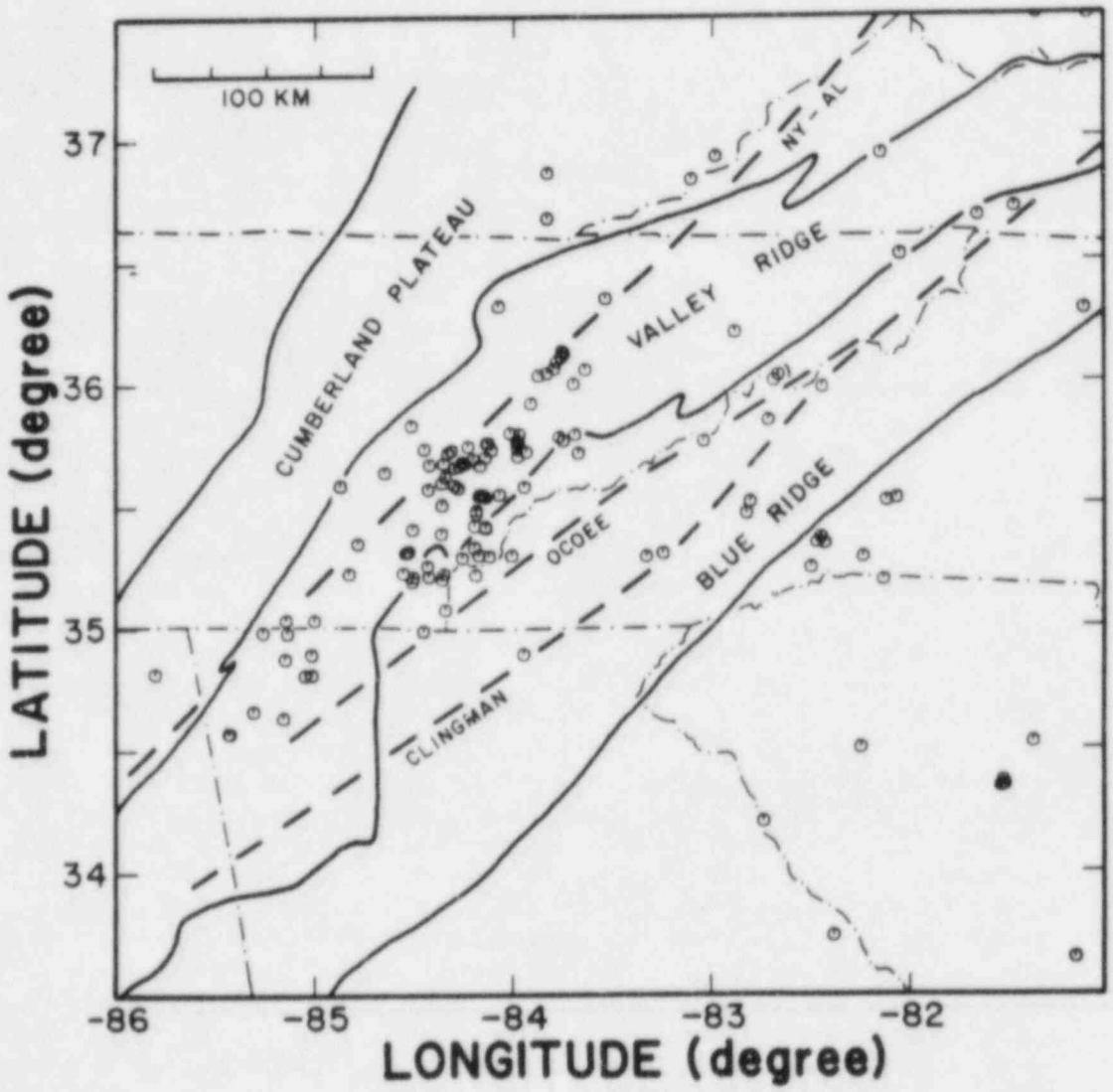

Figure 25: Seismicity and Generalized Geology. Seismicity from 1981 through 1983 with general geologic provinces (between the heavy solid lines) and aeromagnetic lineaments (dashed lines: New York-Alabama (northernmost), Clingman (southernmost), and Ocoee (center); from Johnston and others, 1985).

along northwest trending nodal planes for the mainshock (Bollinger and others, 1976). Aftershocks yielded mechanism solutions different from those found for the main shock (Bollinger and others, 1976; Guinn, 1980). Herrmann (1979), using primarily surface wave data, obtained a focal mechanism for the main shock that exhibited primarily strike-slip motion along north or east trending nodal planes (see Johnston and others, 1985, their Figure 8).

Installation of the Southern Appalachian Regional Seismic Network (SARSN) in eastern Tennessee and western North Carolina was initiated by the Tennessee Earthquake Information Center (TEIC) in early 1981, and was completed some two years later (Figure 26). Additionally, the Tennessee Valley Authority (TVA) has also operated from four to seven auxiliary stations in the area since the early 1980's. Good hypocenter location capability for the region was achieved by mid-1981. Over half the earthquakes occurring from September 1981 through 1983 are considered to be reliably located (ERH $\leq$ 2 km) and to have good depth control (ERZ $\leq$ 2 km; Johnston and others, 1985).

Most earthquakes that have been located thus far in eastern Tennessee are in the crystalline basement, well beneath the Appalachian decollement found at about 5 km depth. Focal depths range from 3 to 25 km with a mode and mean of 13 km. Between 80% and 90% of the 101 events located by TEIC from 1981 to 1983 lie between the northeast trending New York-Alabama (NY-AL) aeromagnetic lineament first identified by Watkins (1964) and later studied by King and Zietz (1978), and the Clingman and Ocoee aeromagnetic lineaments defined by Nelson and Zietz (1983) and Robert Butler (personal comm.; Johnston and others, 1985; Figure 25). According to Johnston and others (1985), these lineaments bound the "Ocoee Basement Block" in which the majority of earthquakes in the east Tennessee region are generated. The number of earthquake occurrences decreases eastward through the Blue Ridge and Piedmont provinces of North Carolina. The neighboring Cumberland Plateau province to the west is virtually aseismic.

Recently published focal mechanisms from the eastern Tennessee region exhibit generally north-south (right-lateral) or east-west (left-lateral), nearly vertical nodal planes, with predominantly strike-slip motion (Reinbold and others,1983; Johnston and others, 1985). From the general north-south elongation of isoseismal contours from some felt shocks along with and the general northeast trend of epicenters, Johnston and others (1985) conclude that fault movement is probably along the north-south planes.

DATA ACQUISITION

Data were collected from visual and film recorders at TEIC and TVA data centers that had been telemetered from a total of 24 stations in Tennessee, North Carolina, Virginia, Kentucky, Georgia, and Alabama (see Figure 26). All TEIC polarity and amplitude ratio data were read by at least two independent observers. TVA data, which comprises less than 10% of the data base, were unavailable for verification reading.

Hypocenters were located by TEIC using the HYPO71 program (Lee and Lahr, 1975) and a crustal velocity model developed by Moore

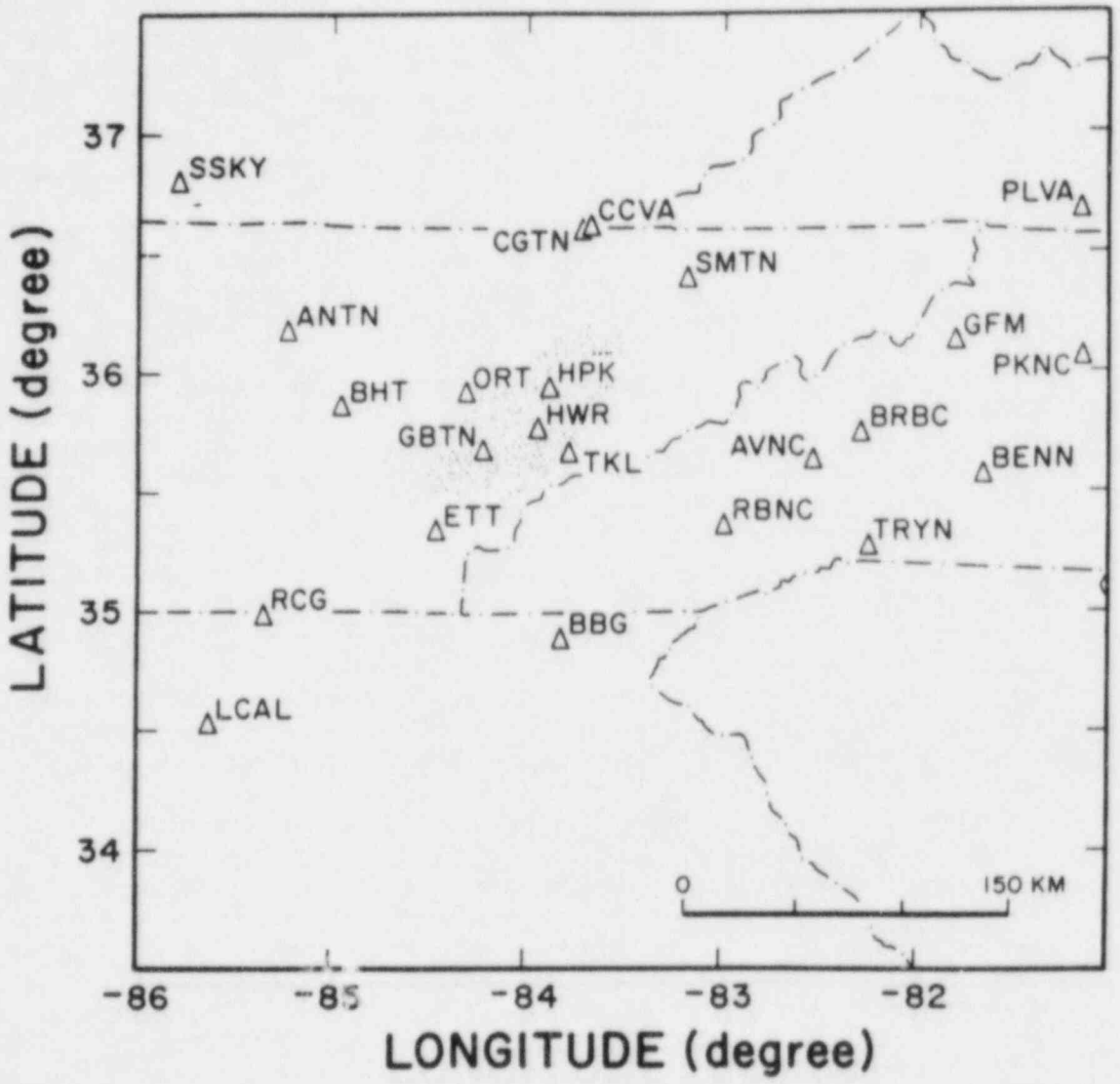

Figure 26: Location of Seismic Stations. Locations of seismic stations (open triangles with 3 or 4 letter station code) from which data was derived. Stipled area indicates general location of the epicenters for the seismic events analyzed in this study.

(1979). Arrival time data, epicenter to station azimuths, and departure angles (measured from downward vertical) are taken from the TEIC locations. Azimuths and departure angles not available in the TEIC listings were calculated by a ray tracing program (RAYFIND; Snoke, written comm., 1984).

P-wave polarities are considered reliable at all epicentral distances provided the first motion signal-to-noise ratio is large, i.e., the first motions are impulsive. Theoretically, first motions are not altered by refractions, and therefore, no attempt to distinguish between direct and refracted arrivals was made.

P and S-wave amplitudes are altered in differing amounts as they propagate through the earth. Furthermore, differences in compressional and shear motion, as measured at the earth's free surface on a vertical seismometer, must also be taken into account. Thus, both raypath (particularly anelastic attenuation and geometrical spreading) and free surface corrections must be applied to the recorded amplitude data to estimate the true source amplitude characteristics.

The effect on amplitude measurements of later arriving primary phase scatter is avoided, or at least significantly reduced, by choosing the largest P or S amplitude within the first one-and-a-half cycles of the respective phase. Emergent or ambiguous arrivals are not used. Because free surface corrections vary rapidly for incident angles between 30° and 37°, amplitudes that have calculated P or S wave surface incident angles between 27° and 40° are also not used. Arrival times are computed for direct waves and for head waves critically refracted off the first layer beneath the hypocenter. Possible interference of direct and refracted waves can then be avoided by rejecting any data with calculated head wave arrival times within 0.2 to 0.3 seconds of the direct phase. Since there is no conclusive evidence of a geologic structure that corresponds to the middle velocity boundary which is capable of producing critically refracted head waves (see GC01, Figure 28), corrections for these head waves are probably less important than those for critical refractions off other boundaries, e.g., the MOHO. Also, according to Kisslinger (1980), refracted waves may theoretically be used to determine valid amplitude ratios. In this study, some amplitude ratios are obtained from head wave arrivals that were calculated to arrive 0.2 to 0.3 seconds before the direct wave. Free surface and geometrical spreading corrections are applied to the remaining data.

Other basic assumptions in this study are that the differences in the anelastic attenuation are negligible and, hence, also the frequency content of P and S waves for epicentral distances less than 100 km (Kisslinger, 1980). At greater epicentral distances, these differences are assumed to be significant enough to prohibit the valid use of ratio data. Differences in the transmission of P and S-wave energies across a boundary are considered negligible. Finally, although departure angles for both P and S-waves differ slightly when variable Vp/Vs ratios are used, they are assumed herein to be the same. This difference is also considered negligible.

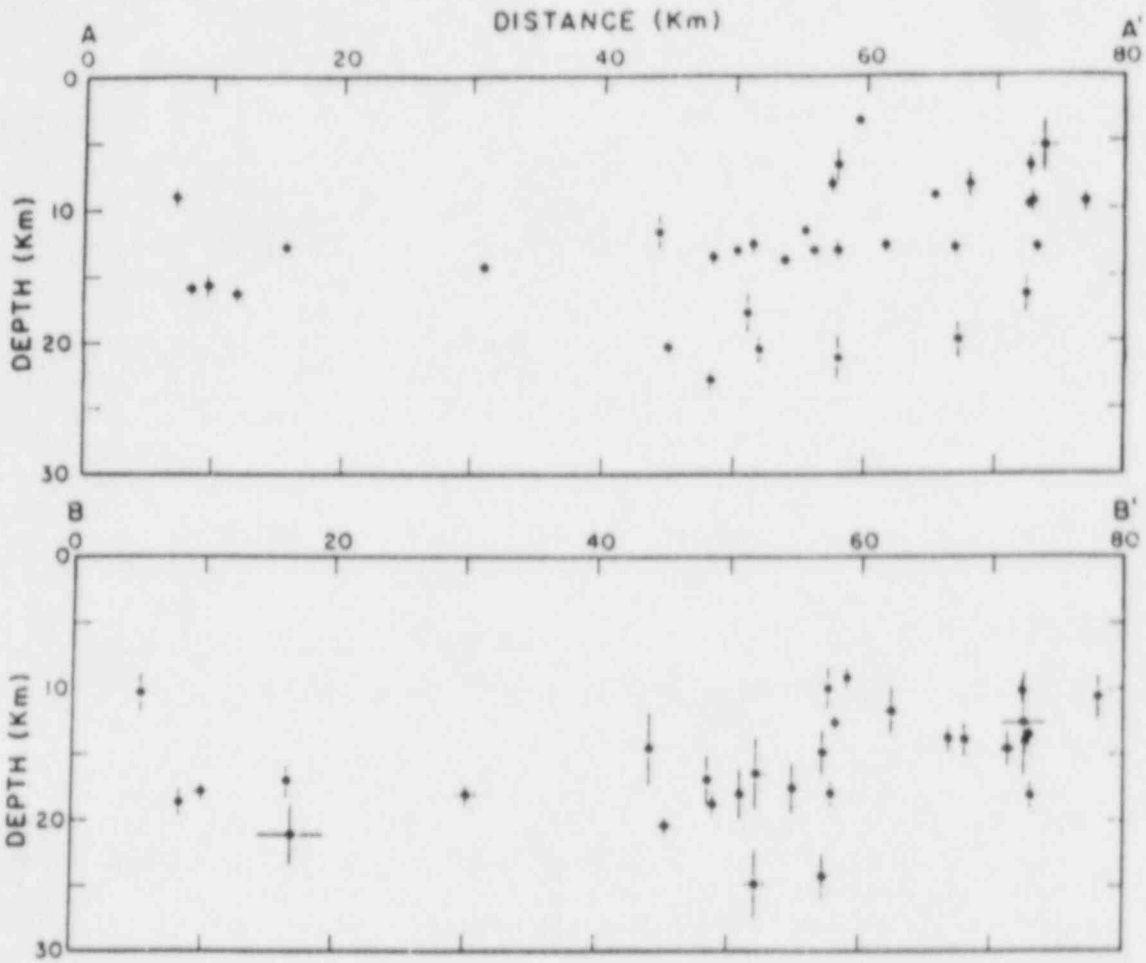

Figure 27: Depth Distribution of Events Located with GC01 and STEP2 Models. Cross section A-A' is the depth distribution of events located with GC01 velocity model (see Figure 28). Note the concentration of events above and the depletion of events at, and just below, the 14.7 km discontinuity. A-A' corresponds to profile lines in Figures 24 and 29. Cross section B-B' is the depth distribution of events located with STEP2 velocity model (see Figure 28). Note the more continuous distribution of events near 15 km depth. The orientation of B-B' is similar to A-A', and is shown in Figure 29.

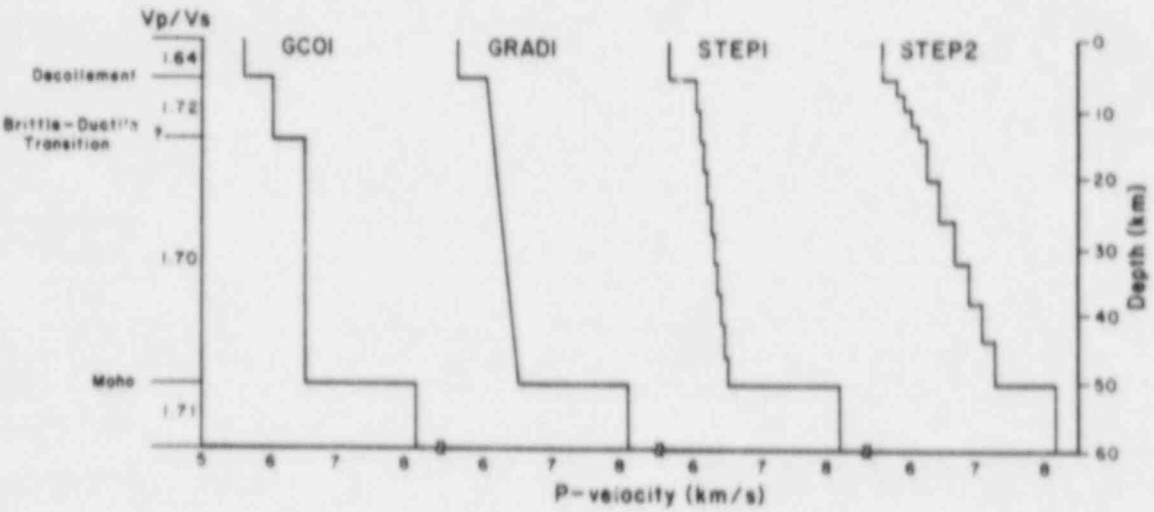

Figure 28: Velocity Models. Velocity models used to determine hypocentral locations with generalized geologic interpretations and Vp/Vs ratios on left, and depth in km on right. The original TEIC locations used a constant Vp/Vs ratio value of 1.73.

DATA PROCESSING

The determination of focal mechanism solutions is influenced by the distribution of data points on the focal sphere. That is, as azimuths and departure angles are changed, so too will the number and type of acceptable fault plane solutions change. This is especially true when a continuous type of data, such as amplitude ratios, is used to determine the mechanism. Whereas only those polarities near nodal planes constrain critically the focal mechanism, all of the amplitude ratios contribute equally to focal mechanism determinations, regardless of their location on the focal sphere. Furthermore, the free surface and raypath corrections applied to the amplitude ratios are path dependent, and any change in hypocenter location will, in general, also produce a change in the amplitude ratio value. Thus, given the presence of errors, relatively small changes in the focal sphere position of amplitude ratios, especially in those regions of the focal sphere where the ratios change rapidly, can alter dramatically the resulting focal mechanism solutions.

Departure angles depend on epicenter location and, particularly, on the generally less well-determined focal depth. For epicentral distances comparable to the focal depth, a small change in focal depth can produce a relatively large change in departure angle. This effect decreases as epicentral distances become larger, but it does continue to influence the possible focal mechanisms.

Often the simplest velocity model calculated from arrival time data consists of a few constant velocity layers. Such models probably do not represent the true geologic structure. The data may collectively be "averaging over," and hence be insensitive to (with respect to time) these velocity discontinuities. Thus, hypocentral locations which are judged to be statistically good may, in fact, have large errors associated with them.

Nicholson and Simpson (1984) showed that, for computer located earthquakes in California, the hypocenters were clustered distinctly above discontinuities in the velocity model. Conversely, they showed that velocity model-independent hypocenters computed from Wadati and Riznichenko plots were scattered more uniformly with depth. A possible model-dependent clustering of seismic events may be seen in eastern Tennessee where both the mode and mean depth of hypocenters are 13 km, near the 14.7 km deep velocity discontinuity (see Figure 27; Johnston and others, 1985). Nicholson and Simpson (1984) also found that, while P and S velocities tend to increase or decrease at the same depths, they do not do so proportionally. Closing of saturated microcracks due to increased lithostatic loading with depth, and changes in lithology can both produce different rates of change in P and S velocities. Hence, to accurately model the local velocity structure, separate P and S velocities must be used (Nicholson and Simpson, 1984; Nicholson and others, 1984). This usually involves the use of Vp/Vs ratios that vary from layer to layer.

Another potential problem with large velocity discontinuities is that critical refractions from such boundaries have the same departure angle regardless of epicentral distance. At epicentral distances found in eastern Tennessee, these refractions exert a strong control on the rays that arrive at a distant station. This effect increases

as hypocentral depth approaches the velocity discontinuities. Thus, a simple velocity model that is adequate for time-dependent hypocentral locations may be inappropriate for raypath-dependent focal mechanism determinations.

In summary, focal mechanisms that utilize amplitude ratios are especially sensitive to hypocentral locations and thus are velocity model dependent. To obtain accurate focal mechanisms, independent P and S velocity models are often required (variable Vp/Vs ratios) and the effects of velocity layering on focal depth and raypath projections must be reduced insofar as is possible.

Testing of Velocity Models

As previously mentioned, all SARSN events are located with the HYPO71 locating program (Lee and Lahr, 1975) and the Moore (1979) crustal velocity model (GCO1 in Figure 28). Three potential problems can arise from the use of the Moore model to locate eastern Tennessee events: 1) the model was determined primarily in the Valley and Ridge province of southwestern Virginia while SARSN stations are located in the Blue Ridge province of North Carolina and the Valley and Ridge and Cumberland Plateau provinces of Tennessee, 2) HYPO71 uses a single Vp/Vs ratio for the entire velocity model rather than the layered Vp/Vs ratios defined by the Moore model, and 3) the middle boundary's (14.7 km depth) influence on hypocentral locations, especially the focal depth. However, TEIC conducted locational stability tests using the GCO1 model, and determined that it performs reasonably well in eastern Tennessee (Brewer and others, 1982; see Appendix F).

The following summary of velocity model testing is discussed in more detail in Appendix F. The HYPOELLIPSE locating program (Lahr, 1984) was employed in this study to locate five well recorded events utilizing the GCO1 velocity model with variable Vp/Vs ratios and with a single Vp/Vs ratio. The constant Vp/Vs ratio appears to locate epicenters with error statistics comparable to those for variable Vp/Vs ratios. The variable Vp/Vs ratios, however, obtained generally deeper and statistically better depth estimates. Similar results were found by Nicholson and Simpson (1984) and Nicholson and others (1984) who relocated earthquakes in California and the New Madrid Seismic Zone using independent P and S velocity models. They also found that epicentral locations were not significantly affected, but that focal depths increased noticeably and systematically.

The hypocentral control of the middle velocity boundary could be effectively eliminated by replacement with a gradient velocity increase between the upper and lower boundaries (see GRAD1 in Figure 28). Unfortunately, HYPOELLIPSE cannot simultaneously apply both a gradient velocity model and variable Vp/Vs ratios to locate events. It can, however, employ a 12-step velocity model (approximation to a gradient velocity model) with variable Vp/Vs ratios. Retaining the decollement and MOHO velocity boundaries allows a gradient model to be approximated by 10 steps (see STEP1 in Figure 28). The efficacy of this approximation was tested by locating five well recorded events with both GRAD1 and STEP1 velocity models, and comparing the results. STEP1 was found to adequately substitute for GRAD1.

Two 12-layer velocity models were postulated (STEP1 and STEP2 in Figure 28) and used to locate seven well- and one poorly-recorded earthquakes. The STEP2 model was judged to be superior because it obtained horizontal (11 of 16) and vertical (6 of 8) error estimates that were smaller than STEP1, plus its quality evaluations, especially those for focal depth (6 of 7), were also consistently better.

STEP2 was then selected as a test velocity model for the study area. Its advantages include the use of variable Vp/Vs ratios and the elimination of the strong locational control of the middle velocity boundary. Earthquakes for which focal mechanisms had been previously obtained were relocated using the arrival time data from the original TEIC locations and the STEP2 velocity model. The new azimuths and departure angles were then used to obtain focal mechanisms. All polarity and amplitude data were processed in the same manner as was previously done, except that only head waves off the decollement or MOHO layers were considered capable of interfering with direct arrivals. New amplitude ratio corrections, consistent with the new hypocentral locations and velocity model, were applied.

Computer Focal Mechanism Determinations

FOCMEC (Snoke and others, 1984) is a computer program that systematically searches the focal sphere for focal mechanisms consistent, within prescribed error limits, with the input polarity and amplitude ratio data. It is used to determine families of valid solutions. Input and output files for FOCMEC are presented in Appendix H. In FOCMEC, a searching algorithm examines the focal sphere for acceptable focal mechanism solutions by relating the observed data to a rotating set of orthogonal B, A, and N axes, where B is the null axis, and A and N are the poles (normals) to the nodal planes. The density of focal sphere coverage is controlled by a preset increment of axes rotation. The 5° increment of focal sphere coverage used for all events herein tests more than 25,000 possible orthogonal nodal plane orientations within the focal sphere.

In FOCMEC, polarity data are analyzed first to determine if they are consistent with each pair of orthogonal nodal planes. If the number of polarity errors is within a pre-specified number of allowable errors, then the difference between theoretical amplitude ratios and the corresponding observed (Sv/P)z amplitude ratios is compared to the preset error allowance. All ratios and ratio error allowances are represented as logarithms to insure linearity of the differences. If the number of acceptable ratio differences (within the preset error allowance) is less than a specified number of allowed ratio errors, a valid solution is declared and its parameters are output. The B, A, and N axes are then incremented for the next iteration.

Solution Selection

A complete search of the focal sphere generally results in not one but rather a family of solutions. From this family of solutions, a preferred solution is selected by analyzing the root-mean-square (RMS) error for the ratios calculated by FOCMEC. This family,

however, is nonunique, and is dependent primarily upon the polarity and amplitude ratio error limits. Varying those error limits can be expected to produce a different family of solutions. The problem would then arise of selecting the overall preferred solution for an event for which there were more than one family of solutions. The solution selection process is summarized below and is explained in detail in Appendix G.

In general, the family of solutions with the least number of polarity errors is selected as the preferred family of solutions, from which the overall preferred solution is to be chosen. This is because polarities are a discrete data type and are generally more accurately determined, and hence, more objective than amplitude ratios, which depend upon two continuously varying observations (P- and S-wave amplitudes) subject to coda interference and a number of velocity model dependent corrections. If, however, the family of solutions with an increased polarity error allowance also has a reduction of two or more ratios and/or substantial improvement in the RMS statistics, then it would become the preferred family. The overall preferred solutions, plotted with the polarity and ratio data, are presented with their respective family of solutions in Figures 33 through 50.

DISCUSSION OF RESULTS

In this study, focal mechanisms have been obtained from two different earthquake location data sets, each of which was generated with a different velocity model (GC01 and STEP2). The GC01 model was developed from a large crustal refraction arrival time data base, and has been stringently tested in different sub-regions of the Southern Appalachian region (Moore, 1979; Bollinger and Wheeler, 1982; Brewer and others, 1984; Chapman and Bollinger, 1985). Additionally, the Virginia Tech Seismological Observatory and TEIC have collectively located over 150 earthquakes in the past five years with the GC01 model.

The STEP2 model was subjectively created to reduce certain biases in the GC01 model (single Vp/Vs ratio and hypocentral control of middle velocity boundary) in an effort to obtain better focal depth and departure angle estimates. The primary objective was to test the stability of the focal mechanism solutions derived from the GC01 data set. That is, how and to what extent, did the assumptions used to develop the STEP2 velocity model affect focal mechanism solutions? Recall that the STEP2 model is, however, only speculative. The GC01 data set and its resulting focal mechanisms will therefore be employed as the definitive solutions, with the STEP2 set of mechanism solutions used primarily to probe for mechanism solution stability.

Hypocentral Locations

As mentioned previously, events relocated with the STEP2 model were observed to have consistently deeper focal depths and relatively unchanged epicentral locations. Both velocity models located nearly all of the earthquakes in the basement; only one of the 37 earthquakes in the study area is located in the overlying sedimentary layers with the GC01 model, and none of the 28 earthquakes relocated with the

STEP2 model has focal depths less than 8 km. Thus, a major proportion of the seismic energy in the study area is being released within the crystalline basement below the detached upper layers. Johnston and others (1985) also found most of the earthquake activity in eastern Tennessee occurring within the basement.

Effect of Amplitude Ratios on Focal Mechanisms

In this study, amplitude ratios were of great value in determining focal mechanism solutions in three important ways. First, roughly half (51% or 153 of 311) of the data used to obtain mechanism solutions are amplitude ratios. Hence, when amplitude ratios are included, more events have acceptably constrained mechanism solutions than when only polarities are used. For example, many events (8 of 18) have five or less polarities which cannot by themselves adequately constrain the nodal plane orientations. However, well constrained families of solutions are obtained for those same events when amplitude ratios are included.

Secondly, in every case, amplitude ratios exert a stronger constraint on the dip, strike and rake angles of solutions than do the polarity data. Since amplitude ratios become more sensitive to nodal plane orientations with increasing dip angle, they are very useful in determining dip and rake angles. In cases where the polarity data would allow both dip-slip and strike-slip solutions, the amplitude ratios consistently restricted the rake angles to those indicating predominantly strike-slip motion.

Finally, amplitude ratios provide an objective method of selecting a preferred solution through the use of the RMS errors for the ratios. Such statistics, discussed in Appendix G, have proved invaluable in accessing the fit of the solutions to the data.

Nodal Plane Orientations

Both SEFM and CFM solutions obtained for earthquakes located with the GC01 velocity model exhibit predominantly strike-slip motion along nearly vertical north-south (right-lateral) or east-west (left-lateral) oriented nodal planes (see Figures 29 and 30, and Table 10). Eighty-eight percent (45 of 51) of the strike, dip, and rake angles for both SEFM and CFM solutions lie within 30° of a perfectly vertical, north-south or east-west, strike-slip solution (see Table 11). Standard deviations for strike, dip, and rake angles range from 8° to 23°. P-axis trend and plunge angles average N48°E, -4° for the SEFM solutions and N54°E, -12° for the CFM solutions, with standard deviations ranging from 11° to 25° (Table 10). These orientations are very similar to N46°E, 13° average P-axis orientation determined for the Giles County, Virginia region (Munsey, 1984). P-axis orientation angles for SEFM solutions were plotted with respect to both time and depth. Within the constraints of the data, the orientations of P-axes do not exhibit a dependence with time, since all orientations may be produced by the same maximum compressive stress orientation. The orientations of P-axes do, however, have a suggestion of depth dependence (Figure 31). As depth increases, both P-axis trend and plunge angles appear to become systematically restricted to an apex

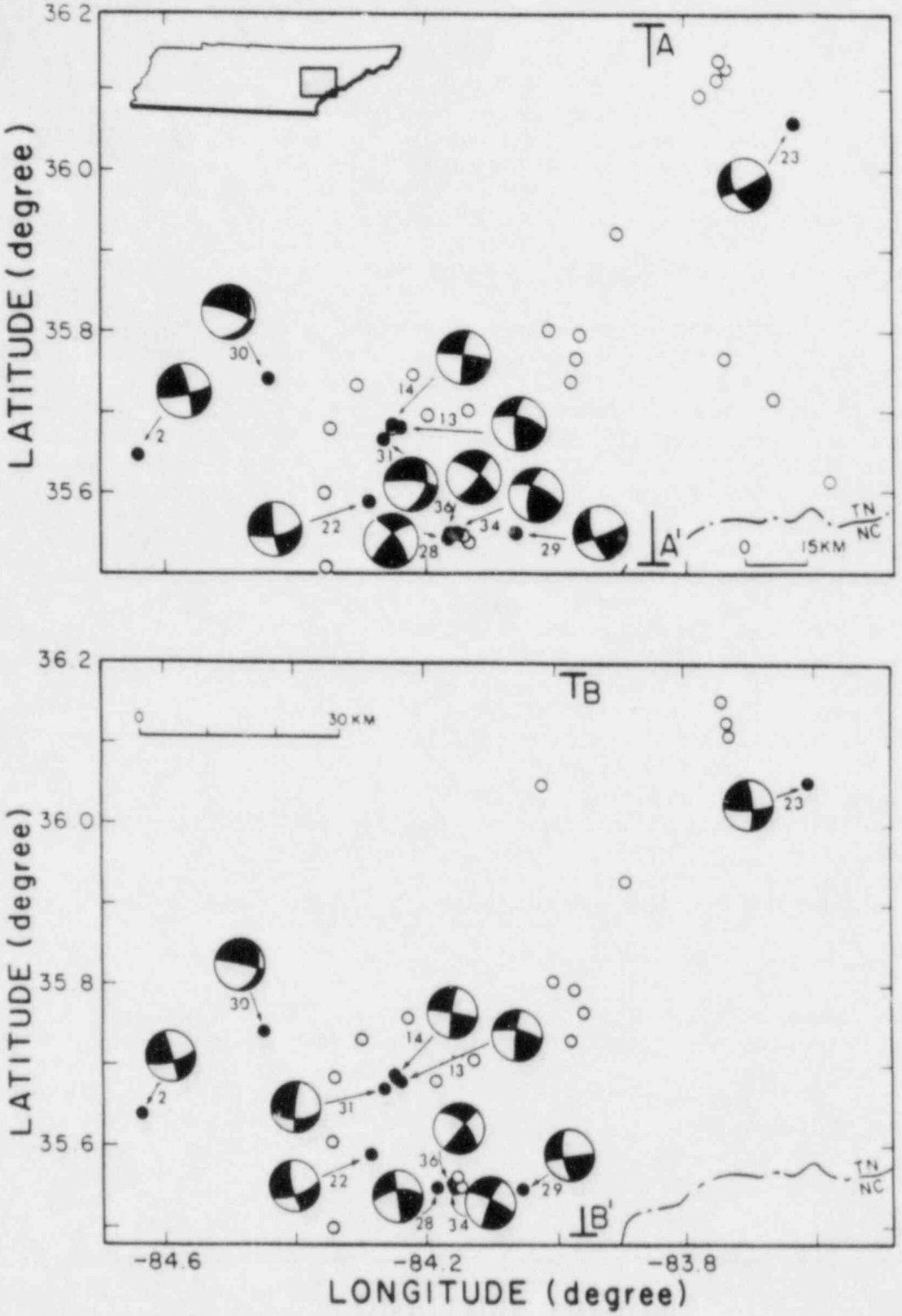

Figure 29: SEFM Solutions for GC01 and STEP2 Data. SEFM solutions for eastern Tennessee study region (inset map). Upper map shows GC01 solutions, lower map shows STEP2 solutions. Note the slight changes in epicenter locations. Some events in upper map are not shown on lower map. Each solution is labeled with a chronologic event number. All solutions are equal area, lower hemisphere projections, with the compressional quadrant shaded. Vertical section plots along A-A' and B-B' are shown in Figure 27.

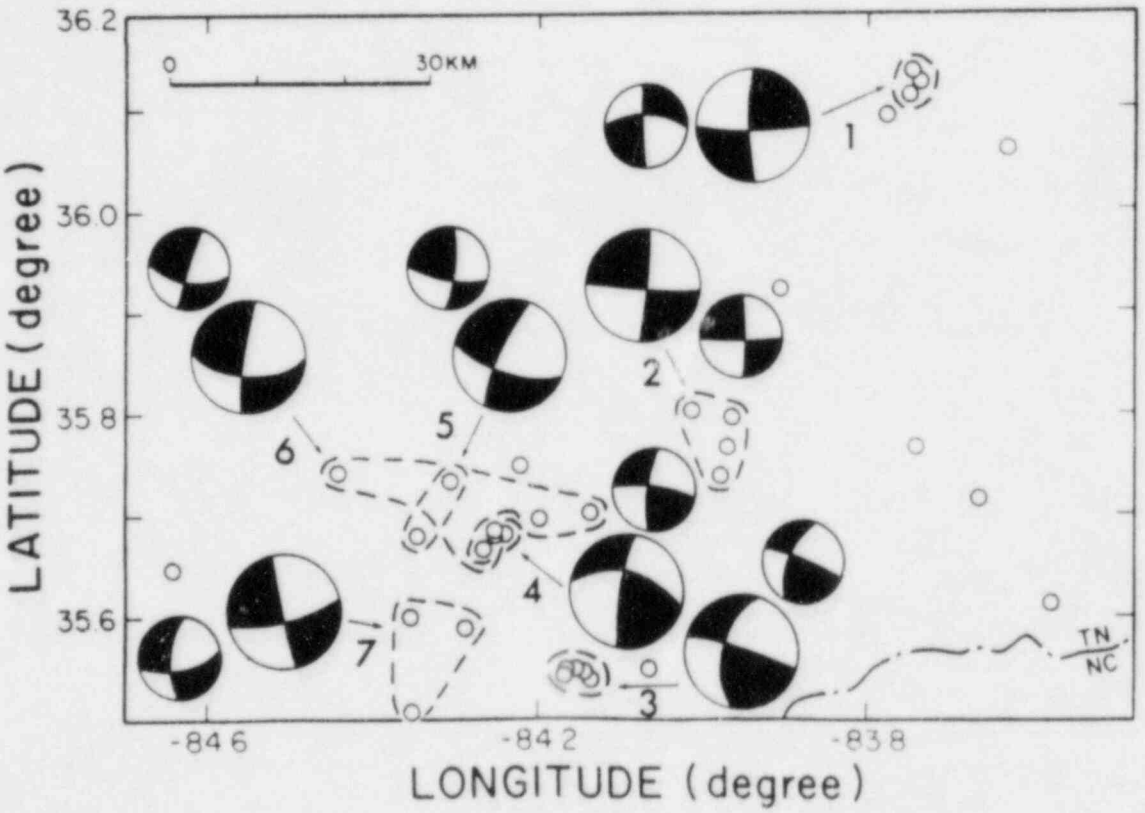

Figure 30: CFM Solutions for GC01 and STEP2 Data. CFM solutions for the eastern Tennessee region. Events composited together are grouped by dashed lines. Large mechanism diagrams represent velocity model GC01 solutions, smaller mechanism diagrams represent velocity model STEP2 solutions. Map and mechanism projections the same as in Figure 29.

TABLE 10

SEFM and CFM P-axis and Nodal Plane Orientations *

	SEFM			CFM		
	GC01	STEP2	DIF/SD	GC01	STEP2	DIF/SD
P Trend	48 +- 23	49 +- 19	5	54 +- 11	52 +- 11	18
P Plunge	-4 +- 25	-2 +- 22	9	12 +- 16	13 +- 11	9
North						
Strike	8 +- 23	6 +- 18	11	8 +- 11	7 +- 11	9
Dip	65 +- 20	76 +- 19	58	79 +- 10	75 +- 9	44
Rake	16 +- 9	19 +- 11	33	19 +- 13	16 +- 8	38
East						
Strike	97 +- 23	95 +- 18	11	97 +- 11	98 +- 12	9
Dip	77 +- 8	72 +- 12	63	71 +- 13	75 +- 8	50
Rake	26 +- 20	15 +- 19	58	12 +- 10	16 +- 9	44

* P-axis and nodal plane orientations and standard deviations for SEFM and CFM from GC01 and STEP2 data set. Nodal plane orientations are divided into northernmost and easternmost trending planes. DIF/SD is the percent of difference between GC01 and STEP2 averages compared to the smallest standard deviation between the two.

TABLE 11

Percent of Nodal Planes within 30° of Vertical, N-S or E-W Strike-slip Solution

	GC01			STEP2		
	Strike	Dip	Rake	Strike	Dip	Rake
SEFM	82	86	77	91	86	86
CFM	100	100	100	100	100	100
TOTAL	88	91	85	94	91	91
OVERALL	88%			92%		

* The percentage of strike, dip, and rake angles that are within 30° of a perfectly vertical, north-south or east-west, strike-slip solution for SEFM, CFM, and a combination of both SEFM and CFM for GC01 and STEP2 data sets. The overall percentage combines all strike, dip, and rake angles for both SEFM and CFM for GC01 and STEP2 data sets.

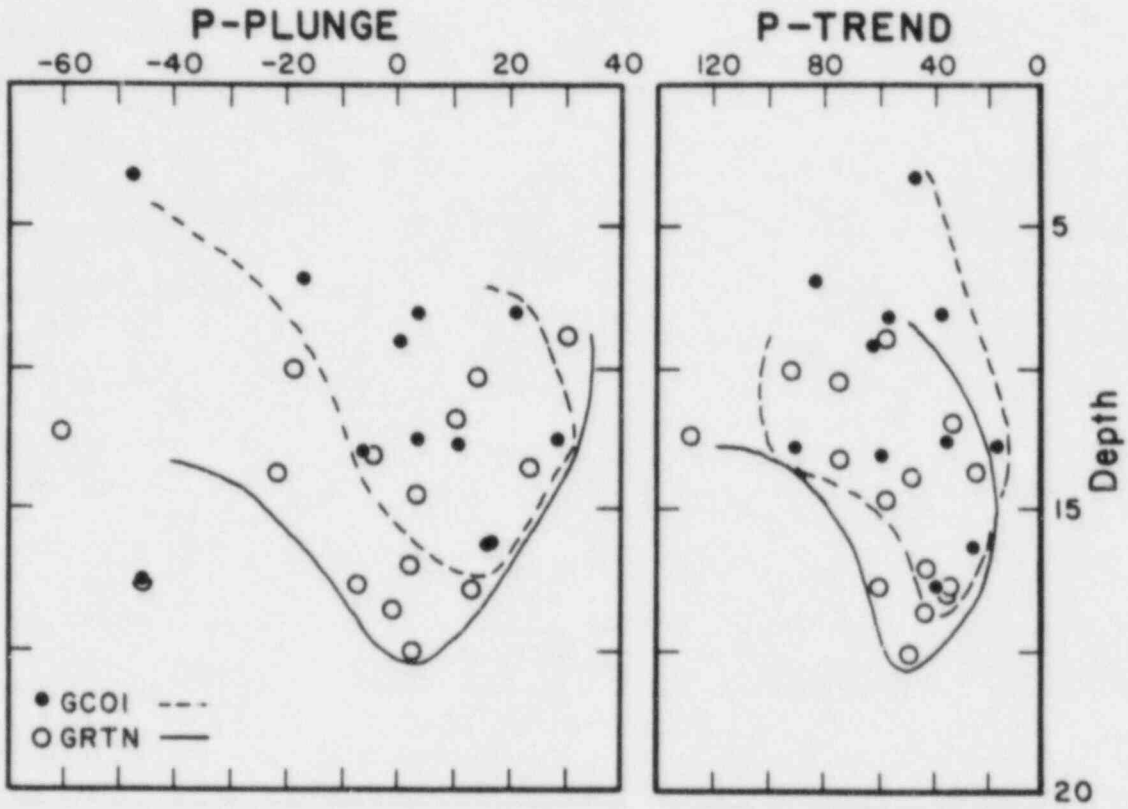

Figure 31: P-Axis Versus Depth. P-axis orientations (plunge and trend in degrees) versus focal depth in km for the mechanism solutions resulting from the use of the GCOI and STEP2 velocity models. Solid and dashed lines are empirical bounds to P-axis orientations with depth, and are drawn by eye.

near N40° to 50°E, and 5° to 10°, respectively. This aspect of the P-axis orientation will be discussed further in the next section. Similar plots of T-axis orientations indicate no dependence with either time or depth.

Primary exceptions to the general orientation of nodal planes are in the southernmost region of the study area where two SEFM events (#28 and 36) have nodal planes that are oriented more than one standard deviation clockwise of the regional average (see Figure 29), and in the northernmost region of the study area where the sense of slip for a CFM (#1) is opposite that of all other solutions (see Figure 30). A SEFM solution (#23) approximately 15 km southeast of CFM #1 exhibits an expected slip direction, i.e., right-lateral along north-south planes or left-lateral along east-west planes. Assuming that SEFM #23 resulted from the inferred regional stress field (approximately N50°E), the slip direction exhibited by CFM #1, would require a change in the orientation of the regional stress field by 20° to 40° within a distance of 15 km. In any event, CFM #1 is inconsistent with the inferred regional stress field, and this mechanism has therefore been omitted from all calculations of averages. We do not have an explanation for this disparity but will continue to seek clarification. Our suspicion at this stage is the presence of undetected error(s). We continue to investigate this result.

Other exceptions are SEFM #23, 30 and 31, whose north-south oriented nodal planes dip more horizontally than the regional average. This would indicate that either strike-slip motion occurred along an inclined north-south fault plane or that dip slip motion occurred along a vertical east-west plane.

SEFM and CFM solutions obtained for events located with the STEP2 velocity model are remarkably similar to those obtained with the GOO1 model. Nodal plane and P-axis orientations are well within one standard deviation of those found with GOO1 locations (see Figures 29 and 30, and Table 10). Strike, dip, and rake angles between the two sets of solutions (those obtained from GOO1 and STEP2 locations) differ at most by 2°, 11°, and 11°, respectively, and P-axis trend and plunge angles differ by no more than 2° each. Similar to the GOO1 results, the STEP2 set of solutions has exceptions in the southernmost region where one SEFM event (#36) has nodal planes that are oriented more clockwise than the regional average and in the northernmost region where the CFM solution (#1) exhibits a sense of slip opposite that of all other solutions. In addition, SEFM #30 has a near horizontal north-south trending nodal plane. Other differences are the sub-vertical dips exhibited by the east-west nodal planes of SEFM #31 and 28.

Apparently, the magnitude of change produced in event location (most notably in focal depth) by the two different velocity models does not significantly affect the ultimate mechanism solution. This is because changes in the departure angle, which is the principal focal mechanism parameter altered by the relocations, produce only radial (along radii of the focal sphere) changes in the location of data on the focal sphere. For this case, polarities will only modify the dip angle and not the strike of nodal planes. Also, for predominantly strike-slip solutions such as those obtained for eastern

Tennessee, amplitude ratios affect primarily the location of the B-axis (null axis) and only to a minor extent the nodal plane dip and strike. The combined effect of the polarities and ratios is to move the B-axis about with relatively minor associated changes in the nodal plane strike. The most notable changes would then be in the dip and rake angles of the nodal planes. For the solutions obtained in this study, the greatest differences between the solutions obtained from GC01 and STEP2 data sets are indeed the dip and rake angles (see Table 10, especially DIF/SD). Crosson and Endo (1982) also showed that small changes in event location produced by a gradient velocity model, principally those in focal depth, influence primarily dip-slip events and the dip angle of nodal planes. Strike-slip events with nearly vertical nodal planes remained relatively unchanged. Nevertheless, the similarity of solutions with two different velocity models supports the presence of stablity in the focal mechanisms.

In-situ Stresses

A homogeneous and fracture free material subjected to a triaxial stress will fail along either of two planes oriented at an angle of 45° or less to the maximum compressive stress (sigma-one) and parallel to the intermediate compressive stress (e.g., Anderson, 1951). The orientation of sigma-one would then correspond exactly to that of the P-axis determined from focal mechanism solutions. However, if the earthquake is caused by slip along a pre-existing fault and/or the property of internal friction is taken into account, then the sigma-one is not simply related to the P-axis but may, in principle, lie anywhere in the quadrant containing the P axis (McKenzie, 1969).

Assuming that earthquakes in eastern Tennessee occur along pre-existing fractures and that the orientation of stresses is generally uniform throughout the region and constant through the short time frame of our observations, then the distribution of P-axes from numerous focal mechanisms should define a quadrant, or sector, wherein the sigma-one is located. The average P-axis orientation can further constrain the region of sigma-one, but may be biased by any concentrations present in the number and/or orientation of pre-existing fractures. However, because the sigma-one can lie anywhere in the quadrant containing the P-axis, then numerous nodal plane orientations could also, in principle, limit the region in which the sigma-one can lie. The applicability of this "sector method" increases directly with the number of different fault orientations and slip directions, and is not biased directly by fault concentrations, since only those extreme fault orientations that will slip in a given stress regime will form the sigma-one limits.

The sector method was used to determine a region for the sigma-one from both SEFM and CFM solutions obtained with GC01 locations (Figure 32). The CFM solutions (with only 12 nodal planes) constrained the region of sigma-one to the outer portions of the northeast and southwest quadrants. Addition of the SEFM solutions (with 22 nodal planes) further constrained the region of sigma-one to between N38°E and N63°E with plunges ranging from about 12° to -25°. Similar, but less constrained regions were found using nodal planes from STEP2 located events. These SEFM solutions restricted the region

to between N38°E and N76°E, with plunge angles of about 15° to -40°. Thus, all earthquakes in the region (except those in the northernmost region that were deleted, i.e., CFM #1) could have been induced by a uniform sigma-one of northeasterly orientation, and sub-horizontal plunge. This orientation is very similar to that determined for the Giles County, Virginia region by Munsey (1984), and is consistent with the east to northeast sigma-one trend determined for the midcontinent region by Zoback and Zoback (1980).

Average P-axis orientations for SEFM and CFM from both locational models are plotted on each focal sphere containing the sigma-one limits, and all lie near the center of each region (figure 32). This suggests that fractures in the region tend to be somewhat multi-directional but rather uniformly distributed throughout the region. That is because any nonuniform distribution or concentrations of fault plane orientations would bias the average P-axis orientation, and offset it from the center of the region of sigma-one.

If, as Raleigh and others (1972) suggest, the region in which the sigma-one is likely to be found is more reasonably restricted to near 30° about the focal mechanism computed P-axis, then the regional stress field would be further constrained to between N48°E and N53°E, with plunges ranging from about 0° to -15° (GCO1) or between N48°E and N66°E, with plunge angles from 5° to -30° (STEP2). The average P-axes would still be located within these more restricted regions.

One line of evidence supporting the general N48°E to N66°E orientation of the sigma-one is the systematic restriction of the P-axis trends to near N40 to 50°E with depth (see Figure 31). For vertical, strike-slip events, the sigma-one and least compressive stress (sigma-three) are horizontal, and the intermediate compressive stress (sigma-two) is vertical. Assuming that the sigma-one remains constant with depth and the sigma-two increases with depth, then the possible orientations for which fault slip will decrease with depth toward an angle of 30° from the sigma-one. The value at which the P-axis trend is restricted toward with depth (apex) should be 45° from this fault orientation, or 15° from the sigma-one. The apex values for the GCO1 and STEP2 data sets are N40°E and N50°E, respectively. Within the constraints of these data sets, which are in themselves biased with depth, the inferred sigma-one is consistent with the aforementioned N48°E to N53°E (GCO1) to 66°E (STEP2) defined by the nodal planes.

Geologic Model - Comparison to Giles County, Virginia

The Giles County Seismic Zone, 300 km to the northeast, has been the subject of several recent papers (Bollinger and Wheeler, 1982; Munsey, 1984; Munsey and Bollinger, 1984) and is one of the better understood seismically active sub-regions in the Southern Appalachians. Bollinger and Wheeler (1982) suggested that seismicity in Giles County is occurring along compressionally reactivated Iapetan (Eocambrian normal faults restricted to a sub-vertical, tabular zone striking northeast. Munsey (1984) and Munsey and Bollinger (1984) have since proposed the possibility of additional fault orientations and slip motion to the northeast and southwest of the zone. These new fault orientations (vertical, north-northwest trending faults with

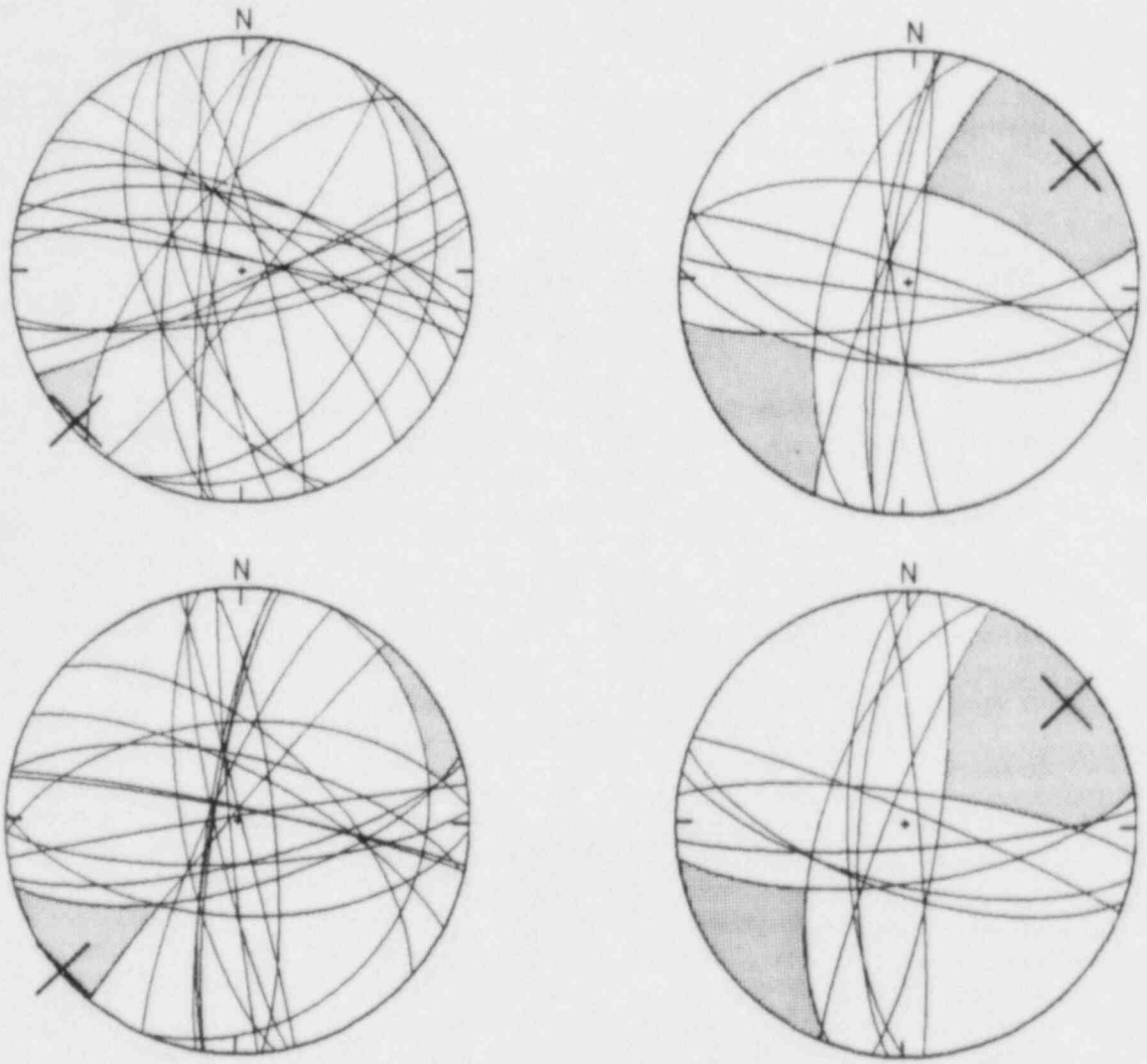

Figure 32: Limits for the Maximum Compressive Stress. Regions in which the maximum compressive stress can exist based upon the assumptions that all fault movement in the study area is due to the same maximum compressive stress orientation, and that the maximum compressive stress can be located anywhere in the dilatational quadrant. Top: GC01 data; SEFM on left and CFM on right. Bottom: STEP2 data; SEFM on left and CFM on right.

both right-lateral and reverse slip) are also consistent with the stress regime inferred for the main north-northeast striking zone.

Wheeler and Bollinger (1984) have also suggested that the current seismicity in the eastern Tennessee-North Carolina border area may be occurring along compressionally reactivated extensional fractures that formed during the rifting of the Proto-Atlantic. By analogy with the North American Mesozoic and other passive margin normal faults, Bollinger and Wheeler (1982) argue that Iapetan normal faults should strike northeast to north-northeast, dip steeply, and may be formed as far inland as 250 to about 450 km from the continental edge. Eastern Tennessee focal mechanisms exhibit generally northerly, steeply dipping nodal planes. Furthermore, the band of eastern Tennessee seismicity is located from 250 to 350 km cratonwards (westward), and trends approximately parallel to, the Piedmont gravity and magnetic lineaments, which have been interpreted to mark the eastern edge of the North American craton (Rankin, 1975; Hatcher and Zietz, 1980).

A major distinction between the two sub-regions is the tabular trend of hypocenters in Giles County, and the diffuse distribution of hypocenters in eastern Tennessee. Other dissimilarities are the underlying basement rock types and the proximity of each sub-region to the Precambrian continental margin. Giles County is underlain by granitic Grenville basement, and is located about 100 km nearer the Piedmont gravity and magnetic lineaments than the eastern Tennessee sub-region, which is underlain by Ocoee basement rocks separated from Grenville basement by the New York-Alabama and Clingman lineaments (see Johnston and others, 1985). These dissimilarities, however, may be interrelated. That is, the granitic Grenville rocks may have undergone a different magnitude of extension and may have reacted differently to such a stress regime than the probably petrologically different Ocoee rocks. Such differences may be reflected in the patterns of seismicity observed in each area.

In short, the seismicity of eastern Tennessee may be due to compressionally reactivated Iapetan normal faults similar to those proposed for the Giles County Seismic Zone, but the evidence presented herein is not conclusive. Future delineation of faults from seismic reflection profiles and/or hypocenter lineations are obviously needed.

CONCLUSIONS

Eleven SEFM and seven CFM were obtained from two different hypocenter data sets that were derived from a 4-layer velocity model (GC01) using a constant Vp/Vs ratio and with a 12-layer velocity model (STEP2) using variable Vp/Vs ratios. STEP2 was defined in an effort to obtain improved depth estimates and a more uniform distribution of ray departure angles. The individual earthquakes analyzed were the same for each set of solutions.

On the average, the resulting focal mechanisms for individual events are quite similar between the GC01 and STEP2 data sets. While a few events may show significant differences, a majority (29 of 36) of the focal mechanism solutions have strike, dip, and rake angles that differ by less than one standard deviation between themselves.

The (SV/P)z amplitude ratios significantly improved the determination of focal mechanism solutions in three important ways.

First, the addition of amplitude ratio data allows more events to have acceptably constrained solutions than when only polarity data are used. Secondly, ratios restrict, at least to some extent, the strike, dip, and rake angles determined by polarities, producing better constrained results. In this study, amplitude ratios were often necessary to distinguish between primarily strike-slip and dip-slip events. Thirdly, the RMS errors and other statistics generated from the amplitude ratio data provide an objective method in selecting a preferred solution from the family of solutions generally obtained.

The detailed geologic structures involved in the earthquake process remain unresolved. The general orientation of fault planes and some insights into the faulting process, however, have been described. Below, in summary form, are the basic conclusions of this study.

1. A major proportion of the seismic energy release in the study area has occurred in the basement, below the detached upper sedimentary layers. Both velocity models (GC01 and STEP2) employed to locate hypocenters confirm this factor.

2. Fault motion for SEFM and CFM solutions is predominantly strike-slip along nearly vertical north-south (right-lateral) or east-west (left-lateral) nodal planes. The average P-axis trend is about N50°E, with a nearly horizontal plunge. This orientation is consistent with both the P-axis orientation determined for the nearby Giles County, Virginia region (Munsey, 1984) 300 km to the northeast and the inferred trend of the sigma-one for the midcontinent region (Zoback and Zoback, 1980).

3. Limits placed by the GC01 based focal mechanism results on the region in which the maximum compressive stress can exist, based on the assumption that it may lie anywhere in the quadrant containing the P-axis, were about N38°E to N63°E, with plunges ranging from about 12° to -30°. The STEP2 based mechanism data set constrained the region from about N38°E to N76°E, with plunge angles of about 15° to -40°. The average P-axis orientation for SEFM and CFM solutions from both locational models each lie near the center of these regions of maximum compressive stress. That the average P-axis, which may be biased by concentrations in fault plane orientations, is so located suggests that fractures in the region are rather uniformly distributed throughout the region.

4. Two sub-regions of the study area have exceptions to the preceding general orientation of nodal planes and/or P-axes. First, nodal planes for some events in the southernmost region are oriented more clockwise than the regional average. These focal mechanisms are, nevertheless, consistent with the inferred regional stress regime. Secondly, the CFM in the northernmost study area exhibits a sense of slip that is opposite that of all other solutions and is thereby

inconsistent with the inferred regional stress field. We suspect error but have no confirmation for the source of this apparent local variation in the regional stress field.

ACKNOWLEDGMENTS

Dr. J. A. Snoke contributed numerous computer programs without which this project would have been impossible. We thank him for this and for his many invaluable insights and discussions into the analysis and interpretation of the results. Further discussions and advice were obtained from Mr. Jeff Munsey, Mr. Matthew Sibol, Mr. Martin Chapman, and Mr. Rick Davison. To these people we are also indebted. Finally, we thank Dr. E. S. Robinson for his critical review of this paper.

Dr. Arch Johnston and Mr. William Seay, directors of the Tennessee Earthquake Information Center and Tennessee Valley Authority Seismological Data Centers, respectively, provided the data used in this investigation. The Tennessee Valley Authority provided financial support throughout the project for one of us (AGT).

This research was supported in part by the Office of Nuclear Regulatory Research under Contracts NRC-04-77-134 and NRC-04-79-214.

REFERENCES

Anderson, E. M. (1951). The Dynamics of Faulting, Edinburgh, Oliver and Boyd, 206 p.

Bollinger, G. A. (1973). Seismicity of the Southeastern United States, Bull. Seism. Soc. Am., 63, 1785-1808.

Bollinger, G. A., C. J. Langer, and S. T. Harding (1976). The eastern Tennessee earthquake sequence of October through December, 1973, Bull. Seism. Soc. Am., 66, 525-547.

Bollinger, G. A., and R. L. Wheeler (1982). The Giles County, Virginia, Seismogenic Zone - Seismological Results and Geological Interpretations, U.S. Geol. Survey Open-File Report 82-585, 136 p.

Bollinger, G. A., and R. L. Wheeler (1983). The Giles County, Virginia, seismic zone, Science, 219, 1063-1065.

Brewer, S., J. Cornwell, and A. C. Johnston (1983). A study of the reliability of depth determinations using SARSN data, Tenn. Eq. Info. Center Spec. Report #10, 26 p.

Chapman, M. C., and G. A. Bollinger (1985). Reliability of focal depth estimates from a small network, Eqke. Notes, 55, p. 13.

Coffman, J. L., C. A. von Hake, and C. W. Stover (1982). Earthquake History of the United States, Publication 41-1, rev. ed. (through 1970), reprinted 1982 (with supplement (1971-1980)), U.S. Dept. of Commerce and Interior, Boulder, Colorado, 260 p.

Cook, F. A., D. S. Albaugh, L. D. Brown, S. Kaufman, and J. Oliver (1979). Thin-skinned tectonics in the crystalline southern Appalachians; COCORP seismic-reflection profiling of the Blue Ridge and Piedmont, Geology, 7, 563-567.

Crosson, R. S., and E. T. Endo (1982). Focal mechanisms and locations of earthquakes in the vicinity of the 1975 Kalapana earthquake aftershock zone 1970-1979: implications for tectonics of the south flank of Kilauea Volcano, Island of Hawaii, Tectonics, 1, 495-542.

Dewey, J. W., and D. W. Gordon (1984). Maps showing recomputed hypocenters of earthquakes in the eastern and central United States and adjacent Canada, 1925-1980, U. S. Geol. Survey Misc. Field Studies, Map MF-1699.

Guinn, S. A. (1980). Earthquake focal mechanisms in the southeastern United States, U. S. Nuclear Regulatory Commission Report NUREG/CR-1503, Washington, D. C., 150 p.

Harris, L. D. (1976). Thin-skinned tectonics and potential hydrocarbon traps-illustrated by a seismic profile in the Valley and Ridge province in Tennessee, J. Research U. S. Geol. Survey, 4, 379-386.

Hatcher, R. D., Jr., and I. Zietz (1980). Tectonic implications of regional aeromagnetic and gravity data from the southern Appalachians, in The Caledonides in the U.S.A., Wones, D. R., ed., VPI&SU Memoir #2, Blacksburg, VA, 235-244.

Herrmann, R. B. (1979). Surface wave focal mechanisms for eastern North American earthquakes with tectonic implications, J. Geophys. Res., 84, 3543-3552.

Johnston, A. C., D. J. Reinbold, and S. I. Brewer (1984). Seismotectonics of the Southern Appalachians, being edited for publication in Bull. Seism. Soc. Am., 23 p.

King, E. R., and I. Zietz (1978). The New York-Alabama lineament: geophysical evidence for a major crustal break in the basement beneath the Appalachian basin, Geology, 6, 312-318.

Kisslinger, C. (1980). Evaluation of S to P amplitude ratios for determining focal mechanisms from regional network observations, Bull. Seism. Soc. Am., 70, 999-1014.

Lahr, J. C. (1984). HYPOELLIPSE/VAX: A computer program for determining local earthquake hypocentral parameters, magnitude, and first motion pattern, U.S. Geol. Survey Open-File Report 84-??, 60 p.

Lee, W. H. K., and Lahr, J. C. (1975). HYP071 (revised): A Computer Program for Determining Hypocenter, Magnitude, and First Motion Pattern of Local Earthquakes, U. S. Geol. Survey Open-File Report 75-311, 114 p.

McKenzie, D. P. (1969). The relation between fault plane solutions for earthquakes and the directions of the principal stresses, Bull. Seism. Soc. Am., 59, 591-601.

Moore, T. P. (1979). Crustal velocity structure in southwestern Virginia, Virginia Polytechnic Institute and State University, M. S. Thesis, 75 p.

Munsey, J. W. (1984). Focal mechanisms for Virginia earthquakes, Virginia Polytechnic and State University, M. S. Thesis, 214 p.

Munsey, J. W., and G. A. Bollinger (1984). Focal mechanisms for Giles County, Virginia and vicinity, Eqke. Notes, 55, p. 8.

Nava, S., and S. Everett, ed. (1984). Tenn. Eqke. Info. Center Qtrly. Seism. Bull., 5, No. 1, 48 p.

Nelson, A. E., and I. Zietz (1983). The Clingman lineament, other aeromagnetic features, and major lithotectonic units in part of the southern Appalachian mountains, Southeastern Geology, 24, 147-157.

Nicholson, C. and D. W. Simpson (1984). Changes in Vp/Vs with depth: implications for appropriate velocity models, improved earthquake locations, and material properties of the upper crust, Bull. Seism. Soc. Am., in press.

Nicholson, C., D. W. Simpson, S. Singh, and J. E. Zollweg (1984). Crustal studies, velocity inversions and tectonics: results from a microearthquake survey in the New Madrid Seismic Zone, J. Geophys. Res., 89, 4545-4558.

Raleigh, C. B., J. H. Healy, and J. D. Bredhoeft (1972). Faulting and Crustal Stress at Rangely, Colorado, in Flow and Fracture of Rocks, Heard, H. C., I. Y. Borg, N. L. Carter, and C. B. Raleigh, ed., Am. Geophys. Union, Washington, D. C., 275-284.

Rankin, D. W. (1975). The continental margin of eastern North America in the Southern Appalachians: the opening and closing of the proto-Atlantic ocean, Am. Jour. Sci., 275-A, 298-336.

Reinbold, D., and J. Cornwell (1983). The Greenback, Tennessee earthquakes of 24 September 1982 and their tectonic associations, Tenn. Eqke. Info. Center Spec. Report #9, 32 p.

Sibol, M. S., and Bollinger, G. A., ed. (1984). Hypocenter listing from Southeastern U. S. Seismic Network Bulletins no. 1-12, SEUSSN Bull No. 12A, 44 p.

Sibol, M. S., G. A. Bollinger and E. C. Mathena (1984). Seismicity of the Southeastern United States, SEUSSN, Bull. No. 14, 53 p.

Snoke, J. A., J. W. Munsey, A. G. Teague, and G. A. Bollinger (1984). A program for focal mechanism determination by combined use of polarity and SV-P amplitude ratio data, Eqke. Notes, 55, p. 15.

Tzeng, W. S. and L. T. Long (1982). Investigation of SV- to P-wave amplitude ratio for determining focal mechanism, Eqke. Notes, 53, 39-40.

Watkins, J. S. (1964). Regional geologic implications of the gravity and magnetic fields of a part of eastern Tennessee and southern Kentucky, U.S. Geol. Survey Prof. Paper 516A, 17 p.

Wheeler, R. L. and G. A. Bollinger (1984). Seismicity and suspect terranes in the southeastern United States, Geology, 12, 323-326.

Zoback, M. L. and M. Zoback (1980). State of stress in the conterminous United States, J. Geophys. Res., 85, 6113-6156.

APPENDIX E.

APPENDIX F.

APPENDIX G.

APPENDIX H.

These appendices may be found in the form of microfiche in the jacket at the back of this report.

NRC FORM 335 (2-84) NRCM 1102, 3201, 3202

U.S. NUCLEAR REGULATORY COMMISSION

BIBLIOGRAPHIC DATA SHEET

SEE INSTRUCTIONS ON THE REVERSE

1. REPORT NUMBER (Assigned by TIDC and Vol. No., if any)

NUREG/CR-4288

2. TITLE AND SUBTITLE

Focal Mechanism analyses for Virginia and Eastern Tennessee Earthquakes (1978-1984)

3. LEAVE BLANK

4. DATE REPORT COMPLETED

MONTH: April | YEAR: 1985

5. AUTHOR(S)

G. A. Billinger, A. G. Teague, J. W. Munsey
A. C. Johnson

6. DATE REPORT ISSUED

MONTH: June | YEAR: 1985

7. PERFORMING ORGANIZATION NAME AND MAILING ADDRESS (Include Zip Code)

Seismological Observatory
Virginia Polytechnic Institute and State University
Blacksburg, VA 24061

Tennessee Earthquake Information Center
Memphis State University
Memphis, TN 38152

8. PROJECT/TASK/WORK UNIT NUMBER

9. FIN OR GRANT NUMBER

FIN B6249 & B6675

10. SPONSORING ORGANIZATION NAME AND MAILING ADDRESS (Include Zip Code)

Division of Radiation Programs and Earth Sciences
Office of Nuclear Regulatory Research
U.S. Nuclear Regulatory Commission
Washington, DC 20555

11a. TYPE OF REPORT

Technical

b. PERIOD COVERED (Inclusive dates)

12. SUPPLEMENTARY NOTES

13. ABSTRACT (200 words or less)

Focal mechanisms are presented for 11 earthquakes from the Giles County, Virginia, seismic zone and its vicinity and for 12 earthquakes from the Central Virginia seismic zone. These earthquakes ($0 \leq M < 4$) were monitored by local networks between January 1978 and October 1984. In Giles County, the data base consists of 43 P-wave polarities and 50 SB to P amplitude ratios (SV/P) that yielded six single event focal mechanisms (SEFM's) and five composite event focal mechanisms (CFM's). In Central Virginia, 79 P-wave polarities and 51 SV/P ratios are used to determine 11 SEFM's and four CFM's. A computer program FOCMEC was used to determine the focal mechanism solutions. The results for the Giles County seismic zone show mainly strike-slip mechanisms on steeply dipping ($73° \pm 16°$) NNE (right lateral motion) and ESE (left lateral motion) trending nodal planes. However, some (4/11) of the solutions show similar movement on nodal planes rotated 45° counterclockwise. The P axes in Central Virginia are generally northeast trending for shallow earthquakes (> 8 km) and northwest trending for deeper ones (< 8 km). In Giles County, where the seismic activity is occurring beneath the Appalachian decollement, faulting and inferred stress orientations are more uniform than in Central Virginia, some 200 km away, where the seismicity is occurring near and above the decollement.

14. DOCUMENT ANALYSIS - a. KEYWORDS/DESCRIPTORS

Focal Mechanisms
Earthquakes
Seismicity
Giles County
Tennessee
Virginia

b. IDENTIFIERS/OPEN ENDED TERMS

15. AVAILABILITY STATEMENT

Unlimited

16. SECURITY CLASSIFICATION

(This page) Unclassified

(This report) Unclassified

17. NUMBER OF PAGES

18. PRICE

UNITED STATES
NUCLEAR REGULATORY COMMISSION
WASHINGTON, D.C. 20555